Comparative gene expression of different African horse sickness virus strains

by

Carolina Elizabeth de Wet

Submitted in partial fulfilment of the requirements for the degree

Magister Scientiae

In the Faculty of Natural & Agricultural Sciences
University of Pretoria

Pretoria

(2017)

UNIVERSITEIT VAN PRETORIA
UNIVERSITY OF PRETORIA
YUNIBESITHI YA PRETORIA

DECLARATION

I, ***Carolina Elizabeth de Wet***, declare that the thesis / dissertation, which I hereby submit for the degree *Magister Scientiae* at the University of Pretoria, is my own work and has not previously been submitted by me for a degree at this, the University of Pretoria, or any other tertiary institution.

SIGNATURE: ……...

DATE: ……..…..

ACKNOWLEDGEMENTS

I wish to thank the following parties for their contribution to my work:

Vida van Staden, my supervisor, for her guidance and enduring patience throughout this project.

Prof Jacques Theron, my co-supervisor, for his advice, counsel and guidance on this project.

The National Research Foundation and the University of Pretoria for the funding that sustained the expenses of this project.

The Department of Genetics and my colleagues from the Orbivirus Research Group for the fun and great memories.

Flip Wege for his wisdom and tremendous assistance with the tissue culturing work throughout this project.

Grandpa Lourens and Granny Pat De Wet for materialising the childhood dream of obtaining tertiary education.

My parents, John and Sarie de Wet for being the best life coaches one could ever ask for – you have taught me all the hard life lessons in the best way!

To my sisters Jeanne and Frances, for their constructive criticisms, healthy sibling-rivalry and always being my best cheerleaders to excel in all I do.

Lastly and most importantly, to the most wonderful husband, Chris-Jan, whose unmeasured support, exuberant patience, enduring love and shared late nights carried me through this endeavour to help me make this a success.

En al sou ek die gawe van profesie hê en al die geheimenisse weet en al die kennis, en al sou ek al die geloof hê, sodat ek berge kon versit, en ek het nie die liefde nie, dan sou ek niks wees nie.
1 Kor 13:2

~ Vir Oupa Willie & Ouma Lutha Manning ~

SUMMARY

Comparative Gene Expression of Different African Horse Sickness Virus Strains

by

Carolina Elizabeth de Wet

Supervisor: Dr Vida van Staden
Department of Genetics
University of Pretoria

Co-supervisor: Prof Jacques Theron
Department of Microbiology
University of Pretoria

For the degree *Magister Scientiae*

Currently orbiviruses are recognised as causing worldwide emerging and re-emerging disease outbreaks including African horsesickness (AHS), a devastating disease of equids. AHS is endemic to sub-Saharan Africa, and of great economic importance in South Africa. AHS is a non-contagious arboviral disease with a mortality rate of up to 90% in susceptible horses. The disease is caused by African horsesickness virus (AHSV) and transmitted through species of the biting midge *Culicoides*. AHS can present with different disease severity and varying mortality rates, and to date no known correlation exist between specific serotypes and specific clinical forms. AHS disease pathogenesis is complex, and the result of an interaction of both viral and host factors. When using a tissue culture model system there are less variables, and one should theoretically be able to pinpoint viral genes or proteins that contribute to cellular cytopathic effect (CPE) with greater accuracy and ease.

AHSV is a member of the *Orbivirus* genus, within the *Reoviridae* family, and is one of nine genera with a characteristic segmented double stranded RNA genome. This genome organisation allows the formation of genetic reassortants, which have assisted in revealing the functions of specific viral proteins. In a previous study eight AHSV strains, representing three different serotypes and five reassortant, were compared and differences observed with respect to virus release, effects on membrane permeability, cytotoxicity and cell viability, timing and extent of CPE, and induction of apoptosis. As the molecular basis for these differences were not fully understood, the aim of this study was to monitor different stages of the AHSV lifecycle of these strains to propose a cause for the diverse cytopathogenesis phenotypes observed. To accomplish this, systematic comparisons of gene expression studies on the three parental and five reassortant AHSV strains were done in both a mammalian and insect tissue culture system. This study set out to monitor different AHSV replication cycle stages, and focused mainly on i) transcription, ii) translation, iii) genome segment packaging and dsRNA synthesis, and iv) virus release since little was known about the discrepancies in replication kinetics between the different strains.

In this investigation, varying degrees of CPE were observed in cultured mammalian cells upon infection with the different AHSV strains. Results suggested that a reassortant combination of genome segments 5 (NS1) and 10 (NS3) influenced the time of onset and severity of CPE observed *in vitro* in mammalian tissue cultures. Monitoring protein synthesis with Western blot assays, suggested probable interaction between the proteins encoded by AHSV-2 segments 5 and 10. When heterologous relative to the backbone genome, this reassortment combination produced a more severe cytopathic phenotype compared to the AHSV-2 parent. It may be hypothesised that the interaction between AHSV NS1 and NS3, when originating from the same parental strain, may play a role in the rate of onset of CPE and consequently influence the severity of cytopathicity *in vitro*, at least with respect to AHSV-2, -3 and -4. However, this was only observed when monitoring VP7 but not NS1 and NS2 protein synthesis levels. Moreover, similar findings were not observed when monitoring virus dsRNA synthesis levels or virus yield. Results further indicated no significant differences between the parental and reassortant strains when monitoring protein synthesis levels, dsRNA synthesis levels and virus yield in insect cell cultures.

In our study the replication kinetics for the different reassortment progeny indicated changes in early replication stages only in infected mammalian cells. Although reassortant strains with an AHSV-2 NS1/NS3 recombination achieved changes early during virus replication, late virus replication stages remained unchanged. Results suggested that no specific step during virus replication was more efficient, as indicated by the parameters monitoring replication kinetics. We have also shown that replication kinetics in insect cells appear to be unchanged, at least during the replication steps monitored. This suggested that the cause for superior *in vitro* cytopathogenic strains in mammalian cells, but not in insect cells, grants merit for further investigation of host cell interactions and responses.

LIST OF ABBREVIATIONS

°C	degrees Celsius
β-	beta
β_2MG	β_2-microglobulin
β-ME	β-mercaptoethanol
µCi	microCurie
µg	microgram
µl	microlitre
µm	micrometer
35S-Met	Sulpher-35 radio isotope labelled Methionine
40S	eukaryotic small ribosomal subunit
AdoHCy	S-adenosyl homocysteine
AdoMet	S-adenosyl methionine
ADP	adenosine diphosphate
AHS	African horsesickness
AHSV	African horsesickness virus
ANOVA	analysis of variance
ATP	adenosine triphosphate
ATPase	adenylpyrophosphatase
bp	base pairs
BR	biological replicate
BSR	a clone of baby hamster kidney cells
BTV	blue tongue virus
cDNA	complimentary DNA
CLP	core-like particle
cm	centimeter
CO_2	Carbon dioxide
Cp	crossing point
CPE	cytopathic effect
CTD	C-terminal domain
ddNTP	dideoxynucleoside triphosphate

DeltaDD	dynamic difference
dH_2O	distilled water
DNA	deoxyribonucleic acid
DNase	deoxyribonuclease
dNTP	deoxynucleoside triphosphate
ds	double stranded
DVD	aspartic acid - valine - aspartic acid motif
EDTA	ethylenediaminetetra-acetic acid
EEV	equine encephalosis virus
EHDV	epizootic haemorrhagic disease virus
eIF4G	eukaryotic translation initiation factor 4 G
ELISA	enzyme-linked immunosorbent assay
EtBr	ethidium bromide
EtOH	ethanol
G	glycine
g	relative centrifugal force
GAPDH	glyceraldehyde-3-phosphate dehydrogenase
GDP	guanosine diphosphate
GMP	guanosine monophosphate
GTase	guanylyltransferase
GTP	guanosine triphosphate
HCl	hydrochloric acid
HK	housekeeping gene
HRP	horse radish peroxidase
HSD	honestly significant difference
IFNAR	interferon alpha / beta receptor
KCl	potasium chloride
kDa	kilodalton
KH_2PO_4	potassium dihydrogen phosphate (anhydrous)
L	large segment
LiCl	lithium chloride
M	medium segment

MEM	minimum essential medium
MeOH	methanol
Met / M	Methionine
mg	miligrams
Mg_2^+	magnesium ion
$MgCl_2$	magnesium chloride
min	minutes
mM	milimolar
MOI	multiplicities of infection
mRNA	messenger RNA
MTase	methyltransferase
MVB	multivesicular body
$Na_2HPO_4 \cdot 2H_2O$	disodium hydrogen phosphate (hydrated)
NaCl	sodium chloride
NaOAc	sodium acetate
nm	nanometer
NS	non-structural
NS1	non-structural virus protein 1 (genome segment 5)
NS2	non-structural virus protein 2 (genome segment 8)
nt	nucleotide
NTD	N-terminal domain
NTE	sodium chloride, Tris, EDTA
-OH	hydroxyl
ORF	open reading frame
p.i.	post-infection
p11	subunit of the cellular calpactin complex, a cellular binding partner of NS3
PAGE	polyacrylamide gel electrophoresis
PBS	phosphate buffered saline
PCR	polymerase chain reaction
PD	polymerase domain
pfu	plaque forming units
pH	potential of hydrogen

P_i	inorganic phosphate
pmol	picomol
PP_i	pyrophosphate
PSAP	late-domain motif, recruits the cellular protein Tsg101
PSB	protein solvent buffer
qPCR	quantitative PCR
RdRp	RNA-dependent RNA polymerase
rMVA	recombinant modified vaccinia virus Ankara
RNA	ribonucleic acid
rpm	revolutions per minute
RTase	RNA 5'-triphosphatase
RT-PCR	reverse transcription PCR
rt-qPCR	quantitative real-time PCR
SDS	sodium dodecyl sulphate
sec	seconds
Seg	segment
Sf	*Spodoptera frugiperda* cell line
sp.	species (singular)
spp.	species (plural)
ss	single stranded
Syt1	cellular synaptotagamin-1 protein
TAE	Tris, Acetic acid and EDTA
TBE	Tris, Boric acid and EDTA
TEMED	N,N,N',N'-tetramethylethylene diamine
TR	technical replicate
Tris	Tris hydroxymethyl aminomethane
Tsg101	tumor susceptibility gene 101, a component of the ESCRT-I complex
UHQ	ultra-high quality
UK	United Kingdom
USA	United States of America
UTP20	small subunit processome component 20 homolog
UV	ultra violet

V (amino acid)	valine
V (current)	voltage
v/v	volume per volume
VIB	virus inclusion bodies
VP	virus protein
VP7	Virus protein 7 (AHSV genome segment 7)
w/v	weight per volume

LIST OF BUFFERS

5% Blocking Solution:

1 × PBS buffer containing 5% (w/v) milk powder

NTE Buffer:

100 mM NaCl, 10 mM Tris-HCl, 1 mM EDTA, pH 7.4

1 × Phosphate-buffered Saline (PBS):

PBS; 137 mM NaCl, 2.7 mM KCl, 4.3 mM $Na_2HPO_4 \cdot 2H_2O$, 1.5 mM KH_2PO_4, 0.5% (v/v) Triton X-100

3 × Protein Solvent Buffer (PSB)

188 mM Tris-HCl (pH 6.8) 6% SDS, 30% Glycerol, 15% β-mercaptoethanol and 0.005% bromophenol blue

0.01 M STE Buffer:

10 mM NaCl, 1 mM $MgCl_2$, 1 mM Tris-HCl, pH 7.4

0.15 M STE Buffer:

150 mM NaCl, 1 mM EDTA, 1 mM Tris-HCl, pH 7.4

0.15 M STM Buffer:

150 mM NaCl, 5 mM $MgCl_2$, 10 mM Tris-HCl, pH 7.4, 0.5% Triton X-100

1 × TAE Buffer:

4 mM Tris-HCl, 0.1% (v/v) Glacial acetic acid, 0.2 mM EDTA, pH 8.0

1 × TBE Buffer:

0.1 M Tris-HCl, 0.1 M Boric acid, 2 mM EDTA, pH 8.0

Transfer Buffer:

25 mM Tris-HCl, 192 mM Glycine, 20% (v/v) MeOH

1 × Tris-glycine Running Buffer:

25 mM Tris-HCl, 250 mM glycine

LIST OF FIGURES

Figure 1: Agarose gel confirming PCR amplification of the S7 target region. Both gels include a 100 bp DNA size marker (lane 1 & 5) with sizes indicated on left, negative controls (lane 2 & 6) and target specific amplification for segment 7 of AHSV-2 (lanes 3 & 4) and AHSV-4 (lanes 7 & 8). **33**

Figure 2: PCR amplification results indicating the segment 5 target region. Lane 1 shows the 100 bp DNA size marker with sizes indicated on the left, a negative control (lane 2) followed by amplification of a region of segment 5 of AHSV-2 (lanes 3 & 4), AHSV-3 (lanes 5 & 6) and AHSV-4 (lanes 7 & 8). **34**

Figure 3: PCR amplification results of a segment 5 target region for: A) AHSV-2; B) AHSV-3 and C) AHSV-4 using primer concentrations of 10 pmol (lane 3), 20 pmol (lane 4), 25 pmol (lane 5) or 30 pmol (lane 6); a DNA size marker (lane 1) with sizes indicated on the left, and a negative control (lane 2) were included. **35**

Figure 4: Results indicating segment 5 amplification from a temperature gradient PCR ranging from 55.5°C (lane 2) to 65.5°C (lane 13) in 1°C increments. A DNA size marker (lane 1), with sizes indicated on left, was also included. **35**

Figure 5: PCR amplification results showing amplification of a segment 8 target region. A DNA size marker (lane 1, showing sizes on left) and a negative control (lane 2) were included. Target-specific amplification shown for segment 8 of AHSV-2 (lanes 3 & 4), AHSV-3 (lanes 5 & 6) and AHSV-4 (lanes 7 & 8). **36**

Figure 6: Agarose gel electrophoresis results showing PCR amplification of the segment 10 target region of AHSV-2 (lanes 3 & 4), AHSV-3 (lanes 5 & 6) and AHSV-4 (lanes 7 & 8). A DNA size marker depicted in lane 1 with sizes indicated on left and negative control (lane 2) were also included. ... **36**

Figure 7: Nucleotide alignment of four segment 10 sequences available on Genbank. Accession numbers represent the sequences as follows: AHU59279 (AHSV-2), DQ868782 and D12479 (AHSV-3), DQ868783 (AHSV-4). RT-NS3F and RT-NS3R indicate the forward and reverse primer sequences, respectively (5'-3' orientation). **37**

Figure 8: Sequence alignment of four Genbank sequences for segment 10 and consensus sequences obtained from sequencing experiments for AHSV-2 (Consensus2), AHSV-3 (Consensus3) and AHSV-4 (Consensus4). The highlighted regions in the bottom 3 sequences are the targeted region from which serotype-specific primer sets were designed for each AHSV serotype studied. **38**

Figure 9: Agarose gel electrophoresis results showing PCR amplification of the segment 10 target regions from newly synthesised cDNA of A) AHSV-2, B) AHSV-3 and C) AHSV-4 in lanes 4 and 5 of each gel image. Lanes 6 and 7 represent amplification results from the sequencing cDNA control samples. A DNA size marker with the sizes indicated on the left (lane 1), a negative control (lane 2) and a Vero cell cDNA control (lane 3) were included in all gels. **39**

Figure 10: Amplification results of a gradient PCR showing amplification of the segment 10 target region of A and C) AHSV-2, B and D) AHSV-3 and E) AHSV-4. In all gel images lane 2 shows results at 50°C and lane 13 shows results at 60°C annealing temperatures. Lane 1 in all gel images contains a DNA size marker with the sizes indicated on the left. Gel images A and B show electrophoresis of PCR amplicons on agarose gel prepared with TAE buffer. Gel images C, D and E show electrophoresis of PCR amplicons on agarose gel prepared with TBE buffer. For all gels the annealing temperatures were: 50°C (lane 2), 50.2°C (3), 50.7°C (4), 51.6°C (5), 52.7°C (6), 54°C (7), 55.4°C (8), 56.8°C (9), 58.1°C (10), 59.2°C (11), 60°C (12), 60.4°C (13). **40**

Figure 11: PCR amplification results of housekeeping genes GAPDH (lanes 3-5 and β_2MG (lanes 7-9) from uninfected Vero cells. Negative controls were included for the GAPDH primer set (lane 2)

and β_2MG primer set (lane 6). Lane 1 contains a DNA size marker with the sizes indicated on the left. **41**

Figure 12: Real-time PCR amplification results for the A) β_2MG primer set with B) corresponding standard curve calculated, and the C) GAPDH primer set with D) corresponding standard curve calculated. **42**

Figure 13: Electrophoresis results of the real-time PCR amplification of the A) β_2MG primer set and B) GAPDH primer set. In both gel images three technical replicates each are shown for the negative controls (lanes 1-3), with serial cDNA dilutions of 10^{-1} (lanes 4-6), 10^{-2} (lanes 7-9), 10^{-3} (lanes 10-12), and 10^{-4} (lanes 13-15). Lane 16 contains a DNA size marker with the sizes indicated on the right. **43**

Figure 14: PCR amplification of cDNA using A) the GAPDH primer set and B) the β_2MG primer set. Lane 1 contains a DNA size marker with the sizes indicated on the left and lane 2 a negative control. cDNA was synthesised from uninfected Vero cells (lane 3) or from cells infected with AHSV-2 (lane 4), AHSV-3 (lane 5) or AHSV-4 (lane6). **44**

Figure 15: Relative quantification ratios calculated as *Target* over *Reference* This experiment shows the ratios for β_2MG : GAPDH. The blue bars indicate the *one-to-one* pairing ratio calculated using the crossing point concentrations. The red bars indicate the normalised quantification ratios calculated. The error bars indicate standard deviation. Samples assigned as “Mock” were unifected cells. AHSV-2, AHSV-3 and AHSV-4 assigned samples indicate that those cells were infected with the assigned virus. No data was recorded for AHSV-4-infected cells at 24 hours p.i. **45**

Figure 16: Microscope photos indicating the level of CPE at the indicated times post-infection from three parental AHSV serotypes and five reassortant virus strains. Results are shown for both unsynchronised infections (MOI 0.1 pfu/cell) and synchronised infections (MOI 2 pfu/cell). **47**

Figure 17: Western blot analyses using anti-VP7 (A), anti-NS1 (B) or anti-NS2 (C) antibodies. Each blot shows a protein size marker with the sizes indicated on the left (lane 1), a mock-infected sample (lane 2) and AHSV-3-infected cells (lane 3). **49**

Figure 18: Western blot analysis results with corresponding quantification results showing A) VP7, B) NS1 and C) NS2, respectively, from AHSV-2, AHSV-3 and AHSV-4. Each blot shows a protein size marker (PR) with the sizes indicated on the left and a mock (M)-infected sample. **50**

Figure 19: β-Actin protein levels in Vero cells. Cells were mock-infected, or infected with AHSV at an MOI of 0.1 pfu/cell, and harvested at A) 16 h p.i., B) 24 h p.i. or C) 48 h p.i. A representative Western blot is shown on the left. In each blot Lane 2 contains a mock-infected sample, Lanes 3-5 the parental serotypes and Lanes 6-10 the reassortant virus strains in the same order as on the graphs. The graphs shown on the right, represent the average volume intensity values obtained from the quantification of multiple blots as detailed in Table 3. Error bars indicate the standard deviation. **54**

Figure 20: β-Actin protein levels in Vero cells. Cells were mock-infected, or infected with AHSV at an MOI of 2 pfu/cell, and harvested at A) 8 h p.i., B) 16 h p.i. and C) 24 h p.i. A representative Western blot is shown on the left. In each blot Lane 2 contains a mock-infected sample, Lanes 3-5 the parental serotypes and Lanes 6-10 the reassortant virus strains in the same order as on the graphs. The graphs shown on the right, represent the average volume intensity values obtained from the quantification of multiple blots as detailed in Table 3. Error bars indicate the standard deviation. **55**

Figure 21: VP7 protein levels in Vero cells. Cells were mock-infected, or infected with AHSV at an MOI of 0.1 pfu/cell, and harvested at A) 8 h p.i., B) 16 h p.i., C) 24 h p.i. and D) 48 h p.i. A representative Western blot reacted with anti-VP7 antibody is shown on the left. In each blot Lane 2 contains a mock-infected sample, Lanes 3-5 the parental serotypes and Lanes 6-10 the reassortant

virus strains in the same order as on the graphs. The graphs shown on the right, represent the average volume intensity values (dark blue bars), and the adjusted values (light blue bars). Error bars indicate the standard deviation. Numbers above bars indicate statistical significant difference to that parental strain. **57**

Figure 22: NS1 protein levels in Vero cells. Cells were mock-infected, or infected with AHSV at an MOI of 0.1 pfu/cell, and harvested at A) 16 h p.i., B) 24 h p.i. and C) 48 h p.i. A representative Western blot reacted with anti-NS1 antibody is shown on the left. In each blot Lane 2 contains a mock-infected sample, Lanes 3-5 the parental serotypes and Lanes 6-10 the reassortant virus strains in the same order as on the graphs. The graphs shown on the right, represent the average volume intensity values (dark blue bars), and the adjusted values (light blue bars). Error bars indicate the standard deviation. No NS1 proteins were detected at 8 hours post-infection. **58**

Figure 23: NS2 protein levels in Vero cells. Cells were mock-infected, or infected with AHSV at an MOI of 0.1 pfu/cell, and harvested at A) 8 h p.i., B) 16 h p.i., C) 24 h p.i., and D) 48 h p.i. A representative Western blot reacted with anti-NS2 antibody is shown on the left. In each blot Lane 2 contains a mock-infected sample, Lanes 3-5 the parental serotypes and Lanes 6-10 the reassortant virus strains in the same order as on the graphs. The graphs shown on the right, represent the average volume intensity values (dark blue bars), and the adjusted values (light blue bars). Error bars indicate the standard deviation. Numbers above bars indicate statistical significant difference to that parental strain. **59**

Figure 24: VP7 protein levels in Vero cells. Cells were mock-infected, or infected with AHSV at an MOI of 2 pfu/cell, and harvested at A) 8 h p.i., B) 16 h p.i. and C) 24 h p.i. A representative Western blot reacted with anti-VP7 antibody is shown on the left. In each blot Lane 2 contains a mock-infected sample, Lanes 3-5 the parental serotypes and Lanes 6-10 the reassortant virus strains in the same order as on the graphs. The graphs shown on the right, represent the average volume intensity values (dark blue bars), and the adjusted values (light blue bars). Error bars indicate the standard deviation. **60**

Figure 25: NS1 protein levels in Vero cells. Cells were mock-infected, or infected with AHSV at an MOI of 2 pfu/cell, and harvested at A) 16 h p.i. and B) 24 h p.i. A representative Western blot reacted with anti-NS1 antibody is shown on the left. In each blot Lane 2 contains a mock-infected sample, Lanes 3-5 the parental serotypes and Lanes 6-10 the reassortant virus strains in the same order as on the graphs. The graphs shown on the right, represent the average volume intensity values (dark blue bars), and the adjusted values (light blue bars). Error bars indicate the standard deviation. Again, no NS1 proteins were detected at 8 hours post-infection. **61**

Figure 26: NS2 protein levels in Vero cells. Cells were mock-infected, or infected with AHSV at an MOI of 2 pfu/cell, and harvested at A) 8 h p.i., B) 16 h p.i. and C) 24 h p.i. A representative Western blot reacted with anti-NS2 antibody is shown on the left. In each blot Lane 2 contains a mock-infected sample, Lanes 3-5 the parental serotypes and Lanes 6-10 the reassortant virus strains in the same order as on the graphs. The graphs shown on the right, represent the average volume intensity values (dark blue bars), and the adjusted values (light blue bars). Error bars indicate the standard deviation..... **62**

Figure 27: Pulse labelling results for the four different optimisation experiments. Visualisation of bands from an overnight exposure onto an autorad-screen. Lanes 1-6 show results for experiment A, Lanes 7-12 show results for experiment B, Lanes 13-18 results for experiment C and Lanes 19-24 for experiment D. In all experiments the lanes were loaded in the order: AHSV-2, AHSV-3, AHSV-4, R4-$2_{4, 5,7,10}$, R4-$2_{7,10}$ and R4-2_{10}. **68**

Figure 28: Pulse labelling results from infected cells labelled at A) 5-8 hours p.i., B) 13-16 hours p.i. and C) 21-24 hours p.i. Visualisation of labelled proteins from overnight exposure. Position of the protein marker is indicated on the left. Protein bands for VP7, NS1 and NS2 are indicated with arrows on the right. For each image, samples were loaded in the order: L1: Mock-infected sample,

L2: AHSV-2, L3: AHSV-3, L4: AHSV-4, L5: R3-$2_{3,5}$, L6: R3-$2_{5,10}$, L7: R4-2_{10}, L8: R4-$2_{7,10}$, L9: R4-$2_{4,5,7,10}$. **69**

Figure 29: VP7, NS1 and NS2 protein synthesis levels during A) 5-8, B) 13-16 and C) 21-24 hours p.i. for the different AHSV strains studied. Pulse labelling, using ^{35}S-Met, were done at the three time intervals indicated. At 5-8 and 21-24 hours p.i., more than one replicate for each set of data was available to calculate average volume intensities and error bars are shown, indicating standard deviation. Numbers above bars indicate statistical significant difference to that parental strain. ... **71**

Figure 30: RNA PAGE results showing the three parental strains, Lanes 1 and 5: AHSV-2, Lane 2: AHSV-3, Lane 6: AHSV-4 and Lanes 3, 4, 7, 8 and 9: the five reassortant strains. The genome segments are indicated to the left of the image. **75**

Figure 31: RNA PAGE results showing virus dsRNA levels at: A) 24 hours p.i. from Vero cells infected at an MOI of 2 pfu/cell and B) 48 hours p.i. from Vero cells infected at an MOI of 0.1 pfu/cell. AHSV-2, AHSV-3 and AHSV-4 were loaded in Lanes 1-3, respectively. The reassortant virus strains were loaded in the order: R3-$2_{3,5}$, R3-$2_{5,10}$, R4-2_{10}, R4-$2_{7,10}$ and R4-$2_{4,5,7,10}$ in Lanes 4-8. Only genome segments 1-3 are shown, indicated to left of image. **76**

Figure 32: Averaged volume intensity values of A) virus dsRNA levels for Seg-3 at 24 hours p.i., cells were infected at an MOI of 2 pfu/cell. B) Virus dsRNA levels at 48 hours p.i., cells were infected at an MOI of 0.1 pfu/cell. Error bars indicate standard deviation. Numbers above bars indicate statistical significant difference to that parental strain. **77**

Figure 33: Titration results shown for yield of newly assembled infectious AHSV particles at A) 24 hours p.i. for a synchronous infection (MOI 2 pfu/cell) and B) 48 hours p.i. for an unsynchronous infection (MOI 0.1 pfu/cell). The graphs represent the average of three biological replicates for each strain at the two time points. Error bars indicate standard deviation. Numbers above bars indicate statistical significant difference to that parental strain. **80**

Figure 34: Results showing a representative blot for AHSV proteins studied with a corresponding graph indicating the quantified protein levels synthesised up to 8 days post-infection. For each blot a size marker (Lane 1) is indicated with sizes on the left. For each blot Lane 2 indicates the mock-infected sample and Lanes 3-10 show the AHSV results for A) VP7, B) NS1 and C) NS2. NS1 results are indicated with arrow. Results from Western blots are indicated in the same order as shown on graphs. Error bars on graphs represent standard deviations. **84**

Figure 35: A) Results showing virus segment 3 dsRNA levels at 8 days p.i. in infected KC cells. Genome segments indicated to left of image. Samples on gel loaded in same order as indicated on graph. B) Average virus segment 3 dsRNA levels at 8 days p.i. for the 8 different virus strains as indicated. Error bars indicate standard deviation. **86**

Figure 36: Titration results showing average yield of new infections AHSV particles from infected KC cells at 8 days p.i. Error bars indicate standard deviations. **87**

LIST OF TABLES

Chapter 1:

Table 1: Summary of the AHSV genome segments arrangement, the proteins they encode, molecular mass and size, and the location of each protein **7**

Chapter 2:

Table 2: Summary of primers used for PCR amplification experiments **28**

Table 3: Summary of primary antibodies used for Western blot analyses **31**

Table 4: Summary of primers used for RT-PCR and sequencing of the NS3 genes of AHSV-2, -3 & -4 ..... **37**

Table 5: Summary of the three AHSV serotype specific primer set sequences **38**

Table 6: Summary of Western blots done for housekeeping protein β-Actin **52**

Table 7: Summary of Western blot analyses to study virus protein expression **53**

Table 8: Adjustment factors* calculated from β-Actin at each time point within each infection trial **56**

Table 9: Summary of the calculations done for the one-way ANOVA analyses **64**

Table 10: One-way ANOVA analyses results from immunoblot assays on infected mammalian cells **65**

Table 11: Summary of the *post-hoc* multiple comparisons test on virus protein levels that revealed statistically significant difference **66**

Table 12: Preparation of four experiments A-D indicating different volumes of variables tested in combination to each other **67**

Table 13: Summary of ANOVA analyses results from pulse labelling assays on infected Vero cells **73**

Table 14: Results from *post-hoc* multiple comparisons test from pulse labelling assays on infected Vero cells **74**

Table 15: One-way ANOVA results from virus dsRNA levels at 24 and 48 hours p.i. monitored in infected Vero cells **78**

Table 16: Summary of the *post-hoc* multiple comparisons test on virus dsRNA levels from infected Vero cells **78**

Table 17: One-way ANOVA results from virus titrations at 24 and 48 hours p.i. to monitor yield of newly assembled infectious AHSV particles **81**

Table 18: Summary of the *post-hoc* multiple comparisons test results on virus titrations at 24 and 48 hours p.i. **82**

Table 19: Summary of the one-way ANOVA results for AHSV VP7, NS1 and NS2 protein levels from infected KC cells **85**

Table 20: Summary of the *post-hoc* multiple comparisons test results for virus protein synthesis at 8 days p.i. **85**

Table 21: Summary of one-way ANOVA results for virus dsRNA levels at 8 days p.i. in infected KC cells **87**

Table 22: Summary of the one-way ANOVA results for new infectious AHSV particles from infected KC cells **88**

Table 23: Summary of the *post-hoc* multiple comparisons test results for virus yield at 8 days p.i **88**

TABLE OF CONTENTS

DECLARATION ..... **i**
ACKNOWLEDGEMENTS ..... **ii**
SUMMARY ..... **iii**
LIST OF ABREVIATIONS ..... **v**
LIST OF BUFFERS ..... **x**
LIST OF FIGURES ..... **xi**
LIST OF TABLES ..... **xv**

CHAPTER 1: LITERATURE REVIEW **2**
1 INTRODUCTION **2**
2 AFRICAN HORSESICKNESS VIRUS AETIOLOGY **2**
3 GLOBAL IMPLICATIONS **3**
3.1 The Current BTV status in Europe **3**
3.2 Current Vaccines for AHSV **3**
3.3 AHSV Vaccine Development **4**
4 EPIDEMIOLOGY OF THE AHSV **5**
4.1 AHS Pathogenesis **5**
4.2 Vector Species and Transmission of AHS **5**
5 MOLECULAR BIOLOGY OF ORBIVIRUSES **6**
5.1 Viral Genome **6**
5.2 Structural Proteins **8**
VP1 ..... *8*
VP2 ..... *8*
VP3 ..... *9*
VP4 ..... *9*
VP5 ..... *9*
VP6 ..... *9*
VP7 ..... *10*
5.3 Non-structural Proteins **10**
NS1 ..... *10*
NS2 ..... *11*
NS3 ..... *11*
NS4 ..... *12*
5.4 The Orbivirus Replication Cycle **13**
Entry into host cells and uncoating of virus particles *13*
Transcription and replication *13*
Translation of viral transcripts *15*

Assembly of the virus particles *15*
Release of virus particles *17*
5.5 Cytopathicity **18**
5.6 Reassortment Capability of the Orbiviruses **19**
6 CONCLUDING REMARKS **20**
7 AIMS AND OBJECTIVES **20**

CHAPTER 2: MONITORING GENE EXPRESSION OF DIFFERENT AHSV STRAINS IN MAMMALIAN AND INSECT CELLS

1 INTRODUCTION **22**
2 MATERIALS AND METHODS **24**
2.1 Cells **24**
2.1.1 Mammalian cells *24*
2.1.2 Insect cells *24*
2.1.3 Light microscopy *24*
2.2 Viruses **24**
2.2.1 AHSV strains *24*
2.2.2 Virus titration *25*
2.3 Sample Preparation for Protein Analyses **25**
2.3.1 Sample preparation *25*
2.3.2 Sub-cellular fractionation *26*
2.4 RNA Isolation **26**
2.5 Reverse Transcription for First Strand cDNA Synthesis **27**
2.6 Conventional PCR **27**
2.6.1 PCR ampification *27*
2.6.2 PCR product purification *28*
2.7 Real-time qPCR **29**
2.8 Gel Electrophoresis **29**
2.8.1 Agarose gel electrophoresis *29*
2.8.2 RNA PAGE *29*
2.8.3 SDS-PAGE *30*
2.9 Sequencing **30**
2.10 Immunoblot Assays **30**
2.10.1 SDS-PAGE and Western blot analyses *30*
2.11 ^{35}S-Met Pulse Labelling **31**
2.12 Statistical Analyses **32**
3 RESULTS **33**
3.1 Virus Primary Transcription **33**
3.1.1 Optimising cycling conditions for PCR amplification of four viral genes *33*

VP7 gene *33*
NS1 gene *34*
NS2 gene *36*
NS3/NS3A gene *36*
3.1.2 Selection of suitable housekeeping genes for RT-qPCR analyses *40*
3.1.3 Monitoring the transcriptional stability of β_2MG and GAPDH in infected mammalian cells *43*

3.2 Host Cell Cytopathicity Monitored by Light Microscopy **46**

3.3 Analyses of Viral Protein Synthesis by Immunoblot Assays **48**
3.3.1 Optimisation of the antibody detection conditions for three AHSV proteins *48*
3.3.2 Detection of VP7, NS1 and NS2 protein levels by Western blot *51*
3.3.3 Protein levels expressed from the housekeeping gene, β-Actin, at different times *53*
β-Actin (MOI = 0.1 pfu/cell) *54*
β-Actin (MOI = 2 pfu/cell) *55*
3.3.4 Virus protein levels for VP7, NS1 and NS2 at different times *56*
3.3.5 Statistical analyses of VP7 and NS2 immunoblot data *63*

3.4 Analyses of Viral Protein Synthesis by Pulse Labelling **67**
3.4.1 Optimising virus infections and pulse labelling in mammalian cells *67*
3.4.2 Monitoring time-specific virus protein synthesis using ^{35}S-Methionine pulse labelling *68*
3.4.3 Statistical analyses of VP7, NS1 and NS2 pulse labelling data *72*

3.5 Analyses of Virus dsRNA Production in Infected Mammalian Cells **75**
3.5.1 Optimising total RNA isolation and virus dsRNA purification *75*
3.5.2 Monitoring virus dsRNA levels *76*
3.5.3 Statistical analyses of AHSV segment 3 dsRNA levels at 24 and 48 hours p.i. *77*

3.6 Analyses of Virus Yield through Titration **79**
3.6.1 Assaying virus yield from infected mammalian cells following an unsynchronised and synchronised infection *79*
3.6.2 Statistical Analyses of virus yield results at 24 and 48 hours p.i. *81*

3.7 Monitoring Virus Protein Synthesis, Virus dsRNA and Virus Yield in Infected Insect Cells **82**
3.7.1 Analyses of viral protein synthesis by immunoblot assays *83*
3.7.2 Analyses of viral dsRNA levels in infected insect cells *86*
3.7.3 Assaying virus yield from infected insect cells through titration *87*

4 DISCUSSION AND CONCLUDING REMARKS **89**

REFERENCES **98**

CHAPTER 1 : LITERATURE REVIEW

LITERATURE REVIEW

1 INTRODUCTION

Orbivirus, one of the largest virus genera within the *Reoviridae* family, is one of nine genera with a characteristic segmented double stranded RNA genome. The *Orbivirus* genus contains 19 serogroups, which were established and confirmed through various serological and molecular analyses (Belaganahalli *et al*., 2015; Calisher and Mertens, 1998). The focus of this study is on African horsesickness virus (AHSV) which can manifest in four clinically distinct forms in equid species. African horsesickness (AHS) can present itself with varying mortality rates, and to date no known correlation exist between specific serotypes and specific clinical forms. AHS disease pathogenesis is complex, and the results of an interaction of both viral and host factors. When using a tissue culture model system there are less variables, and one should theoretically be able to pinpoint viral genes or proteins that contribute to cellular cytopathogenesis with greater accuracy and ease.

In viruses with a segmented genome previous studies using genetic reassortants have assisted in revealing the functions of specific viral proteins. The investigation undertaken here was a direct follow up on the findings of Meiring *et al*. (2009) and Venter (2014). In their studies they compared properties of three parental (AHSV-2, AHSV-3, AHSV-4) and five reassortant (R3-$2_{3,5}$; R3-$2_{5,10}$; R4-2_{10}; R4-$2_{7,10}$; and R4-$2_{4,5,7,10}$) AHSV strains. They observed differences with respect to virus release, effects on membrane permeability, cytotoxicity and cell viability, timing and extent of CPE, and induction of apoptosis. Conclusion from their work included a role for NS3 in influencing virus release and yield, and a combined contribution of NS1 and NS3 to virus-induced CPE and cell death by a replication-dependent effect on apoptosis. It is however not yet known which aspects of the viral life cycle potentially underlie these observed differences.

For this study, different stage of the life cycle of eight AHSV strains was comparatively assessed to determine factors that contribute to the diverse cytopathogenic phenotypes observed for these strains *in vitro*. Systematic comparisons were performed on parental and reasortant AHSV strains of their gene expression in mammalian as well as insect cell culture systems. Ultimately the intention of the study was to observe different stages in the AHSV replication cycle by investigating and comparing transcription, translation, core packaging, and virus release of eight AHSV strains.

2 AFRICAN HORSESICKNESS VIRUS AETIOLOGY

Of the 19 serogroups, the prototype bluetongue virus (BTV) was the first orbivirus to be characterised (Verwoerd, 1969; Verwoerd *et al*., 1979), and has subsequently been studied in great detail (MacLachlan *et al.*, 2008; Mertens and Diprose, 2004; Mertens *et al*., 2004; Roy, 1996; Roy, 2008a; Savini *et al.*, 2008; Schwartz-Cornill *et al*., 2008; Wilson *et al.*, 2008). Other orbiviruses closely related to BTV, which are of economic importance, include AHSV and epizootic haemorrhagic disease virus (EHDV) of deer (Verwoerd *et al.*, 1979). Initial studies on BTV established the structure of the virus particles, subsequent research has shown a correlation in structure and function of AHSV virus particles to those of BTV (Gould and Hyatt, 1994; Manole *et al*., 2012; Roy *et al*., 1994b; Verwoerd and Huismans, 1969).

AHSV causes an infectious, non-contagious viral disease in equids and is transmitted by species of *Culicoides* midges (House, 1993; Mellor and Hamblin, 2004). AHSV is composed of a double layered icosahedral protein capsid (Bremer *et al.*, 1990; Oellermann *et al.*, 1970) of which the inner core particle consists of the structural viral proteins VP1, VP3, VP4, VP6 and VP7, and encapsidates a genome comprising 10 double stranded RNA (dsRNA) segments (Grubman and Lewis, 1992; Roy, 1996). The outer protein capsid consists of VP2 and VP5 of which VP2 carries the serotype-specific neutralizing antigen sites similar to the VP2 protein of BTV (Bremer *et al*., 1990). Each structural protein is encoded by one of the RNA segments and in addition to the structural proteins, five non-structural proteins NS1, NS2, NS3, NS3A and NS4 are expressed from the viral genome (Bremer *et al*., 1990; Grubman and Lewis, 1992; Uitenweerde *et al*., 1995; Van Staden *et al*., 1998; Zwart *et al*, 2015). Nine serotypes of AHSV are known at present, all endemic to sub-Saharan Africa (McIntosh, 1958, Howell, 1962).

AHS is a disease affecting mainly equids, and was first reported in Yemen in 1327 when an apparent epidemic occurred. The first time that AHS was recorded in Africa was in 1569 (Roy, 2001), some 60 years after the introduction of horses to the central and eastern parts of this continent (Mellor and Hamblin, 2004). The first reference to AHS in South Africa was by Theiler in 1921 after he confirmed the relationship of seven epizootics of the disease in the Cape Province that occurred between 1780 and 1918 (House, 1993; Mellor and Hamblin, 2004), although it is believed that AHSV outbreaks in this country occurred as early as 1719. From South Africa, introduction to other areas in southern Africa occurred gradually over time, resulting in the current broad geographical distribution of AHS (Roy, 2001).

3 GLOBAL IMPLICATIONS

3.1 The Current BTV status in Europe

The first outbreak of bluetongue in Northern Europe was documented in Belgium in 2006, from where it spread to Luxemburg, Germany and the north-east of France. BTV overwintered in 2006-2007, after which a re-emergence of the virus occurred and spread to Denmark, Switzerland, the Czech Republic and the UK. BTV is now a proven example of a virus that managed to become established in northern Europe, in countries previously considered BTV free (Thompson *et al*., 2012). This is believed to be the result of climate changes in these parts. However, the exportation of animals across this continent and wind-borne midges cannot be excluded as factors pressuring the European dispersal of BTV (Gould and Higgs, 2008; Maan *et al*., 2008; MacLachlan and Guthrie, 2010). Another concern is vector-independent transmission of BTV (Van der Sluijs *et al*., 2014). Cases of transplacental transmission were observed after vaccination with live strains. Before 2005, vaccination against BTV involved administration of modified live virus vaccines. However, after 2005 inactivated vaccines became available (Zientara and Sánchez-Vizcaíno, 2013).

3.2 Current Vaccines for AHSV

There are three existing types of vaccines for AHSV, i.e. live attenuated vaccines, inactivated vaccines and subunit vaccines. However, not all of these vaccines are commercially available or in use (Mellor and Hamblin, 2004). Currently live attenuated (modified-live virus) polyvalent vaccines are in use. In South Africa two polyvalent vaccines are available from Onderstepoort Biological

Products (Onderstepoort, South Africa), containing AHSV types 1, 3 and 4 (bottle 1) and AHSV types 2, 6, 7 and 8 (bottle 2) respectively. Due to severe side effects and fatalities in some vaccinated animals, AHSV-5 has been withdrawn from vaccines. Vaccines against type 8 provides adequate cross protection (Coetzer and Guthrie, 2004). Due to the high cross-reactivity between types 6 and 9, and the fact that AHSV-9 is infrequently isolated in South Africa, type 9 is also omitted from the vaccines. In West Africa a monovalent AHSV-9 vaccine was in use until fairly recently as this was the only serotype circulating in this region (Mellor and Hamblin, 2004). Even animals with no vaccination history test positive for AHSV-9 and it is speculated that this may be a live-attenuated vaccine-derived strain (Oura *et al*., 2012). The responses to monovalent vaccines do not show any significant difference from that of using a polyvalent vaccine and, therefore, the focus should rather be on developing next generation vaccines.

3.3 AHSV Vaccine Development

Later research aimed at finding alternative methods to develop effective vaccines. De la Poza and colleagues (2013) looked at the importance of NS1 when it is included in a recombinant modified vaccinia virus Ankara (rMVA) expressed along with VP2. When IFNAR$^{(-/-)}$ mice were inoculated with the rMVA-VP2,-NS1 from AHSV-4, significant levels of specific neutralising antibodies could be detected for AHSV-4. This was also the case when tested on horses. Furthermore, specific T-cell responses were evident against the virus. Partial protection was manifested against a homologous AHSV-4 (higher virulence) and cross-protection against heterologous AHSV-9 (lower virulence) (De la Grandière *et al*., 2014). Similar studies were performed in horses only using VP2 from AHSV-9. Vaccinated horses showed complete protection against the strain after inoculation with a virulent AHSV-9 (Alberca *et al*., 2014). The inclusion of NS1 showed promising results for novel multiserotype vaccines. The potential of using an rMVA expression model is also encouraging.

Reverse genetics systems have revolutionised advances in virology by permitting study of targeted genetic changes in virus genomes. The development of such technology has led to the understanding of several aspects of the biology and pathogenesis of many viruses. By using the cDNA available for the viral genomes, one can genetically manipulate and modify these genomes to produce live viruses enclosing specifically designed genetic material. Reverse genetics systems and recombinant virus design have become a focus of new efforts to design vaccines that integrates virus-based systems to induce lasting immunity in the host without adverse effects. Recent studies have made progress on the requirements for reverse genetics of both BTV and AHSV (Van Rijn *et al*., 2016). Fully plasmid-based reverse genetics systems have been developed for both BTV (Pretorius *et al.,* 2015) and AHSV (Conradie *et al*., 2016) where viable virus was recovered using cDNA plasmids. Considering that orbiviruses have similar virion structures as well as replication mechanisms, this technique can be applied for other *Orbivirus* members. As a result, the creation of such plasmid-based reverse genetics systems will save resources and increase our understanding of *Orbivirus* replication and virus protein function, transmission and hots-virus-vector interactions, and pathogenesis (Conradie *et al*., 2016; Pretorius *et al.,* 2015; Van Rijn *et al*., 2016).

The ability to manipulate the genome of AHSV to create specific mutants will add to our understanding of AHSV infectivity, replication, pathogenicity, and transmission (Vermaak *et al*., 2015). A major drawback in past studies was the inability to manipulate the segmented genome of AHSV. Another possibility in vaccine development for ASHV will be to target the *Culicoides* midges and this will be probable once we establish a gene profile for these vectors. Unlike other important vectors, including mosquitoes, there appears to be an absence of genetic and genomic tools for

midges (Nayduch *et al*., 2014). Once we can understand the interactions between virus and vector on a molecular level, we may be able to find an effective method to control AHSV. Then we might be able to use methods involving reverse genetics to develop novel recombinant vaccines against AHSV.

Of the seven structural proteins of AHSV (VP1-VP7), VP2 is the serotype specific protein. This serves as a target for neutralising antibodies. Kanai *et al*. (2014) developed a recombinant baculovirus expressing VP2 for every one of the nine serotypes in a baculovirus expression system. The results suggested a dose-dependent response because of the lower serotype-specific antibody titres after immunisation with a cocktail containing all the VP2 proteins. However, the application of a multiserotype subunit vaccine seem to be feasible.

4 EPIDEMIOLOGY OF THE AHSV

4.1 AHS Pathogenesis

Endemic to sub-Saharan Africa, especially in tropical and sub-tropical regions, the disease AHS appears to be seasonal and outbreaks occur annually in susceptible horses (House, 1993). Pathogenesis of the disease consists of two stages, a primary and a secondary viraemia. Primary viraemia involves the initial multiplication of AHSV in regional lymph nodes followed by the distribution of the virus to different target organs via the blood. This leads to the onset of secondary viraemia (Mellor and Hamblin, 2004; Verwoerd and Erasmus, 2004). Four clinically distinguishable forms of the disease are present with mortality as high as 90% in most cases. These forms or syndromes are recognised as the pulmonary/ peracute form, the cardiac/ subacute form, the mixed/ acute form, and the fever form. Clinical signs consistent with all four forms of the disease include fever and congestion of the ocular, nasal and mucosal membranes. Depression precedes death in most cases (House, 1993).

AHS mostly occurs in susceptible horses, mules, donkeys and zebras. Zebras have been shown to have a natural resistance to AHSV (Barnard, 1993), and even though donkeys show some resistance to the disease, research suggests that donkeys are not considered as long term reservoirs of AHSV (Hamblin *et al*., 1998). It has been observed that domestic dogs as well as various other of African carnivores may be infected through the consumption of infected horse meat (Alexander *et al*., 1995).

4.2 Vector Species and Transmission of AHS

The Afro-Asiatic midge *Culicoides imicola* has been indicated as the most prominent vector species of AHSV (Bakhoum *et al*., 2013; House, 1993). These midges prefer a warm climate and thus the prevalence of disease appears to be temperature dependent (Mellor *et al*., 1998). Adult *C. imicola* can be seen during spring to summer when temperatures are favourable for breeding. Although a drop in temperature may result in the virus halting replication, replication will resume once the climate becomes favourable again. This observation has led to the suggestion that the virus can overwinter in its insect vector (Mellor *et al*., 1998). Recent studies indicated that another species of midge (*C. bolitinos*) serves as a vector of AHSV. These midges occur in cooler regions of South Africa, where *C. imicola* are mostly absent (Venter *et al*., 2000). Other *Culicoides* species associated with AHSV

transmission include *C. pulicaris*, *C. obsoletus*, *C. cataneii*, and *C. lailae* present mostly in Northern Europe and the United Kingdom (Diarra *et al*., 2014; House, 1993).

Little is known about the virogenesis of AHSV in the *Culicoides* species (Paweska *et al*., 2003). After inoculating field-collected midges of the *C. bolitinos* and *C. imicola* species with vaccine strains of AHSV, it was clear that the midges were susceptibility to oral infection. However, the replication tested below threshold levels for most of the virus strains tested. Further assessment is required to determine the potential transmission of vaccine strains by *Culicoides* species.

Although midges from *Culicoides* species have been implicated as the major biological vectors of AHS, experimental infections with *Aedes* spp. mosquitoes have been observed. The virus has also been isolated from a camel tick (*Hyalomma dromedarii*) and from a tick associated with dogs (*Rhiphicephalus sanguineus*) (House, 1993).

Global changes, especially climate change, may have an influence on the spread of diseases. Impact on the environment is likely to influence the evolution of pathogens, leading to increased risk in disease control (Scheffer *et al*., 2012). The populations of the vectors may also be influenced by the change in conditions and may lead to spread of the vectors to regions previously uninhabited (Guichard *et al*., 2014). French researchers developed a model to assist in prioritising animal health risk (Dufour *et al*., 2008). Resulting from their model, six diseases were identified as priority and included bluetongue, Rift Valley fever, West Nile fever, visceral leishmaniasis, leptospirosis and African horsesickness. As a result recommendations were made to assess and manage risks regarding these diseases. These recommendations included development of epidemiological surveillance, increase knowledge of epidemiological cycles, inspire research into these diseases, and involve cross-border efforts to control the diseases. Therefore, biosecurity risks of both AHSV and BTV need to be reconsidered.

5 MOLECULAR BIOLOGY OF ORBIVIRUSES

5.1 Viral Genome

The first orbivirus genome to be fully characterised was that of BTV. The BTV genome consists of ten linear double stranded RNA (dsRNA) segments, each encoding at least one functional polypeptide, and in total comprising approximately 19 200 bases. AU nucleotides constitute 57% and GC 43% of the genome. The 5’ and 3’ terminal hexanucleotide ends of the positive RNA strand are conserved with the 5’ terminal sequences being GUUAAA and the 3’ terminal sequences ACUUAC (Grimes *et al*., 1998; Mertens and Sangar, 1985). Furthermore, once transcribed from the dsRNA genome, each of the 10 mRNA segments has partial inverted complementarity at the 5’ and 3’ terminal sequences. This enables the mRNA to form complex secondary structures such as end-to-end (panhandle) structures and stem-loop configurations. These secondary structures are proposed to aid in mRNA stability and protect against degradation from endonucleases and exonucleases. Recognition by the viral polymerases is another function of these secondary structures, as well as for association and packaging of the RNA segments. Sung and Roy (2014) suggested that the smallest of the segments, Seg-10, serves as the instigator which triggers RNA-RNA interaction with other smaller segments. After this complex network is formed, the medium and larger size single stranded RNAs (ssRNA) join this network until the whole genome is packaged into the capsid. Demonstrated initially in BTV, similar mRNA secondary structures can be found in AHSV

and EHDV too (Roy, 2001). Specific interaction of the participating RNA segments showed that the base pairing, rather than the absolute sequence, was important for the formation of the functional inter-segment complex (Boyce *et al*., 2016). The variation in absolute sequence of complimentary motifs between different *Orbivirus* species may explain why there is no natural reassortment between orbivirus species.

Similar to the BTV genome, the AHSV genome contains ten double stranded RNA segments with an average base composition of 57% AU and 43% GC. The segments are grouped based on size when performing agarose gel electrophoresis. The segments are designated as large (Seg-1 to Seg-3), medium (Seg-4 to Seg-6) or small (Seg-7 to Seg-10).

Table 1 gives a summary of the AHSV RNA segments and their encoded proteins. Unlike BTV RNA segments, the 5' and 3' terminal sequences of AHSV are not conserved amongst all nine serotypes. Generally the 5' terminal sequence is 5' GUUA...3' and the 3' terminal sequence is 5'...ACUAC 3' (Roy *et al*., 1994b; Roy, 2001). The 5' non-coding region size ranges between 12-35 base pairs whereas the 3' non-coding region size ranges between 29-100 base pairs (Bremer, 1976; Bremer *et al*., 1990; Grubman and Lewis, 1992; Roy *et al*., 1994b).

Table 1: Summary of the AHSV genome segments arrangement, the proteins they encode, molecular mass and size, and the location of each protein

RNA Segment	Size (bp)	Protein	Molecular Mass (kDa)	Location
Seg-1	3954	VP1	149	Core
Seg-2	2926	VP2	111	Outer Capsid
Seg-3	2770	VP3	103	Core
Seg-4	1981	VP4	76	Core
Seg-5	1769	NS1	59	Outer Capsid
Seg-6	1638	VP5	64	Infected Cell
Seg-7	1156	VP7	38	Core
Seg-8	1124	NS2	40	Infected Cell
Seg-9	1046	VP6 NS4	35 23	Core Infected cell
Seg-10	822	NS3/NS3A	25/24	Infected Cell

Adapted from (Belhouchet *et al*., 2011; Bremer, 1976; Bremer *et al*., 1990; Firth, 2008; Grubman and Lewis, 1992; Roy *et al*., 1994b)

5.2 Structural Proteins

Although great morphological similarity exist between AHSV and BTV (Bremer, 1976; Huismans and Els, 1979; Oellermann *et al*., 1970), protein structures and functions were deduced initially from studies done on BTV (Martinez-Torrecuadrada *et al*., 1994; Verwoerd and Erasmus, 2004). The BTV viral proteins range in sizes between 25 and 149 kDa and early studies by Bremer (1976) affirmed that the AHSV proteins are similar in size. In both BTV and AHSV the triple-layered capsid is made up of three minor proteins (VP1, VP4 and VP6), that constitute 6% of the total protein, and two major proteins (VP3 and VP7). Collectively the three minor core proteins synthesise the virus mRNA (Roy, 2008a,b). The outer capsid of BTV and AHSV is composed of two major proteins VP2 and VP5. Together the four major proteins constitute 94% of the total protein. Each protein is encoded by one of the RNA segments (Grubman and Lewis, 1992).

VP1

VP1, encoded by segment 1 in BTV and AHSV (Grubman and Lewis, 1992; Roy, 1996; Vreede and Huismans, 1998), is the largest of the minor proteins and is designated the putative RNA-dependent viral RNA polymerase (Roy, 2008b). The polymerase domain for BTV VP1 has been identified between amino acids 582-882 and its enzymatic efficiency is stabilised through the N- and C-terminals (Roy 2008a). VP1 interaction with other viral proteins has suggested its specificity for viral mRNA, RNA replicase activity and synthesis of all RNA strands using ssRNA as templates (Boyce *et al*., 2004; Roy 2008a; Urakawa *et al*., 1989). Studies have shown that this protein interacts with the major core protein VP3 and efficiently binds nucleotide triphosphates (Roy *et al*., 1996). VP1 is highly conserved amongst the nine different AHSV serotypes as was demonstrated with hybridisation studies (Bremer *et al*., 1990).

VP2

VP2 is encoded by segment 2 (Grubman and Lewis, 1992) and is a major protein of the outer capsid (Mertens *et al*., 1984). This spike-like protein is the cellular receptor binding protein of the virus, determine the specific virus serotype (Huismans and Erasmus, 1981; Huismans *et al*., 1985; Huismans *et al*., 1987a), and is responsible for eliciting a virus-neutralising antibody response (Burrage *et al*., 1993; Martinez-Torrecuadrada *et al*., 1994; Vreede and Huismans, 1994). Studies have shown that the major antigenic domain of VP2 is in the central region, from amino acids 200 to 413 (Martinez-Torrecuadrada and Casal, 1995). The protein is hydrophilic in nature that forms trimers, stabilised by disulphide bonds, in the cytoplasm and consist of of many charged residues (Hassan and Roy 1999; Hewat *et al*., 1992). The VP2 protein is highly variable among the nine different AHSV serotypes homology between the serotypes varying between 47.6% and 71.4% (Bremer *et al*., 1990; Manole *et al*., 2012; Potgieter *et al*., 2003). In a recent study by Van de Water and colleagues (2015) exchange of AHSV VP2 was studied between nine different reverse genetics generated strains (AHSV1LP-AHSV9LP), differing only in the serotype determining VP2 encoding Seg-2. Single Seg-2 exchange between all nine strains appeared more flexible than between BTV strains. Their findings indicated that CPE for all nine reverse genetics strains were similar although serotypes 1-3 and 7 indicated lower titres compared to AHSV4LP. Van de Water *et al*. (2015), concluded that exchange of AHSV Seg-2 could affect virus growth kinetics irrespective of which serotype specific VP2 was translated.

VP3

VP3, encoded by segment 3, acts as scaffolding proteins on which VP7 proteins assemble to form the core like particles (Roy, 1996) which determine the internal organization of the viral genome (reviewed in Mertens *et al*., 2004). During assembly of the core, VP3 interacts with the three minor proteins VP1, VP4 and VP6 and binds to viral RNA (Roy, 2008b). Research has established the conserved nature of this highly basic protein specifically amongst different BTV strains (Maree *et al*., 1998; Purdy *et al*., 1984; Roy, 1996; Williams *et al*., 1998).

VP4

VP4 is encoded by segment 4 and is the second largest of the minor core proteins (Roy, 2008a). Encapsidation and functioning of the VP4 is dependent on dimerization of the protein by means of a conserved C-terminal leucine-zipper motif (Ramadevi *et al*., 1998; Roy 1996). This protein has different enzymatic activities all catalysing 5' cap formation of the viral mRNA. These enzyme functions are RNA 5'-triphosphatase, guanylyltransferase, and a methyltransferase type 1 and 2 activity (Grubman and Lewis, 1992; Martinez-Costas *et al*., 1998; Ramadevi and Roy, 1998; Ramadevi *et al*., 1998). RNA 5'-triphosphatase functions in creating 5' diphosphate ends on mRNA transcripts. The 5' termini is GMP capped using triphosphate bonds, assisted by VP4 guanylyltransferase activity. The 5' cap and second 5' nucleotide of mRNA is methylated by the guanine-7-methyltransferase and 2'-O-methyltransferase respectively. This is achieved by using S-adenosyl-L-mehionine as a substrate. The inhibitory effect of the by-products from these enzymatic activities are prevented by the VP4 pyrophosphatase function.

VP5

VP5 is encoded by segment 6 and forms part of the orbivirus outer capsid (Grubman and Lewis, 1992; Verwoerd *et al*., 1972) and, similar to VP2, possesses antigenic specificity although it is not involved in virus neutralisation (Roy *et al*., 1994b). VP5 shows similar secondary structures to that of the fusion proteins of certain enveloped viruses. It was suggested that VP5 is a membrane binding protein and pH-dependant conformational changes may allow membrane fusion and syncytium formation. BTV VP5 plays a role in viral release from endosomal compartments into the cytoplasm due to its function as a membrane penetration protein (Forzan *et al*., 2004; Hassan *et al*., 2001). Furthermore, VP5 copurifies with lipid raft domains, demonstrating its role in membrane targeting. This postulate was supported by the observation of a conserved membrane docking domain on VP5, similar to the Syt1 protein of the soluble N-ethylmaleimide-sensitive fusion attachment protein receptor family (Bhattacharya and Roy, 2008).

VP6

VP6, encoded by segment 9 (Grubman and Lewis, 1992), is a helicase protein that demonstrates a high affinity for both single and double stranded RNA molecules (De Waal and Huismans, 2005; Roy *et al*., 1990;) and may function to unwind the double stranded RNA genome prior to complementary strand RNA synthesis (Anthony *et al*., 2011; Roy *et al*., 1994b). Furthermore, VP6 has ATPase activity, and thus in the presence of ATP and magnesium ions, can bind to both blunt ended double

stranded RNA or RNA with a short 5' or 3' overhang (Stauber *et al*., 1997). This protein also interacts with the VP3 protein during core-like particle (CLP) assembly (Mertens *et al*., 2004).

VP7

VP7 is encoded by segment 7 (Grubman and Lewis, 1992), and shows a high degree of conservation among different AHSV serotypes. Characteristically rich in hydrophobic amino acids, VP7 constitutes one of the major components of the inner core particle (Roy *et al*., 1994b). It was found that the VP7 forms crystalline-like particles in infected insect cells that do not form part of the core structure (Bekker *et al*., 2014). Mutation studies confirmed that the relationship between VP7 and VP3 is due to conserved cysteines in VP7, each at positions 15 and 65 of the protein, and a conserved lycine at position 255 (Le Blois and Roy, 1993). Suggested to be the group specific antigen, VP7 fails to elicit a neutralizing antibody response, and this was supported by ELISA testing and Western blot studies (Martinez-Torrecuadrada *et al*., 1996; Oldfield *et al*., 1990).

5.3 Non-structural Proteins

NS1

NS1 is encoded by segment 5 of the genome and is highly conserved among the different BTV serotypes, which can be detected in perinuclear locations and in more abundant quantities than any other BTV proteins (Huismans and Els, 1979; Roy *et al*., 1994a). This non-structural protein is 5.5 nm in diameter and generally arranged as dimer-like structures. The NS1 protein was observed to form tubular structures in insect cells expressed by recombinant baculoviruses, similar to the tubular structures present during viral replication in infected cells (Maree and Huismans, 1997; Van Staden *et al*., 1998). Tubular structures were analysed through cryoelectron microscopy and found to be about 52.3 nm in diameter and 1000 nm in length configuring to a helical structure. Containing about 21 or 22 NS1 dimers per turn, the tubules exist in two pH-dependent conformational state (Hewat *et al*., 1992). Studies confirmed that tubule formation in BTV was due to the two conserved cysteine residues at position 337 and 340 as well as the N- and C-termini (Monastyrskaya *et al*., 1994). It is believed that these proteins play a role in transport of the mature virus particles to the cell plasma membrane, although conclusive evidence on the function of NS1 has not yet been obtained (Owens *et al*., 2004). Studies on AHSV NS1 protein by Maree and Huismans (1997) found that these proteins, like BTV NS1, assemble into tubular structures. However, AHSV NS1 tubules are morphologically different to that of BTV NS1 and are distinguished by the absence of a ladder-like structure and a lower sedimentation value. Furthermore, the structure of AHSV NS1 was investigated by *in vitro* studies with NS1 expressed in recombinant baculoviruses in insect cells, and was confirmed to be approximately 23 nm in diameter and up to 4 µm in length (Maree and Huismans, 1997).

It was believed that NS1 play a role in transport of the mature virus particles to the cell plasma membrane, although more recently the function of NS1 was linked to regulation of viral protein synthesis (Boyce *et al*., 2012; Owens *et al*., 2004). It was shown that NS1 specifically up-regulates the translation of viral mRNAs. This can be ascribed to their unique 5' and 3' UTRs and the absence of a poly-A tail. The consequence of the up-regulation of the translation allows the virus to take over the cell's translational mechanisms and preventing the cell to produce its own proteins (Boyce *et al*.,

2012). NS1 associates with centrosomes and through this interaction NS1 may impede the cell cycle. This then leads to the inhibition of DNA and RNA synthesis and, ultimately, cell death (Shaw *et al*., 2013). NS1 is also speculated to be involved with virus egress as mammalian cells lacking NS1 expression showed no sign of lytic virus release or pathogenesis (Owens *et al*., 2004).

NS2

NS2, encoded by segment 8, is the major component of the virus inclusion body matrix visible in the cytoplasm of infected cells (Roy *et al*., 1994b; Thomas *et al*., 1990). Shown to be highly conserved amongst the different serotypes, NS2 seems to be the only phosphorylated viral protein and is able to bind to single stranded viral RNA (Huismans *et al*., 1987b; Uitenweerde *et al*., 1995). Binding of RNA is a result of positively charged amino acid residues at the N-teminus (Roy *et al*., 1994b). In a study by Kar and colleagues (2007), it was confirmed that a full-length BTV NS2 was sufficient and essential for inclusion body (IB) formation in mammalian cell lines. This resembles VIBs that formed during infections with infectious virus particles. Furthermore, it was established that VP3 associates with the IBs, similarly to their association with NS2 during VIB formation, but that VP7 could only co-localise with NS2 IBs if VP3 was present. Additionally, they confirmed that neither the amino- nor carboxy-terminal truncated NS2 fragments could construct complete IBs and subsequently interfered to a large extent in overall virus syntheses (Kar *et al*., 2007). In 2006 Lymperopoulos and colleagues established that BTV NS2 interacts specifically with a secondary stem-loop conformation present in segment 10 (Seg-10) RNA. RNA regions in three additional segments were mapped which also showed preferential interaction with NS2 of BTV, although no specific stem-loop motif could be observed. Subsequently it was proposed that these interactions between secondary RNA configurations and the NS2 protein could be the basis for discrimination between the different RNA segments during virus assembly (Lymperopoulos *et al*., 2006).

Furthermore, it was established that VP3 associates with the IBs, similarly to their association with NS2 during VIB formation, but that VP7 could only co-localise with NS2 IBs if VP3 was present. Additionally, they confirmed that neither the amino- nor carboxy-terminal truncated NS2 fragments could construct complete IBs and subsequently interfered to a large extent in overall virus syntheses (Kar *et al*., 2007). In 2006 Lymperopoulos and colleagues established that BTV NS2 interacts specifically with a secondary stem-loop conformation present in segment 10 (Seg-10) RNA. RNA regions in three additional segments were mapped which also showed preferential interaction with NS2 of BTV, although no specific stem-loop motif could be observed. Subsequently it was proposed that these interactions between secondary RNA configurations and the NS2 protein could be the basis for discrimination between the different RNA segments during virus assembly (Lymperopoulos *et al*., 2006).

NS3

NS3 and NS3A are both encoded by segment 10, the shortest of the 10 RNA genome segments (Van Staden *et al*., 1995), differing only with respect to the 10 additional amino acids at the N-terminal of NS3. Furthermore, in comparison to the high expression levels of BTV NS3 in a baculovirus system (French *et al*., 1989), AHSV was detected in much lower levels and was only detected with immunoblot or radiolabeling (Van Staden and Huismans, 1991). Comparison of the NS3 gene sequence between different serotypes of AHSV showed a relatively low degree of homology between these strains (Van Niekerk *et al*., 2001b). The direct consequence of genome segment

reassortment between different AHSV serotypes results in high variability within segment 10 which makes it an unreliable indication of the virus serotype (Martin *et al*., 1998). However, some highly conserved features of the AHSV NS3 have been determined, including three features of the N-terminal region. These include the presence of a second in-phase methionine for NS3A translation initiation; at least five proline residues clustered together between amino acids 22 and 34; and a highly conserved region of amino acids from residues 46 to 90, showing a 78% identity and 96% similarity (Van Staden *et al*., 1995). Previous investigations confirmed two hydrophobic regions in the NS3 protein common to BTV, AHSV and other orbiviruses. For AHSV these two regions were mapped at residues 116-137 and 154-170 respectively, and suggested to form transmembrane helices (van Niekerk *et al*., 2001a). Bansal and colleagues (1998) illustrated that both of these domains of BTV NS3 span the membrane. It was also suggested that the glycosylated nature of this protein protected it from degradation (Bansal *et al*., 1998, Wu *et al*., 1992,). In contrast to the BTV NS3 protein, AHSV NS3 of certain serotypes was found to have no glycosylation sequence motifs (Van Niekerk *et al*., 2001a).

Immunogold electron-microscopic analysis illustrated that NS3 was present in perturbed regions of infected Vero cell plasma membranes (Stoltz *et al*., 1996) thus suggesting that it might be related to release of viral particles (Meiring *et al*., 2009). The cytotoxic effect of AHSV NS3 protein on *Spodoptera frugiperda* (Sf9) insect cells was recognized after expressing the recombinant NS3 protein in a baculovirus system. The cytotoxic effect resulted in only 5% of the Sf9 cell population having viability at 48 hours post-infection (p.i.) (Van Staden *et al*., 1995). Another study has shown that changes in the hydrophobic regions of this protein may lead to a loss in cytotoxicity due to loss of membrane targeting. Therefore, NS3 could play a role in viral pathogenesis due to the modification of membrane permeability (Van Niekerk *et al*., 2001b). In addition, the ability of AHSV NS3 protein to influence the pathogenicity and virulence of AHSV was researched in a genomic reassortment study between virulent and avirulent strains. Through use of a murine model, it was confirmed that the exchange of the NS3 gene (segment 10), had a declining effect in the progeny virus' virulence (O'Hara *et al*., 1998), altering the time of release of the virus particle (Martin *et al*., 1998).

NS4

Segment 9 contains an open reading frame (ORF) that almost spans the entire length of this segment that codes for VP6, however, another overlapping ORF was discovered. The product of this overlapping ORF is described as another non-structural protein labelled as NS4 (Belhouchet *et al*., 2011). The small size and low molecular weight of NS4 might be the reason why it took so long before it was discovered. In addition, its low expression levels as well as its irregular expression may have added to the late encounter. Analysis of Seg-9 revealed the existence of two types of AHSV NS4 each of different length and consisting of different amino acid sequences (Zwart *et al*., 2015). These two main types are referred to as NS4-I and NS4-II. NS4 can be located throughout the cytoplasm and nucleus, and is associated with nucleic acid as it shows nucleic acid-binding properties. It was also noted that bacterially expressed recombinant NS4 of both types bind to double stranded DNA (dsDNA) but not dsRNA. The early detection of NS4 in the cytoplasm suggests that it plays a role in virus replication. On the other hand, late detection of NS4 in the plasma membrane indicate potential involvement with virus release.

5.4 The Orbivirus Replication Cycle

Entry into host cells and uncoating of virus particles

Virus entry into susceptible host cells can be ascribed to the two outer capsid proteins of the orbiviruses, VP2 and VP5. VP2 forms the spike-like projections of the outer capsid that are highly variable amongst the different orbiviruses. From preliminary data obtained in a study by Hassan and Roy (1999), the receptors were thought to be glycoproteins. BTV infection was believed to be assisted either by the glycoprotein moiety itself or by a second protein that serves as a co-receptor (Hassan and Roy, 1999). Once VP2 is bound to the host cell receptors, rapid internalisation follow through a clathrin-mediated endocytic pathway. Within the endocytic vesicle, a decreased pH results in the uncoating of the virus, followed by release of the core particle into the cytoplasm. In the case of AHSV-4, uptake into BSR cells was shown to utilize macropinocytosis as the primary entry pathway (Vermaak *et al.,* 2016). The study suggested that entry into BSR cells are dynamin dependent. Vermaak and colleagues (2016) also indicated inhibition of Na^+ / H^+ exchangers, actin polymerisation and cellular GTPases and kinases inhibited AHSV-4 infection. This was evident when binding of AHSV-4 to BSR cells stimulated uptake of micropinocytosis-specific cargo.

The globular VP5 of the outer capsid are associated with membrane fusion during virus entry. Although this protein is generally arranged as trimers in the outer capsid, the monomeric molecule has a characteristic coiled-coil amino domain and globular carboxyl domain linked by a flexible hinge region. Furthermore, the N-terminus of VP5 holds the potential to form two amphipathic helices that result in membrane destabilisation (Hassan *et al*., 2001). Membrane fusion is due to a membrane inserting, hydrophobic region at the N-terminus that is followed by a long heptad repeat region. Membrane fusion with VP5, however, is preceded by a low pH trigger activation step, resulting in an environment similar to that of endosomal cell entry. Subsequently, the low pH causes VP5 to undergo conformational changes, resulting in the fusion competence of this protein however, no proteolytic step is necessary to render the protein functional (Forzan *et al*., 2004). BTV VP5 was found to have the ability to form membrane pores, supporting the fact that VP5 has a cytotoxic effect on susceptible host cells (Hassan *et al*., 2001). Ultimately, the uncoated core particle is released from the endosome into the cytoplasm of the host cell, resulting in subsequent activation of the core particle's transcriptase function (as reviewed in Roy, 2005). *In* vitro studies on BTV showed that uncoating of virus particles occur within one hour after infection and that a second uncoating event, resulting in subcore particles, occur within six hours after initial infection. Subcore particles were demonstrated to be transcriptionally inactive in *in vitro* systems (Huismans *et al*., 1987c).

Transcription and replication

Once the core particle is uncoated, the core is changed to biochemically active. It becomes a nano-scale transcription machine containing the virus genome packaged as a liquid crystal array (Diprose *et al*., 2001; Mertens and Diprose, 2004). Multiplication and transcription of the ten double stranded RNA segments take place simultaneously and repeatedly, although not in equimolar amounts, within the virus core at the transcriptional active site. Orbiviruses follow an overall similar strategy to that of reoviruses and rotaviruses. Negative sense RNA strands enter the polymerase active site after being separated by the virus helicase enzyme (VP6) and positive sense mRNA molecules are transcribed in the presence of Mg^{2+} ions. Following transcription with the virus RNA-dependent RNA polymerase (RdRp) enzyme (VP1), resulting parent-daughter duplexes are capped with the virus

mRNA capping enzyme (VP4) and separated. Subsequent release of progeny RNA molecules occur through pores at the five-fold axis as a result of Mg^{2+} ions creating an expansion site, extruding 5'-capped RNA molecules into the host cytoplasm (Diprose *et al*., 2001; Mertens and Diprose, 2004).

VP6 (35.7 kDa), the smallest of the minor proteins of the inner core particle, was demonstrated with *in vitro* studies to have helicase activity (Stauber *et al*., 1997). This enzyme was observed to have high binding affinity for double stranded (ds) RNA molecules that are blunt-ended or staggered with 5' or 3' overhangs, functioning to unwind the duplex molecule preceding transcription. Furthermore, high affinity was observed for ssRNA molecules of both polarities. VP6 was found to have a similar hexameric morphology that is shared by other helicase enzymes, and can form stable ring-like structures in the presence of nucleic acid molecules. Studies by Kar and Roy (2003) confirmed that VP6 has multiple oligomeric forms. Furthermore, site-directed mutagenesis studies confirmed that the VP6 protein has ATP binding, ATP hydrolysis and RNA unwinding abilities (Kar and Roy, 2003; Kar *et al*., 2005). They further demonstrated that ATP binding is due to a single lysine within a functional motif, an ATPase domain (AxxGxGK(110)V) (Kar and Roy, 2003; Mertens and Diprose, 2004; Mertens *et al*., 2004; Roy, 2005; Roy, 2008b; Stauber *et al*., 1997). Hydrolysis of ATP into ADP and inorganic phosphate (P_i), due to the ATPase activity of VP6, provide the necessary energy to separate the two parental RNA strands for transcription to commence (reviewed in Mertens and Diprose, 2004).

In 1989 Urakawa and colleagues demonstrated through a poly(A) polymerase assay system that VP1 of BTV functions as an RNA-dependent RNA polymerase. In 2004 Boyce and colleagues confirmed with purified VP1, that this protein has a processive replicase activity in the absence of any other viral protein (Boyce *et al*., 2004, Urakawa *et al*., 1989). VP1 (149.5 kDa) is the independent virus RNA-dependent RNA polymerase that is able to initiate *de novo* BTV minus strand synthesis and is responsible for transcription and synthesis of mRNA molecules. Studies on the VP1 of BTV showed that the protein comprise of three distinguishable domains - the N-terminal domain (NTD), the C-terminal domain (CTD) and the polymerase domain (PD). Furthermore, this central PD was observed to have similar morphology to that of other RNA-dependant RNA polymerases, containing multiple conserved sequence motifs (motifs A-D). It also has a canonical thumb, palm and finger folds organisation (Wehrfritz *et al*., 2007).

Further investigation confirmed that a catalytic GDD motif (motif C) was present in the central part of the PD. However, a fragment containing the PD only, showed catalytic activity only when it was associated with the NTD and the CTD but not when isolated, although its nucleotide binding ability was not lost. As reviewed by Roy (2008a), it seemed that the VP1 fragments only showed polymerase activity when all three fragments of VP1 were reconstituted.

Once progeny positive strand mRNA molecules have been transcribed, these molecules are released into the host cells cytoplasm. However, foreign mRNA can easily be detected by the host cell's protective immune response unless the molecules are protected by 5' capping, such as observed in the orbiviruses. VP4 (76.4 kDa) is an enzyme with RNA 5'-triphosphatase (RTase) activity, guanylyltransferase (GTase) and methyltransferase (Type 1, N7MTase and Type 2, 2'OMTase) functions (Martinez-Costas *et al*., 1998; Ramadevi and Roy, 1998; Ramadevi *et al*., 1998). The configuration of VP4 is elongated forming discrete domains. Capping of the 5' end of an mRNA molecule occur in a series of reactions (as reviewed by Mertens and Diprose, 2004). Firstly, the gamma phosphate on the 5' G, of positive sense RNA, is removed by the nucleotide phosphohydrolase activity of VP4. Inorganic phosphate (P_i) is released as byproduct. Secondly, the GDP or GTP is added as GMP to the 5' end, releasing P_i or PP_i. Consequently a GpppG 5'-5'

linked structure is the result at the 5' end. Finally, *S*-adenosyl methionine (AdoMet) is exploited by the methyltransferase activity of VP4, and two methyl groups are added onto the 5'-cap structure, one on position N7 of the terminal 5' guanosine and one on the 2'-OH of the penultimate guanosine. *S*-adenosyl homocysteine (AdoHCy) is finally released as by-product (Furuichi *et al*., 1975; Furuichi *et al*., 1976; Mertens and Diprose, 2004; Sutton *et al*., 2007).

Translation of viral transcripts

After positive sense mRNA strands are synthesised and released into the host cytoplasm, rapid inhibition of the host's cellular macromolecular synthesis is observed. Throughout the infection cycle, virus proteins are expressed and the first virus proteins can be detected from as early as two to four hours post-infection. A rapid increase in the rate of translation persists until around 11-13 hours post-infection. Translated proteins continue to accumulate throughout the infection cycle until assembly of new virus particles and cell lysis (Huismans and Van Dijk, 1990). In the case of reoviruses, infected host cell's mRNA competes with the viral mRNA for transcription. From their kinetic analysis study, Ray and colleagues (1983) proposed that a discriminatory initiation factor must bind to the mRNA before interaction with the 40S ribosomal subunit occurs. This is believed to be the competitive message between the different mRNA species (Ray *et al*., 1983). In the case of rotavirus translation, only 5'-capped viral mRNA is translated. Interaction between the host cell's translation initiation factor (eIF4G) and viral non-structural protein (NSP3, bound to the mRNA 3'-consensus end) initiate translation (Vende *et al*., 2000). Thus a cytotoxic effect results due to a competitive interaction between the host cell and virus structures (complete review by Roy in Fields Virology, 2001).

Assembly of the virus particles

The site for early virus particle assembly is the large granular matrices dubbed VIBs. These VIBs are formed in the cytoplasm of infected host cells (Mertens *et al*., 2004) from as early as four hours post-infection (Brookes *et al*., 1993). The non-structural viral protein NS2 is responsible for the formation of the VIBs, therefore explain the abundance of NS2. As the virus infection progresses, the amount of NS2 protein increases, resulting in the increased association of this protein with other viral proteins and ssRNA. The functional domain implicated in VIB formation is situated at the protein's C-terminal end (Kar *et al*., 2007). Studies by Thomas and colleagues (1990) and later by Modrof and colleagues (2005) indicated that only phosphorylated NS2 proteins were able to form the cellular aggregates that resulted in VIBs. Their studies have indicated that NS2 is phosphorylated post-translationally by a cellular protein kinase and that the phosphorylation sites are two serine residues at positions 249 and 259 respectively. The phosphorylated NS2 exhibited strong ssRNA binding activity (Modrof *et al*., 2005; Thomas *et al*., 1990). Direct interaction of the minor core proteins (VP1, VP4 and VP6) and the major core protein VP3 with NS2 is constantly observed particularly in the absence of other viral protein associations. However, direct interaction of NS2 with the major core protein VP7 is only observed when it is co-localised with VP3. Although phosphorylation of NS2 is necessary for VIB formation, it is possible for NS2 to assemble as small multimers that could attach to other viral proteins without being phosphorylated. It was concluded that neither phosphorylation of NS2 nor the formation of VIBs were essential for the recruitment of the core proteins (Huismans *et al*., 1987c; Kar *et al*., 2007; Modrof *et al*., 2005; Roy, 2008b; Thomas *et al*., 1990).

One of the phenomena concerning the BTV replication cycle is the mechanism of ssRNA recruitment and selection instigated by Seg-10 (Sung and Roy, 2014). This mechanism is necessary so that each core particle has one copy of each of the ten genome segments. It is known that the NS2 protein has multiple RNA binding sites and that it can readily recruit RNA molecules to initiate core assembly. Studies on BTV NS2 protein confirmed that NS2 selects for BTV RNA rather than non-specific RNAs. This is due to putative hairpin structures formed by the different ssRNA molecules of BTV. Hairpin loop structures are found in both coding and non-coding regions of the ssRNA molecules. These structures are absent from the 5' or 3' terminal conserved regions that form a potential panhandle structure due to partial complementary sequences at the 5' and 3' termini. Subsequent chemical and enzymatic probing provided proof that the NS2 then indeed binds to these hairpin loop configurations (Huismans *et al*., 1987c; Lymperopoulos *et al*., 2003; Lymperopoulos *et al*., 2006; Roy, 2008b).

The assembly of the core particle is initiated by the interaction of VP3 (103 kDa) decamers as the first stable intermediate of the core assembly pathway. Resolution of the core structure revealed that this structure is an arrangement of 12 VP3 decameres, joined via dimerization domains or decamer-decamer interacting regions (DeltaDD). Furthermore, co-expression studies (Le Blois *et al*., 1991; Loudon and Roy, 1992) indicated an independent association of VP1 and VP4 with VP3 decamers. Together VP1 and VP4 form a flower-like structure directly beneath the five-fold axis and are attached to the base of VP3 (Nason *et al*., 2004). Additionally initiation of the core assembly pathway is due to the simultaneous interaction of both VP1 and VP4 to the VP3 decamers (Kar *et al*., 2004). Results from studies by Kar and colleagues (2004) confirmed that the N-terminal of VP3 is necessary for the binding and encapsidation of the transcription complex components (i.e. VP1 and VP4). This suggests that the VP3 decamer intermediates are most likely responsible for recruiting the transcription complex components prior to completion of the subcore particle (for complete review refer to Roy, 2008a). Association of VP6 with the VP3 decamers have not been established to date. The recruitment and incorporation of VP6 into the core particle, and its association with nucleic acid, has not been confirmed (Roy, 2008a).

Although the core particle of orbiviruses is highly stable, the subcore particle with only VP3 is an unstable molecule and only stabilises once associated with VP7 (38 kDa) trimers. Furthermore, improper integrity of the VP7 trimers subsequently interferes with proper assembly of the CLP (Limn *et al*., 2000). The core surface is composed of 260 VP7 trimers forming a T=13 quasiequivalent icosahedral protein shell, attached to the smooth layer of VP3 protein that act as scaffolds (Limn and Roy, 2003). Through point mutation studies (Le Blois and Roy, 1993; Limn *et al*., 2000; Limn and Roy, 2003), critical residues, responsible for core assembly, were identified. It was observed that the position of these critical residues as well as their nature had a significant effect on the stability of the VP7 lattice, suggesting that the stability of the lattice was not due to automatic trimer formation. However, the precise shape of the trimers added significantly to the stability of the VP7 lattice. Furthermore, it was observed that deletion and extension of the carboxy-terminus prevented CLP formation. Deletion and extension of the amino terminus, however, had no adverse effect on CLP formation. In addition, it was observed that lysine, at position 255, had a critical role in CLP formation. When this residue was substituted by a leucine residue, CLP formation was abrogated (Le Blois and Roy, 1993). It was observed that multiple sheets of VP7 initially form around different nucleation sites. This implies that a few strong VP7 trimer-VP3 contacts operate as initiation sites for the core outer layer assembly that are subsequently filled up with a set of weaker interactions (Limn and Roy, 2003). A complete review on the mutation studies is described by Roy (2008a).

After assembly of a stable core like particle, the outer capsid proteins VP2 and VP5 are recruited for assembly. This necessitates a VP2-vimentin interaction and result in the association of mature VLPs and intermediate filaments. Studies showed that if vimentin structures were absent, a decline in the amount of virus particles released and an increase in cell associated viruses were observed (Bhattacharya *et al*., 2007). Association of VP2 with the CLPs will render the transcriptionally active particle inactive. Bhattacharya and colleagues (2007) established that BTV VP2 associates with vimentin in virus infected cells as well as in the absence of other BTV proteins. They also proposed a control mechanism by which mature virus particles assemble. It was confirmed that vimentin interaction is conferred by the 118 amino acid residue N-terminal at a site mapped specifically between residues 65 and 114. Deletion of this region resulted in abrogation of vimentin and VP2 association. Furthermore, amino acids 70 and 72 (Glycine (G) and Valine (V) respectively) were indicated as important sites for VP2-vimentin interaction. Mutation of these residues to DVD resulted in a diminished VP2-vimentin association (Bhattacharya *et al*., 2007).

The VP2 and VP5 are assembled independently and are attached directly to the VP7 core (Liu *et al*., 1992). A triangular top portion of the VP7 trimers serves as an attachment platform for VP2, where the base of the VP2 interacts with the upper flattish surface of VP7. These interactions occur at amino acid residues 141-143, 164-166, 195-205 and 238-241 of the VP7 protein. VP5 trimers interact with the lower portion of the *β*-barrel domain of VP7. Interaction sites of VP7 were mapped at residues 168-173, 210-215 and 226-234 within the distal *β*-barrel domain. The interaction between VP5 and VP7 were confirmed to be much stronger than the VP2-VP7 interactions. This indicates that dissociation of VP2 from VLPs by monovalent or divalent salts is possible without removing VP5 from the VLP (Huismans *et al*., 1987a). Once the outer capsid proteins are assembled onto the core-like particle, the progeny virus are no longer transcriptionally active, but are primed for release from the infected host cell (Roy, 2005).

Release of virus particles

It has been observed that orbiviruses can be released from an infected cell in one of two ways, either through budding or by lytic release. Additionally the cytopathic effect (CPE) on mammalian cells appears to be much more substantial than the CPE on insect vector cells (Stassen *et al*., 2012). This might be a result of the mechanism of virus release from the infected host cell (Beaton *et al*., 2002). BTV, AHSV and other orbiviruses lack lipid envelopes. These viruses are released from infected vertebrate host cells mainly through cell lysis without acquiring a cell derived lipid membrane (Han and Harty, 2004). Early in the infection cycle, particles were however also observed to bud off from infected cells acquiring, at least temporarily, an envelope and showed to have no viral antigens present on the temporary envelope (Hyatt *et al*., 1989). In contrast, orbivirus release from infected insect vector cells is exclusively nonlytic and appears to have no significant effect on the host cell's viability (Venter *et al*., 2014).

Many independent studies have confirmed the involvement of AHSV and BTV NS3 in virus egress during morphogenesis (Hyatt *et al*., 1989; Stoltz *et al*., 1996; Wirblich *et al*., 2006,). After synthesis of the BTV NS3 proteins they are transported to the cell membrane via the Golgi apparatus, where they are present in both a glycosylated and non-glycosylated form (Wu *et al*., 1992). A study by Hyatt and colleagues (1993) showed that recombinant NS3 expressed in a baculovirus system localised at the site of VLP release and was integrated in the plasma membrane. Therefore, NS3/NS3A was suggested to facilitate mature virion release from infected cells. In addition, BTV NS3 was found to have two cytoplasmic domains connected by two hydrophobic domains that span

the membrane at the site of integration (Roy, 2005). Furthermore, it was observed that NS3 can manipulate the cellular exocytosis pathway to assist in nonlytic release (Beaton *et al*., 2002). This occurs when the cytoplasmic N-terminal domain, containing a putative amphipathic helix in its first 13 amino acid residues, interacts with the calpactin light chain (p11) of the cellular Annexin II complex (Beaton *et al*., 2002). In the normal cellular secretory pathway p11 is thought to be an effector molecule for plasma membrane localization. It forms heterotetramers with the heavy chain (p36) of Annexin II and is involved in membrane associated events reviewed by Roy, 2005. Through their investigation, Beaton and colleagues (2002) demonstrated that NS3 competes with p36 for ligand association at the p11 site on calpactin. It was proposed that NS3-p11 interaction can direct NS3 proteins to active sites of exocytosis, or conversely be part of an active extrusion process. This suggests the involvement of NS3-p11 in linking the cellular membrane at the neck of a mature virus particle to facilitate subsequent membrane fusion (Beaton *et al*., 2002; Bhattacharya and Roy, 2013).

Studies on NS3 have shown that the cytoplasmic N-terminal domain contains a late domain motif. The function of this motif was thought to be responsible for the recruitment of Tsg101. Tsg101 is a protein involved in the early stages of multivesicular body (MVB) biogenesis that is regulated by the heavy chain of calpactin I. MVBs are implicated as transport intermediates in the lysosomal degradation pathway or as a storage intermediate for intracellular vesicles. The MVBs function to sort ubiquitinated cargo into these vesicles for subsequent release as exosomes. Interaction of NS3 and Tsg101 is via a PSAP motif, found at position 41-44 in the BTV NS3 N-terminal domain. Additionally, dynein was shown to play an important role in endosomal/ lysosomal membrane dynamics. Interaction with NS3 was found to be via the light chain A2 of this protein, confirming NS3 protein's ability to act as platform for the recruitment of these cellular proteins. Interaction with the VP2 protein, but not VP5, via the cytoplasmic C-terminal domain of NS3 was confirmed with yeast two-hybrid screening (Beaton *et al*., 2002). Subsequently it was suggested that the outer capsid assembly occurs just prior to VLP release (Beaton *et al*., 2002; Harrison *et al*., 2003; Mayran *et al*., 2003; Roy, 2005; Wirblich *et al*., 2006).

5.5 Cytopathicity

Orbiviruses are of the lesser understood viruses in regards to their molecular elements that brings about virulence. There are indications that BTV and AHSV VP2, VP5, NS3, and to a lesser extent NS1 are involved in determining virulence (Coetzee *et al*., 2012; Huismans *et al*., 2004; Owens *et al*., 2004). During 2015 Janowicz and colleagues used reverse genetics systems to identify the importance of VP2 (virus entry) and NS3 (virus exit) in primary virulence. They also indicated the importance of other proteins that play a role in virulence and pathogenesis.

In a study conducted by Laegreid and colleagues (1992), the viral virulence phenotype of AHSV was shown to be the primary determinant of the clinical disease form. In mammalian cells, AHSV-induced CPE is recognised by cells detaching from one another leaving large intracellular spaces and cells showing signs of rounding (Coetzer and Guthrie, 2004; Laegreid *et al*., 1992; Meiring *et al*., 2009; Stassen *et al*., 2012). The relationship and specifics regarding the dynamics of CPE in model cell systems as opposed to the manifestation in infected horses are relatively unclear.

5.6 Reassortment Capability of the Orbiviruses

Genome-segment reassortment is an important process for genetic exchange to produce evolutionary change in all viruses with segmented genomes. This is a trait regularly observed in members of the *Reoviridae* family (Cowley and Gorman, 1987; Moody and Joklik, 1989; Ramig *et al*., 1989; Roner and Mutsoli, 2007; Tauscher and Desselberger, 1997). In many previous studies there was a lack of clear understanding of its frequency and biological significances. However, it was found that in the case of BTV reassortment is a frequent process that continuously plays an important role in its evolution (Nomikou *et al*., 2015). It was observed that certain segments showed preference to interact with specific segments during reassortment (Seg-1, Seg-2, Seg-5, Seg-8, and Seg-9) leading to the speculation that genome-wide epistasis and functional relationships exist between single proteins and specific genome segments. They also noted that amino acid changes occurred more regularly in newly reassorted virus in positions that showed positive selection. This might be an indication of adaptive dynamics as a consequence of reassortment (Nomikou *et al*., 2015).

Genome reassortment has been observed in both the vertebrate hosts (Samal *et al*., 1987b; Stott *et al*., 1987) and vector hosts (Samal *et al*., 1987a; Walker *et al*., 1989). In 2008 Von Teichman and Smit investigated the ability of natural vaccine reassortant strains of AHSV to revert back to disease causing strains in susceptible horses. It was suggested that the occurrence of such genome segment reassortment increases the genetic diversity of the orbivirus populations. This was investigated in a study by Stott and colleagues (1987) and it was observed that at least six genome segments participated in genome segment reassortment. In addition, they managed to isolate 16 new reassortant strains. Many of the field isolates found to date are speculated to be the result of natural RNA segment reassortment within compatible serogroup populations. Although the prevalence of reassortment within orbivirus serogroups such as BTV and AHSV are recurring, reassortment between different orbivirus serogroups hasn't been confirmed (Roy, 2001). In their study using two BTV strains (BTV-10 and BTV-17), Ramig and colleagues (1989), established that reassortment takes place early on in the replication cycle and that progeny BTV genomes undergo a single round of reassortment. In the study, non-random segregation of genome segments was confirmed in crosses performed at equal and unequal multiplicities of infection.

During co-infection, not only in natural environments but also in tissue culture, reassortment of the genome segments amongst the orbiviruses has been observed. Reassortant strains formed the focus of numerous earlier studies that investigated the gene coding assignments of the different RNA segments within orbivirus serogroups (Cowley and Gorman, 1987; Cowley and Gorman, 1989; Moss *et al*., 1987). Additionally, reassortants have been used to investigate the genes that affect the virulence of serogroups such as BTV and AHSV (Roy, 2001).

Assessing the influences of specific virus proteins by genomic reassortment may assist in revealing the function of virus proteins in segmented RNA virus such as AHSV and BTV (Roner and Mutsoli, 2007; Tauscher and Desselberger, 1997). If one was to utilise the reverse genetics technology available today, it would be possible to perform similar assessments in a direct approach. In a study by Meiring and colleagues (2009), genetic reassortment was performed on different AHSV strains (serotypes AHSV-2, AHSV-3, AHSV-4) to identify the functions of specific viral genes in viral release and cytopathicity. These AHSV strains were selected to represent the three clades namely γ NS3 (AHSV-2), β NS3 (AHSV-3), and α NS3 (AHSV-4) (Meiring *et al*., 2009; Van Niekerk *et* al., 2001b). The findings suggested that exchange of the Seg-10 genome segment, alone or with other segments, resulted in changes concerning virus release, membrane permeability and total virus

yield. Subsequently questions arose regarding the effect of AHSV NS3 on the infected cell's viability as well as the proteins' cytopathicity on infected cells. More unanswered questions remain regarding the differences of these mechanism between parental and reassortant strains, as well as the pathogenic response in insect and mammalian cell cultures.

After co-infection with the different strains (serotypes AHSV-2, AHSV-3, AHSV-4), five reassortant strains were recovered designated as R3-$2_{3,5}$; R3-$2_{5,10}$; R4-2_{10}; R4-$2_{7,10}$; and R4-$2_{4,5,7,10}$ (Meiring *et al*., 2009). In the reassortant (R) designation, the first number refers to the serotype of the backbone parental strain supplying the majority of the genome segments, whereas the second number refers to the serotype of the backbone parental strain that supplies the genome segments indicated as trailing numbers in subscript. These parental strains as well as the five reassortants were described and comprehensively compared in regards to their virus release, influence on membrane permeability, cytotoxicity, cell viability, CPE, and induction of apoptosis (Meiring *et al*., 2009; Venter, 2014).

6 CONCLUDING REMARKS

Orbivirus is one of the largest virus genera within the *Reoviridae* family and the focus of this study is on AHSV. Currently orbiviruses are recognised as causing worldwide emerging and re-emerging disease outbreaks. Specifically AHS, which can manifest in four clinically distinct forms in equid species, is of great economic importance in South Africa. AHS can present itself with varying mortality rates, and to date no known correlation exist between specific serotypes and specific clinical forms. AHS disease pathogenesis is complex, and the results of an interaction of both viral and host factors. When using a tissue culture model system there are less variables, and one should theoretically be able to pinpoint viral genes or proteins that contribute to cellular cytopathogenesis with greater accuracy and ease.

In viruses with a segmented genome, previous studies using genetic reassortants have assisted in revealing the functions of specific viral proteins. The investigation undertaken here was a direct follow up on the findings of Meiring *et al*. (2009) and Venter (2014). In their studies they compared properties of three parental (AHSV-2, AHSV-3, AHSV-4) and five reassortant (R3-$2_{3,5}$; R3-$2_{5,10}$; R4-2_{10}; R4-$2_{7,10}$; and R4-$2_{4,5,7,10}$) AHSV strains. They observed differences with respect to virus release, effects on membrane permeability, cytotoxicity and cell viability, timing and extent of CPE, and induction of apoptosis. Conclusion from their work included a role for NS3 in influencing virus release and yield, and a combined contribution of NS1 and NS3 to virus-induced CPE and cell death by a replication-dependent effect on apoptosis. It is however not yet known which aspects of the viral life cycle potentially underlie these observed differences.

7 AIMS AND OBJECTIVES

The aim of this study was to comparatively assess different stages of the life cycles of eight AHSV strains, in an attempt to identify factors that contribute to the diverse cytopathogenic phenotypes observed for these strains *in vitro*. To accomplish this, systematic comparisons of gene expression studies on three parental and five reassortant AHSV strains were done in both a mammalian and insect tissue culture system. The objectives of this study were therefore to monitor different AHSV replication cycle stages by investigating and comparing i) transcription, ii) translation, iii) genome segment packaging and dsRNA synthesis, and iv) virus release of eight strains of AHSV.

CHAPTER 2 : MONITORING GENE EXPRESSION OF DIFFERENT AHSV STRAINS IN MAMMALIAN AND INSECT CELLS

1 INTRODUCTION

One of the natural phenomena observed amongst segmented genome viruses is the ability to reassort gene segments, which has been observed in many members of the *Reoviridae* family (Cowley and Gorman, 1987; Moody and Joklik, 1989; Ramig *et al*., 1989; Roner and Mutsoli, 2007; Tauscher and Desselberger, 1997). Genome reassortment has been observed in both the vertebrate hosts (Samal *et al*., 1987b; Stott *et al*., 1987) and vector hosts (Samal *et al*., 1987a; Walker *et al*., 1989). Reassortment strains have formed the focus of numerous earlier studies, and could be used to investigate the gene coding assignments of the different RNA segments within orbivirus serogroups (Cowley and Gorman, 1987; Cowley and Gorman, 1989; Moss *et al*., 1987).

Reassortants have also been used to investigate the genes that affect the virulence of serogroups such as BTV and AHSV (Roy, 2001). In one such study by O'Hara and colleagues (1998), reassortant strains, generated from an attenuated AHSV-3^{att} (virulent) strain and a wild type AHSV-8^{wt} (avirulent) strain, gave rise to 3 distinct phenotypes, regarding virulence, when a murine model was infected with the novel reassortant strains. In the fully avirulent phenotype it was suggested that genome segment 2 (encoding outer capsid protein VP2) from the avirulent parent dominated this phenotype. In the fully virulent phenotype, however, it was suggested that VP2 from the virulent parent as well as segment 5 (encoding VP5) and 10 (encoding NS3/NS3a) from the virulent parent conveyed the virulent phenotype on these reassortant strains. In the third phenotype observed, a novel virulent phenotype, considered to be of intermediate virulence compared to the two parental strains, was observed. In each of the cases where an intermediate virulent phenotype was observed, reassortants contained a combination of segments 2, 5 and 6 from the avirulent parent with segment 10 from the virulent parent or segment 10 only from the virulent parent. Their findings suggested that segment 10 can influence virus virulence, and it was proposed that this was mediated via the effect NS3 had on the rate and timing of virion release from infected cells (Martin *et al*., 1998).

In a study by Martin and colleagues (1998), the virulence characteristics and virion release of reassortant strains, generated by O'Hara *et al*. (1998), were investigated. Phylogenetic analysis indicated that the nine serotypes of AHSV can be grouped into three clades on the basis of sequence homology of NS3. AHSV types 4, 5, 6 and 9 were clustered into group α, serotypes 3 and 7 were cluster together in group β and serotypes 1, 2 and 8 were clustered into group γ. In their study they compared the virulence characteristics on infected insect cells from a virulent AHSV-3^{att} parental strain, an avirulent AHSV-8^{wt} parental strain and a reassortant strain (A90) that was identical to AHSV-8 but contained segment 9 and 10 from AHSV-3. They observed that virus release from AHSV-3^{att}-infected cells occurred from 6 hours p.i. but virus release from AHSV-8^{wt}-infected cells showed a significant increase only after 24 hours p.i., and the reassortant strain (A90) showed a similar pattern to the AHSV-3 parental strain. These findings indicated and supported the proposed hypothesis, stating that NS3/NS3a potentially influence the inferred virulence phenotype by altering the time of virus release. More recently Ooms and colleagues (2010) further discovered that regulation of the replication efficiency of mammalian Orthoreovirus is observed after primary transcription and translation. The study suggested that reoviruses have the ability to use its replication complex to mediate a cell-selective viral replication capacity after virus entry.

In a recent study Meiring and colleagues (2009) generated five novel AHSV reassortant strains, and used these to investigate the role of non-structural protein NS3 in specific viral characteristics. Their findings suggested that exchange of the S10 genome segment between the different parental strains (AHSV-2, AHSV-3 and AHSV-4), resulted in changes concerning virus release, membrane permeability and total virus yield. No direct correlation between a specific AHSV NS3 protein and

the infected cell's viability or the viral CPE could be established. However, some indication in results observed suggest that a combination of NS1 and NS3 contributed from the same parental strain, could contribute to this effect, which was formerly suggested in a study by O'Hara and colleagues (1998). This study is a direct follow up from the study by Meiring *et al*. (2009). The aim was to monitor different stages of the AHSV lifecycle to propose a molecular basis evident from different reassortment combinations of related AHSV strains that cause their diverse virulence phenotypes. To accomplish this, systematic comparisons of gene expression studies on parental and reassortant AHSV strains were done in both a mammalian and insect host cell system.

2 MATERIALS AND METHODS

2.1 Cells

2.1.1 Mammalian cells

African green monkey (*Cercopithecus aethiops*) kidney cells (Vero ATCC CCL-81) were obtained from ATCC (Manassa, USA). Vero cells were propagated in Eagle's minimum essential medium (MEM), supplemented with 5% foetal calf serum (both from Sigma, USA) and supplemented with non-essential amino acids (Sigma), fungizone (2.5 µg/ml), penicillin (100 U/ml) and streptomycin (100 µg/ml) (Highveld Biological). Monolayer cell cultures were seeded in 75 cm^2 Nunc™ cell culture flasks or Nunc™ six-well multidish cell culturing plates (Thermo Scientific, USA) and maintained at 37°C, with 5% CO_2, until ~90-100% confluent. Cells were infected with AHSV at a multiplicity of infection (MOI) of 0.1, 1 or 2. Infected cells were incubated at 37°C for 1 hour with gentle rotation at 10 minute intervals to allow for maximum virus adsorption. After virus adsorption, the medium, containing any virus that did not adsorp to cells, was removed and the cells replensished with fresh Eagles's MEM. AHSV-infected cells were harvested when ~95-100% CPE was observed. Cells were loosened for harvesting from flasks by scraping them with a cell scraper or with the plunger of a small syringe if harvested from a multidish plate. All harvested AHSV-infected cell samples were stored at 4°C.

2.1.2 Insect cells

Biting midge (*Culicoides variipennis*) insect cells (KC) were a gift from Dr. A. C. Potgieter (Onderstepoort Veterinary Institute, Pretoria, South Africa). KC cells were propagated in Schneider's Drosophila medium supplemented with glutathione (6 mg/L), L-asparagine (30 mg/L), insulin (4.5 mU/ml), L-glutamine (2 mM) (all Highveld Biological) and 10% (v/v) foetal calf serum (Sigma), fungizone (2.5 µg/ml), penicillin (100 U/ml) and streptomycin (100 µg/ml) (all Highveld Biological). Monolayer cell cultures were seeded in 25 cm^2 Nunc™ cell culture flasks and maintained at 28°C, with humidity, until ~80-100 % confluent. Cells were infected with AHSV at an MOI of 0.1 and incubated at 28°C with humidity. Cells were harvested at 8 days post-infection. Cells were loosened for harvesting from flasks by scraping them with a cell scraper. All harvested AHSV-infected cell samples were stored at 4°C.

2.1.3 Light microscopy

Vero cells, propagated in 75 cm^2 Nunc™ cell culture flasks (Thermo Scientific), were infected with AHSV as previously described (2.1.1). Cells were either infected at an MOI of 0.1 or 2. Microscope images of the infected cells were captured using a DCM300 Digital Camera (Scopetek, China) at 8, 16, 24 and 48 hours post-infection. Images were analysed using the Scopephoto imaging software (Version 3.1.386, Scopetek, 2009).

2.2 Viruses

2.2.1 AHSV strains

The parental African horsesickness virus (AHSV) serotypes, AHSV-2 (82/61), AHSV-3 (M322/97) and AHSV-4 (HS39/97), used in this study were all obtained from the OIE Reference Laboratory at the OVI (Pretoria, South Africa). The AHSV-2 and AHSV-4 strains were originally isolated from spleen or lung samples of dead horses. The AHSV-3 strain was originally isolated from the spleen of a dead dog. These parental serotypes were selected on the basis of their grouping into the three

NS3 phylogenetic clades. Each of the three serotypes were representative of the three clades, namely γ NS3 (AHSV-2), β NS3 (AHSV-3) and α NS3 (AHSV-4) (Meiring *et al.*, 2009; Van Niekerk, *et al.,* 2001b). Purified samples for each serotype were available for use in the lab. Furthermore, five reassortant AHSV strains were investigated in this study, R3-$2_{3,5}$; R3-$2_{5,10}$; R4-2_{10}; R4-$2_{7,10}$ and R4-$2_{4,5,7,10}$. All of the reassortant viruses studied were progeny resulting from co-infection of combinations of two of the three parental strains used in this study. These reassortant strains have been described (Meiring *et al*., 2009).

Nomenclature for the reassortant virus describe both the parental strains from which the reassortant strain originate and the genome segments that were reassorted. The first numeral in the name refers to the parental strain that donated the genome backbone, R3 or R4 refer to AHSV-3 or 4 respectively. The second numeral (-2) in the name identifies the parent (AHSV-2) which has donated the reassorted segments and are indicated in subscript following the second numeral. For example, R3-$2_{3,5}$ is a reassortant between AHSV-3, donating the genome backbone, and AHSV-2, donating genome segments S3 and S5.

When required, various volumes of virus stocks, depending on the size of the tissue culture flask initially used to cultivate virus, were concentrated in order to achieve higher multiplicities of infection (MOI). Harvested cells were initially centrifuged in an Avanti® J-E Centrifuge (Beckman Coulter Inc., Life Sciences, USA) for 10 min at 4°C and 4000 rpm. The cell pellet was resuspended in 1 ml of 2 mM Tris-HCl, containing 0.5% (v/v) Triton X-100 (Sigma). Cells were incubated for 30 min on ice followed by mechanical shearing by ~20 aspirates using a sterile syringe and needle (22 Gauge). Nuclei were removed by centrifugation in a 5415D benchtop microcentrifuge (Eppendorf, Germany) for 2 min at 1500 rpm. The supernatant was transferred onto 1 ml of a 40% (w/v) sucrose cushion and centrifuged in an Optima™ L-100 XP Ultracentrifuge (Beckman Coulter Inc.) for 1 hour at 4°C and 30 000 rpm, using a SW55Ti rotor. Pelleted, purified virus particles were subsequently resuspended in 1500 µl of 2 mM Tris-HCl (pH 7.2) and stored at 4°C.

2.2.2 Virus titration

Virus titrations were carried out on BSR cells. Briefly, 10-fold serial dilutions, using 2 mM Tris-HCl as diluent, were prepared for each sample to be titrated. Monolayers of BSR cells propagated in Nunc™ 6-well multidish cell culturing plates (Thermo Scientific) were infected with the 10^{-4}, 10^{-5} and 10^{-6} dilutions, in duplicate. Infected cells were incubated for 60 min at room temperature with gentle agitation every 12 minutes to ensure virus adsorption. A 0.6% (w/v) agarose solution, prepared using ultra high quality (UHQ) dH_2O and 2 × Eagles MEM, preheated to 50°C in a water bath, were mixed in a 1:1 ratio and gently poured over the infected cells. Infected cells were left at room temperature until the agarose layer polymerised followed by incubation at 37°C for 3-4 days. To visualise plaques, the agarose was stained by adding 0.5 ml/well of 0.1% (w/v) Thiazolyl Blue Tetrazolium Bromide (MTT; Sigma) in 1 × PBS. Cells were left for 24 hours at 37°C. Plaques were subsequently counted and titres (pfu/ml) calculated as 2 × the number of plaques counted × dilution factor.

2.3 Sample Preparation for Protein Analyses

2.3.1 Sample preparation

Infected Vero or KC cells harvested for protein analysis were separated from cell debris in the supernatant before analyses. Briefly, harvested samples were centrifuged in a benchtop Hermle Z216MK refrigerated microcentrifuge (Labnet International, USA) for 10 min at 4000 rpm and 4°C. Pellets were washed in 1 ml 1 × Phosphate-buffered saline (PBS; 137 mM NaCl, 2.7 mM KCl, 4.3 mM $Na_2HPO_4 \cdot 2H_2O$, 1.5 mM KH_2PO_4), containing 0.5% (v/v) Triton X-100 (Sigma), by centrifugation for 10 min at 4000 rpm and 4°C. Pellets were resuspended in 200 µl NTE buffer (100 mM NaCl, 10

mM Tris-HCl, 1 mM EDTA, pH 7.4) and incubated on ice for 30 min. Samples were subsequently lysed by ~20 aspirates using a sterile syringe and needle (22 Gauge) and stored at -20°C.

2.3.2 Sub-cellular fractionation

Sub-cellular fractionation was done based on the method described by Huismans (1979). Briefly, infected Vero cells were harvested and centrifuged for 10 min at 4000 rpm and 4°C. Pelleted cells were resuspended in cold 0.15 M STM buffer (150 mM NaCl, 5 mM $MgCl_2$, 10 mM Tris-HCl, pH 7.4, 0.5% Triton X-100) to a final concentration of 5×10^7 and incubated on ice for 5 min. To remove the nuclei, samples were centrifuged for 5 min at 3000 rpm. Pelleted nuclei were subsequently resuspended in STM buffer to half the original volume, followed by centrifugation for 5 min at 3000 rpm. The supernatants, containing the cytoplasmic extracts, from both centrifugation steps, were pooled and transferred onto 2 ml of a 40% (w/v) sucrose cushion, made up with 0.15 M STE buffer (150 mM NaCl, 1 mM EDTA, 1 mM Tris-HCl, pH 7.4). Samples were centrifuged in an Optima™ L-80 XP Ultracentrifuge (Beckman Coulter) using a SW55Ti rotor for 2 hours at 45 000 rpm. The soluble (S100) fraction was lyophilized and stored at -20°C. The pelleted particulate fraction was resuspended in 0.01 M STE (10 mM NaCl, 1 mM $MgCl_2$, 1 mM Tris-HCl, pH 7.4) buffer to one-fifth the original cytoplasmic extract volume and stored at -20°C. Proteins from the soluble (S100) fraction was separated by SDS-PAGE and analysed.

2.4 RNA Isolation

Total RNA was isolated from previously harvested infected Vero or KC cells. This was done with the aid of the Aurum™ Total RNA Mini Kit (BioRad, Catalog no.: 732-6820). The Spin Protocol for nonadherent cells, as outlined in the manufacturer's manual, was followed. Briefly, harvested cell samples were rinsed in PBS and transferred to the supplied 2 ml capped microcentrifuge tubes. Samples were centrifuged in a benchtop microcentrifuge, at maximum speed (>10 000 rpm) for 2 min and the supernatant discarded. To each tube, 350 µl of the kit-supplied lysis solution, supplemented with 1% β-mercaptoethanol (Merck), were added and cells lysed by aspi rating with pipette. After cell lysis, 350 µl of 70% EtOH was added to each tube and mixed thoroughly by pipetting. Homogenized lysates were transferred into RNA binding columns, assembled with 2 ml capless wash tubes (both supplied) and centrifuged for 30 sec at maximum speed. The filtrate was discarded and the collection tube reassembled. 700 µl of low stringency wash solution (1:4 (v/v), 20 ml concentrated low stringency wash solution diluted in 80 ml 95-100% EtOH) was added to each RNA binding column followed by centrifugation for 30 sec at maximum speed. Again, the filtrate was discarded and the collection tube reassembled. A solution, consisting of 5 µl reconstituted DNase I and 75 µl DNase dilution solution (both supplied), scaled up proportionally to add 80 µl per RNA binding column was prepared and aliquoted to the membrane stack at the bottom of each column. Tubes were incubated for 15 min at room temperature to allow for digestion. After digestion, 700 µl of high stringency wash solution (supplied) was added to each RNA binding column and then centrifuged for 30 sec at maximum speed. The filtrate was discarded, the collection tube reassembled and 700 µl of low stringency wash solution added to each column. Columns were centrifuged for 60 sec at maximum speed and the filtrate discarded. The collection tubes were reassembled and the columns centrifuged for an additional 2 min to remove all residual wash solution. The collection tubes were discarded after centrifugation and the RNA binding columns were placed in 1.5 ml capped microcentrifuge tubes (provided). 50 µl of supplied elution solution was pipetted onto the membrane stacks at the bottom of each RNA binding column and incubated for 1 min to allow the solution to saturate the membrane, followed by centrifugation for 2 min at maximum speed to elute the total RNA from each starting sample. Samples were stored at -20°C until further use.

All centrifugation and incubation steps were carried out at room temperature as per the protocol guidelines. Furthermore, all samples were measured using the NanoDrop® ND-100 spectrophotometer (NanoDrop Technologies, Inc., USA) to obtain the nucleic acid concentrations.

Alternatively, double-stranded virus RNA was isolated and purified with the aid of TRIzol® reagent (Invitrogen, Life Technologies, USA) and LiCl. Briefly, infected Vero or KC cells were harvested and centrifuged in a benchtop Hermle Z216MK refrigerated microcentrifuge (Labnet International) for 10 min at 4°C and 6 200 rpm. Pellets were resuspended in 1 × PBS and centrifuged as before. After centrifugation the pelleted sample was homogenised in 1 ml TRIzol® reagent and incubated at room temperature for 5 min. Chloroform was added to the samples, shaken vigorously, incubated at room temperature for 2 min and centrifuged for 15 min at 4°C and 10 300 rpm. Once samples had separated into phases, the upper aqueous phase was removed and transferred to new microcentrifuge tubes and mixed with isopropanol. Samples were subsequently incubated for 10 minutes at room temperature followed by centrifugation for 10 min at 4°C and 10 300 rpm. The centrifugation step was repeated for 5 min at 4°C and 8 500 rpm to wash the pellet with 1 ml of 75% (v/v) EtOH. The wash solution was removed and the RNA pellet air-dried. The RNA pellet was dissolved in 80 µl of molecular-grade Ambion® Nuclease-free water (Applied Biosystems, Life Technologies, USA) and incubated for 10 min at 55°C in a water bath, followed by addition of 20 µl of 10 M LiCl to a final volume of 100 µl. Samples were incubated overnight at 4°C, followed by centrifugation for 30 min at 4°C and maximum speed to precipitate all single-stranded RNA molecules. The supernatant was transferred to a clean microcentrifuge tube and mixed with 4 µl of 5 M NaCl and 200 µl of 96% (v/v) EtOH. Samples were incubated for 60 min at -20°C and centrifuged for 15 minutes at 4°C and maximum speed. The centrifugation step was repeated to wash the pelleted dsRNA in 70% (v/v) EtOH for 20 min at 4°C and 10 300 rpm. Pelleted dsRNA was briefly air-dried and then resuspended in 50 µl of Ambion® Nuclease-free water.

All samples of purified RNA (mRNA, ssRNA and dsRNA) were stored according to guidelines outlined in Protocol 7.1 from Sambrook and Russell (Vol.1, 2001).

2.5 Reverse Transcription for First Strand cDNA Synthesis

After RNA purification of harvested infected Vero cells, first strand cDNA was synthesised with the aid of the QuantiTect® Reverse Transcription kit (Qiagen, Catalog no.: 205311). The protocol guidelines as outlined by the manufacturer's handbook (01/2009) was followed. Briefly, a master mix containing 7 × gDNA Wipeout Buffer (2 µl), template RNA (up to 1 µg), and RNase-free water (making up the total volume to 14 µl) were prepared on ice and scaled up proportionally for the number of reactions to prepare. However, the total master mix was first prepared, aliquoted followed by the appropriate volume of RNA added. The genomic DNA elimination reactions were incubated for 2 min at 42°C, followed by incubation on ice. A reverse-transcription master mix, containing 1 µl Quantiscript Reverse Transcriptase (containing RNase inhibitor), 4 µl of 5 × Quantiscript RT Buffer (containing Mg^{2+} and dNTPs) and 1 µl Primer Mix (containing an optimised mixture of oligo-dT and random hexamer primers) was prepared on ice and proportionally scaled up for the total number of reactions. 6 µl of reverse-transcription master mix was aliquoted to each genomic DNA elimination reaction followed by incubation for 15 min at 42°C. This was followed by incubation for 3 min at 95°C to ensure inactivation of the Quantiscript Reverse Transcriptase. All samples were stored at -20°C until further use. Again, samples were measured with a spectrophotometer, to determine the nucleic acid concentration in each sample.

2.6 Conventional PCR

2.6.1 PCR ampification

A PCR master mix was prepared and proportionally scaled up for the total number of reactions. The master mix, prepared on ice, contained 5 µl of 5 × GoTaq® Flexi Buffer (Colourless, Promega, USA), 4 µl $MgCl_2$ (25 mM, Promega), 1 µl dNTP mix (10 mM, 0.25 mM of each dNTP, TaKaRa, USA), 2.5 µl forward primer (10 pmol, Whitehead Scientific, USA), 2.5 µl reverse primer (10 pmol, Whitehead Scientific), 0.25 µl GoTaq® DNA Polymerase (5U/µl, Promega, Catalog no.: M8305), and DEPC-treated water to a final reaction volume of 49 µl. Table 2 summarises the primer sets, and their PCR

conditions, used for PCR amplification. Cycling conditions were as outlined: An initial denaturation step and activation of the polymerase enzyme of one cycle for 2 min at 94°C; 30 cycles of a denaturing step for 15 sec at 94°C, followed by an annealing step for 30 sec at the primer set Tm, followed by an extension step for 20 sec at 72°C, one cycle for 5 min at 72°C for final extension. Amplification products were stored at 4°C.

Table 2: Summary of primers used for PCR amplification experiments

Primer	Sequence (5' - 3')	Tm (°C)	Annealing position	Size of primer	Size of amplicon
AHSV-SPECIFIC PRIMERS					
rt-VP7-*F*	CTG GAG ATG TCG TCG CAT GGA ATA C	59,2	656-680	25 nt	138 bp
rt-VP7-*R*	GAG CCA ATT CCG GAA CCG TG	58,9	774-793	20 nt	
rt-NS1-*F*	GCC CGT TTG CCC TTA TAC TG	56,2	603-623	20 nt	149 bp
rt-NS1-*R*	TGA AAT CCT GTG CCG CTC	55,5	733-751	18 nt	
rt-NS2-*F*	TGT GCG CGA GAT CAC CTT G	58,1	610-629	19 nt	102 bp
rt-NS2-*R*	TGT CTT CGT GCC ACA TCA TCT G	57,3	690-711	22 nt	
rt-NS3-*F*	TCA ATG AGA CGT AGG TAT GCG	54,3	316-336	21 nt	145 bp
rt-NS3-*R*	TCT TCG ACA GCC AAC CAT C	54,9	442-460	19 nt	
VERO CELL HOUSEKEEPING GENE PRIMERS					
rt-β_2MG-*F*	ATC CAG CGT GCT CCA AAG ATT CAG	59,5	71-94	24 nt	98 bp
rt-β_2MG-*R*	ATC AGA TGG ATG AAA CCC AGA CAC A	58,1	144-168	25 nt	
rt-GAPDH-*F*	GCA TGG CCT TCC GTG TTC CTA C	60,5	653-674	22 nt	104 bp
rt-GAPDH-*R*	CCT GCT TCA CCA CCT TCT TGA TGT C	59,7	733-757	25 nt	

2.6.2 PCR product purification

PCR products were purified with the aid of the High Pure PCR Product Purification Kit (Roche, Germany, Catalog no.: 11732676001) according to the protocol outlined in the manufacturer's guidelines (Version 01/2008). Briefly, the DNA band of interest was isolated through electrophoresis and cut out of the agarose gel. Excised DNA bands were placed in a 1.5 µl microcentrifuge tube and dissolved in 300 µl binding buffer (supplied) per 100 mg agarose gel (w/v). The excised gel slice, containing the DNA product, was melted in the binding buffer during incubation for 10 min at 56°C with intermittent vortexing every 2-3 minutes. Once the agarose gel had completely dissolved, 150 µl isopropanol per 100 mg initial agarose gel was added to each tube and mixed thoroughly. A kit-supplied High Pure filter tube was assembled with a supplied collection tube for each sample and the entire content of each sample transferred. Samples were centrifuged in a benchtop centrifuge for 30-60 sec and 25°C at maximum speed. The flow-through was discarded, the collection tube reassembled and 500 µl wash buffer added to each sample. Again all samples were centrifuged for 60 sec and 25°C at maximum speed. The previous step was repeated with the modification of adding 200 µl of wash buffer to each sample. After centrifugation the collection tube was discarded with the flow-through and the filter tube reassembled in a clean 1.5 ml microcentrifuge tube (not supplied). A volume of 50 µl of elution buffer was added to each sample and centrifuged for 60 sec and 25°C at maximum speed to elute the DNA into the clean collection tube. Samples were stored at 4°C until further analyses.

2.7 Real-time qPCR

Real-time quantitative PCR was done using the LightCycler® 480 SYBR Green I Master pre-mix kit. The protocol for use with the "LightCycler® 480 Multiwell Plate 384", as outlined in the manufacturer's manual (Roche, V08/2006), was followed. Briefly, a master mix, containing 5 µl of 2 × SYBR Green I Master mix, 1 µl each of forward and reverse primer (20 pmol each) were prepared on ice. The master mix was scaled up proportionally for the number of reactions to run. Aliquots of 7 µl of the prepared master mix were loaded in the wells on a 384 multiwell LightCycler® 480 plate for each reaction. Subsequently, 3 µl of cDNA was added to each well containing SYBR Green I master mix. A 10-fold serial dilution (10^{-1}–10^{-4}) of each cDNA sample to be analysed was prepared and loaded. The plate was covered with multiwell sealing foil and centrifuged for 60 sec at 3 800 rpm to collect the total reaction volume at the bottom of each well. Plates were loaded in the LightCycler® 480 PCR cycler (Roche).

The PCR parameters programmed were one cycle pre-incubation for 5 min at 95°C; an amplification programme of 45 cycles of 10 sec at 95°c, 10 sec at primer Tm and 5 sec (with single acquisition) at 72°C; one cycle for melting curve analysis of 5 sec at 95°C, 1 min at 59°C and a continuous acquisition step at 97°C; followed by one cycle of cooling for 10 sec at 40°C. Before each reaction was run, the programme was further set to "relative quantification" or "absolute quantification" and the wells where samples were loaded were identified by the programme as either "target", "reference", "standard" or "calibrator".

After amplification the data obtained was analysed using the LightCycler® 480 software (v5.1, Roche) on the instrument. Real-time PCR amplification products were additionally visualised on a 2% agarose gel and analysed.

2.8 Gel Electrophoresis

2.8.1 Agarose gel electrophoresis

Success of PCR amplification was visualised on a 2% agarose gel. A 2% (w/v) agarose gel was prepared using agarose powder (Separations, South Africa) dissolved in 1 × TAE buffer (4 mM Tris-HCl, 0.1% (v/v) Glacial acetic acid, 0.2 mM EDTA, pH 8.0) or 1 × TBE buffer (0.1 M Tris-HCl, 0.1 M Boric acid, 2 mM EDTA, pH 8.0) containing 3 µl of 1 mg/ml EtBr (Merck). Once agarose powder was successfully dissolved in the buffer, horizontal slab gels were cast and left to set. Agarose gels ready for use were placed in a Minicell® EC370M electrophoresis tank (Thermo Electron Corporation) and the tank was filled with 1 × TAE or 1 × TBE running buffer. A volume of 8 µl of each sample, mixed with 5 µl of 6 × blue/orange loading dye (Bromophenol blue/ Xylene cyanol), were loaded onto the gel. A DNA molecular size marker, the 100 bp DNA Ladder (Promega, USA, Catalog no.: G2101), was also loaded to determine the sizes of the visualised bands. Samples were electrophoresed at 100 V followed by visualisation on a GelDoc™ XR+ Imaging System UV transilluminator (BioRad Laboratories Inc., USA).

2.8.2 RNA PAGE

Purified AHSV dsRNA samples (2.4) were separated and analysed on a polyacrylamide gel. For each sample 8 µl, mixed with 5 µl of 6 × blue/orange loading dye, was loaded and concentrated on a 3% spacer gel containing 3% (w/v) acrylamide, 0.08% (w/v) N, N' methylene bis-acrylamide, 64 mM Tris-HCl (pH 6.7), 0.15% (w/v) Ammonium peroxydisulfate and 0.15% (v/v) TEMED. Next, AHSV dsRNA genome segments were separated in a 6 or 14% resolving gel containing 6 or 14% (w/v) acrylamide, 0.16 or 0.37% (w/v) N, N' methylene bis-acrylamide, 375 mM Tris-HCl, 0.0625 N HCl, 0.15% (w/v) Ammonium peroxydisulfate and 0.05% (v/v) TEMED. Electrophoresis was carried out in a SE 400 Vertical Slab Gel Unit (Amersham Biosciences, GE Healthcare, Life Sciences, USA) in 1 × Tris-glycine running buffer (25 mM Tris-HCl, 250 mM glycine) at 90 V for 20-22 hours.

Subsequently, gels were stained in 1 × Tris-glycine buffer containing SYBR® Gold nucleic acid gel stain (Invitrogen, Life Technologies) and visualised on a GelDoc™ XR+ Imaging System UV transilluminator (BioRad).

2.8.3 SDS-PAGE

Protein samples were analysed by separation using SDS-PAGE. Samples (10-20 µl) were resuspended in 3 × Protein Solvent Buffer (PSB) containing 188 mM Tris-HCl (pH 6.8), 6% SDS, 30% Glycerol, 15% β-mercaptoethanol and 0.005% bromophenol blue, and denatured, for 5 min at 96°C. Subsequently, samples were concentrated in a 5% stacking gel (5% (w/v) acrylamide, 0.14% (w/v) N, N' methylene bis-acrylamide, 125 mM Tris-HCl (pH 6.8), 0.1% (w/v) SDS, 0.1% (w/v) Ammonium peroxydisulfate and 0.1% (v/v) TEMED) followed by resolving in a 12% separating gel (12% (w/v) acrylamide, 0.32% (w/v) N N' methylene bis-acrylamide, 375 mM Tris-HCl (pH 8.8), 0.1% (w/v) SDS, 0.1% (w/v) Ammonium peroxydisulfate and 0.1% (v/v) TEMED) for 2.5-3.5 hours at 131 V (250 mA). Additionally, 3 µl of a Fermentas PageRuler™ Prestained Protein Ladder (SM0671, Fisher Scientific) molecular mass marker were loaded. Following electrophoresis, gels were stained in Coomassie staining solution (0.3% (w/v) Coomassie brilliant blue G-250, 50% (v/v) MeOH, 10% (v/v) Glacial acetic acid) for 20-30 minutes at room temperature. Subsequently, gels were destained in Destain solution (5% (v/v) Glacial acetic acid, 5% (v/v) MeOH) for 24-26 hours at room temperature and visualised on a GelDoc™ XR+ Imaging System UV transilluminator (BioRad).

If analyses of samples did not continue with Western blotting, gels were vacuum-dried at 80°C, using a SE 1160 DrygelSr Slab Gel Dryer (Hoefer Scientific, USA), until gels were completely dry (~3-4 hours).

2.9 Sequencing

Sequencing of the purified DNA molecules (2.8.2) were done with the aid of the BigDye® Terminator v3.1 Cycle Sequencing Kit (Applied Biosystems). The protocol outlined in the manufacturer's guidelines were followed. Briefly, sequencing reactions including 75-100 ng of DNA, were set up containing 2 µl of 2.5 × Big Dye Terminator Ready Reaction Premix (containing the ddNTPs), 1 µl of 5 × sequencing buffer, 10 pmol of target-specific primer and molecular-grade Nuclease-free water to a final volume of 10 µl. A master mix, scaled up proportionally, were prepared, aliquoted, and the primer and target DNA added last. The cycling conditions were set as follow: An initial denaturation step for one cycle of 1 min at 94°C, followed by 25 cycles of denaturation for 10 sec at 94°C, annealing for 5 sec at 50°C and elongation for 4 min at 60°C.

Extension products were subsequently precipitated using the EtOH/ EDTA/ NaOAc method. Briefly, to each reaction mix 1 µl of 125 mM EDTA, 1 µl of 3 M NaOAc and 25 µl of 100% EtOH was added and incubated for 15 min at room temperature. Samples were centrifuged for 20-30 min at maximum speed and 4°C. The supernatant was discarded and the wash step repeated by adding 100 µl of 70% EtOH and centrifuged for 10-15 min at maximum speed and 4°C. Finally, the supernatant was carefully discarded, the pelleted DNA fragments air-dried and submitted for sequencing. DNA fragments were analysed using the ABI PRISM 3130xl Genetic Analyser (Perkin Elmer, USA). The sequences were aligned and further analysed using the ClustalW multiple sequence alignment interface in BioEdit (Version 5.0.6, Tom Hall, Isis Pharmaceuticals Inc., 2004).

2.10 Immunoblot Assays

2.10.1 SDS-PAGE and Western blot analyses

Proteins were separated using SDS-PAGE as previously described (2.8.3) and subsequently transferred to a Hybond™-C extra nitrocellulose membrane (Amersham Biosciences, Amersham

International plc, UK). Protein transfer was carried out in a submerged VS20WAVE electrophoresis system (AEC Amersham, Cleaver Scientific, USA) filled with Transfer buffer (25 mM Tris-HCl, 192 mM Glycine, 20% (v/v) MeOH) for 1 hour at 100 V. Membranes were rinsed in 1 × PBS for 5 min followed by blocking for 30 min in a 5% blocking solution (1 × PBS buffer containing 5% (w/v) milk powder) with gentle agitation at room temperature. Membranes were then incubated overnight at room temperature, and with gentle agitation, in 1% (w/v) blocking solution containing the primary antibody. Table 3 summarises the different primary antibodies used. Following incubation, membranes were washed 3 times, for 5 min each, in washing buffer (1 × PBS with 0.05% (v/v) Tween-20). Following the wash steps, membranes were incubated for 60 min at room temperature and gentle agitation in 1% (w/v) blocking solution containing Horseradish peroxidase-conjugated Protein A (Calbiochem®, Merck Millipore, Germany; diluted 1:10 000). After antigen detection, the membranes were washed 3 times, for 5 min each, in wash buffer followed by a final wash for 5 min in 1 × PBS. Detection and visualisation was carried out by incubating membranes in an enzyme substrate solution. Membranes were soaked in enzyme substrate solution containing a chromogen (60 mg 4-chloro-1-naphtol (Sigma) in 20 ml ice-cold MeOH mixed with 60 µl hydrogen peroxide in 100 ml 1 × PBS) at room temperature, until bands were visible. Once no more change in band intensity was observed, membranes were rinsed in dH_2O and dried.

Table 3: Summary of primary antibodies used for Western blot analyses

Antibody	Source / Notes	Dilution
anti-G5-VP7	Animal bleeds – Guinea pig, raised against AHSV-9	1:200
anti-NS1-40	Animal bleeds – Guinea pig, raised against AHSV-9	3:200
anti-NS2	Animal bleeds – Guinea pig, raised against AHSV-9	1:200
anti-β-Actin	Abcam Inc, Cambridge, USA	1:100
anti-Lamin A	Abcam Inc, Cambridge, USA	1:100

2.11 ^{35}S-Met Pulse Labelling

Radiolabelling of infected Vero cells was done according to the protocol outlined by Anthony and co-workers (2010). Briefly, 48 well tissue culturing plates containing confluent monolayers of Vero cells were infected at an MOI of 5. Cells were incubated at 37°C followed by depletion from cellular methionine (Met) by substituting the growth medium with 200 µl of Eagle's Met-free growth medium (Sigma) per well. Depletion of cellular methionine was done by incubating cells for 1 hour at 37°C either at 4-5, 12-13 or 20-21 hours post-infection. Radioactive labelled isotope was prepared as a master mix (0.3 % ^{35}S-Met in 1 ml met-free Eagle's MEM; scaled up proportionally) and 200 µl of master mix was added to each well. Cells were pulsed at 37°C for 3 hours, at 5-8, 13-16 or 21-24 hours post-infection. After pulse labelling, cells were harvested and prepared as described in 2.3. Samples were stored at -20°C until analysed by SDS-PAGE (2.8.3).

After SDS-PAGE, vacuum-dried gels were visualised on the VersaDoc Imaging System (BioRad) UV transilluminator. Briefly, a Kodak Imaging Screen-K (20 × 25 cm; BioRad, Catalog no.: 170-7843) were blanked for 15 min using Screen Eraser-K (BioRad). The blank imaging screen and gel were placed in a Konica sample exposure cassette (24 × 30 cm; BioRad) for 22 hours. After exposure, the imaging screen was scanned using the Molecular Imager® (BioRad), connected to the VersaDoc Imaging System to visualise the radiolabelled bands. Gels were analysed using Quantity One® imaging software (Version 4.2.1, BioRad Laboratories, 2000).

2.12 Statistical Analyses

Statistical analysis was done according to the guidelines by Tamhane (1979) and using the statistical program SPSS Statistics (IBM Corp., Version 22, 2013). All analyses were calculated at an alpha level of 0.05 and statistical tests were considered significant if the *p*-value was less than alpha. Briefly, all data sets, where $N > 2$, were tested for normality of data using the *Shapiro-Wilk's* test. Homo- or heteroscedasticity of data was calculated using *Levene's* test for Homogeneity of Variances. Linear Regression, *Student's-t* test or one-way ANOVA analyses were calculated if homogeneity of variance was not violated (*Levene's* test was not significant). Alternatively, ANOVA analyses was run making the *Welch-Satterthwaite* correction if homogeneity of variance was violated (*Levene's* test was significant). Additionally, multiple comparisons tests were done if the one-way ANOVA was significant. *Tukey's HSD post-hoc* multiple comparisons test was considered when the *Welch-Satterthwaite* correction was not made. The *Games-Howell post-hoc* multiple comparisons test was considered if the *Welch-Satterthwaite* correction was made.

3 RESULTS

Reassortment of the African horesesickness virus (AHSV) genome have been shown to have varied virulence phenotypes in infected mammalian cells. It has also been suggested that AHSV NS3 plays an intricate role resulting in changes concerning virus release, membrane permeability and total virus yield. This section describes results from comparative gene expression studies, showing the effect of different reassortment combinations including genome segment S5 or S10 or both.

3.1 Virus Primary Transcription

To identify suitable gene segments for monitoring transcription levels across the different AHSV strains, four genes were initially investigated. Amplification of a target region was tested for one virus core protein coding gene (segment 7) and three non-structural protein coding genes (segments 5, 8 and 10). The aim was to then use one or more of these genes in quantitative real-time PCR (RT-qPCR) assays to compare the timing and levels of transcription at different times post-infection.

3.1.1 Optimising cycling conditions for PCR amplification of four viral genes

Primer sets were available (see Table 2, section 2.6.1) that would amplify a target region of ~120 base pairs (bp) for each of the selected virus genes and these were tested on the parental AHSV strains (AHSV-2, AHSV-3 and AHSV-4). Infected Vero cells were harvested and, with the aid of kits, total RNA was purified from the samples followed by reverse transcription with random hexamer primers to synthesise cDNA. Conventional PCR cycling was then used to determine if the target region was amplified with equally high efficiency in all strains for subsequent application in RT-qPCR.

VP7 gene

Synthesised cDNA was used as template in a PCR reaction with the seg-7 specific primers. An annealing temperature of 64°C was calculated for this primer set and the cycling conditions set accordingly. PCR products were separated on an agarose gel and visualised (Figure 1).

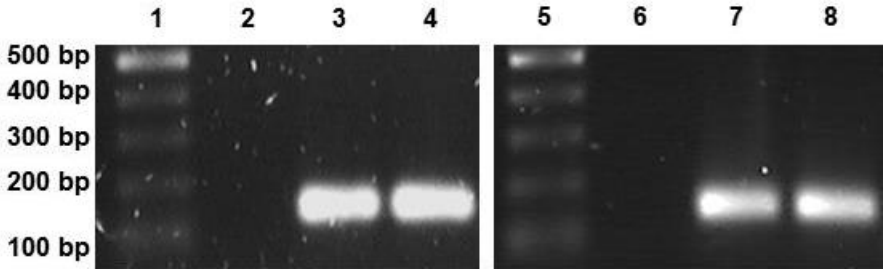

Figure 1: Agarose gel confirming PCR amplification of the S7 target region. Both gels include a 100 bp DNA size marker (lane 1 & 5) with sizes indicated on left, negative controls (lane 2 & 6) and target specific amplification for segment 7 of AHSV-2 (lanes 3 & 4) and AHSV-4 (lanes 7 & 8).

Results for the PCR experiments indicated successful amplification from the primer set used. A negative control indicated no non-specific amplification or contamination and only a single amplification product at the expected size (~138 bp) was observed for AHSV-2 and AHSV-4. Results

for amplification of the target region in AHSV-3 indicated similar amplification efficiency (not shown, imager software for GelDoc™ XR+ Imaging System UV transilluminator at time not available). These results confirmed that the primer set targeting virus genome segment 7 was suitable for use in subsequent RT-qPCR.

NS1 gene

The previous experiment was repeated, using the seg-5 specific primers at a concentration of 10 pmol and an annealing temperature of 56°C. Again, amplicons were separated and visualised on an agarose gel, illustrated in Figure 2.

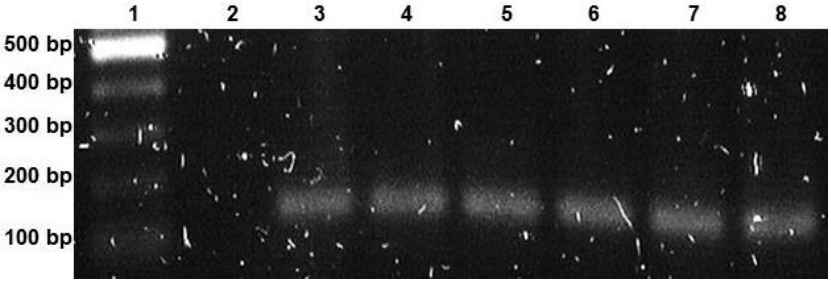

Figure 2: PCR amplification results indicating the segment 5 target region. Lane 1 shows the 100 bp DNA size marker with sizes indicated on the left, a negative control (lane 2) followed by amplification of a region of segment 5 of AHSV-2 (lanes 3 & 4), AHSV-3 (lanes 5 & 6) and AHSV-4 (lanes 7 & 8).

Although amplicons observed were of the expected size (~149 bp) for all three serotypes, amplification did not appear to be optimal. Different primer concentrations were then tested by setting up four different master mixes, with final primer concentrations of 10, 20, 25 and 30 pmol, respectively. All other PCR components were kept the same compared to those for VP7 and NS2 PCR amplification as these were at optimal conditions. Agarose gel electrophoresis was carried out to separate and visualise the amplification results, shown in Figure 3. Results indicated that a primer concentration of 25 pmol or higher yielded very high amplification. However, because limited primer stocks were available, a primer concentration of 20 pmol was decided on to produce sufficient amplification that could be adequately quantified.

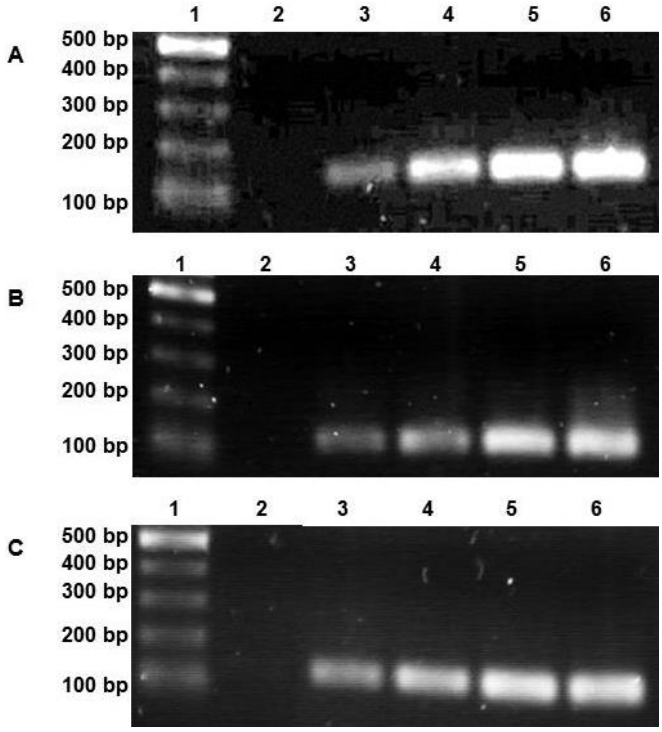

Figure 3: PCR amplification results of a segment 5 target region for: A) AHSV-2; B) AHSV-3 and C) AHSV-4 using primer concentrations of 10 pmol (lane 3), 20 pmol (lane 4), 25 pmol (lane 5) or 30 pmol (lane 6); a DNA size marker (lane 1) with sizes indicated on the left, and a negative control (lane 2) were included.

To confirm if the results obtained were because of primer concentration or annealing temperatures, a gradient PCR experiment was set up to test the primer concentration (20 pmol) at various annealing temperatures ranging from 55.5°C to 65.5°C. Furthermore, where virus cDNA had been used for all the previous experiments, these PCR reactions were set up using a plasmid containing AHSV-3 segment 5 as template. Figure 4 shows results obtained from the gradient PCR experiment.

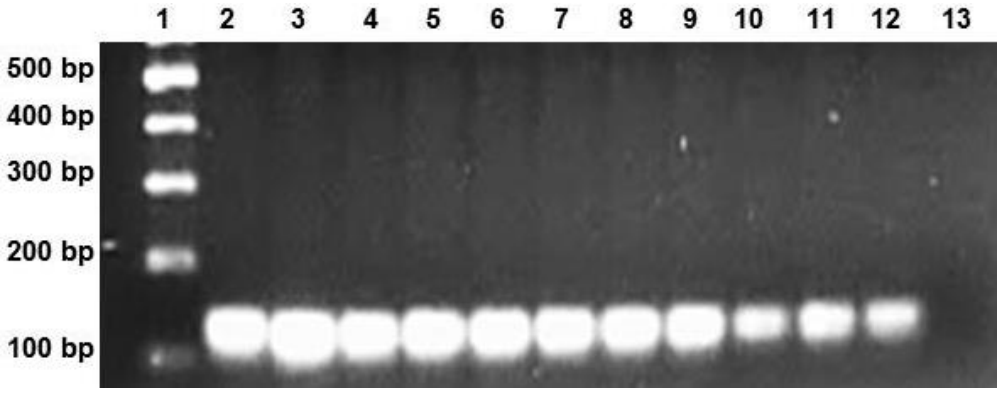

Figure 4: Results indicating segment 5 amplification from a temperature gradient PCR ranging from 55.5°C (lane 2) to 65.5°C (lane 13) in 1°C increments. A DNA size marker (lane 1), with sizes indicated on left, was also included.

It appeared that the optimal annealing temperature for this primer set was indeed 56°C (Lane 3), the temperature used initially. The results indicated amplification conditions to be primer concentration-

dependent and temperature dependent, and the primer set was confirmed to be suitable for use in subsequent RT-qPCR applications.

NS2 gene

To test the primer set designed to amplify a target region within genome segment 8, encoding the virus NS2 protein, a PCR experiment was set up as above. The annealing temperature for this primer set was calculated at 59°C and the cycling conditions set accordingly. To visualise the results, amplicons were electrophoresed on an agarose gel, shown in Figure 5.

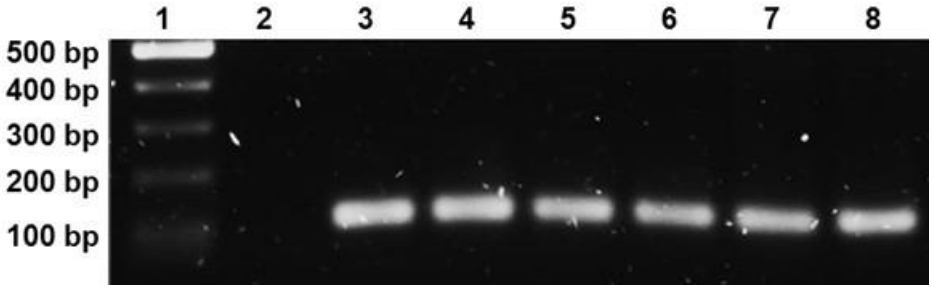

Figure 5: PCR amplification results showing amplification of a segment 8 target region. A DNA size marker (lane 1, showing sizes on left) and a negative control (lane 2) were included. Target-specific amplification shown for segment 8 of AHSV-2 (lanes 3 & 4), AHSV-3 (lanes 5 & 6) and AHSV-4 (lanes 7 & 8).

Results indicated high amplification efficiency of the expected target region from all three AHSV serotypes. Only products of the expected size (~102 bp) and a clean negative control, without non-specific amplification, were observed. It was concluded that this primer set amplified the target region with high efficiency at the tested cycling conditions and could be used in subsequent RT-qPCR applications.

NS3/NS3A gene

The available primer set designed to amplify a target region within segment 10 was designed based on the AHSV-3 NS3 gene sequence. The primers were tested in a PCR experiment with the annealing temperature set at the calculated optimum of 55°C. Results were again visualised on an agarose gel (Figure 6).

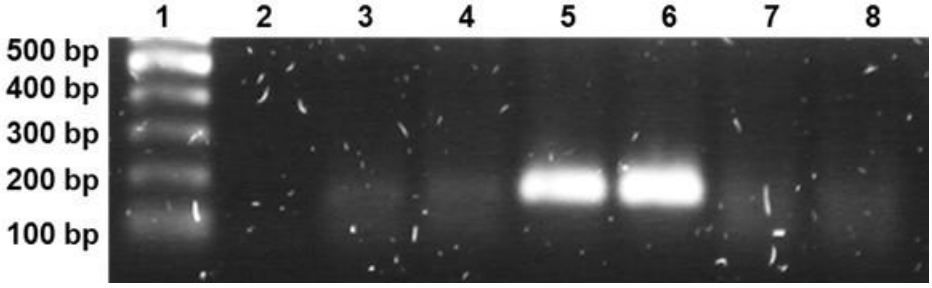

Figure 6: Agarose gel electrophoresis results showing PCR amplification of the segment 10 target region of AHSV-2 (lanes 3 & 4), AHSV-3 (lanes 5 & 6) and AHSV-4 (lanes 7 & 8). A DNA size marker depicted in lane 1 with sizes indicated on left and negative control (lane 2) were also included.

Results showed successful amplification from AHSV-3 only, and the lack of amplification of the segment 10 region from AHSV-2 and AHSV-4. This was attributed to the high variability of this gene amongst the different AHSV serotypes. Further investigation on four segment 10 sequences available on the GenBank database indicated that the primer target region was too variable within AHSV-2 and AHSV-4 for efficient annealing (Figure 7).

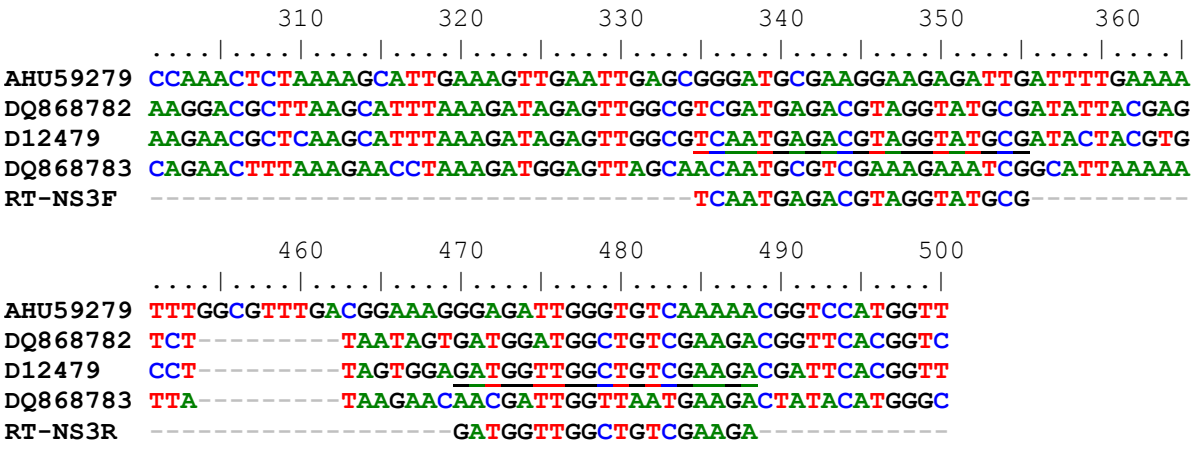

Figure 7: Nucleotide alignment of four segment 10 sequences available on Genbank. Accession numbers represent the sequences as follows: AHU59279 (AHSV-2), DQ868782 and D12479 (AHSV-3), DQ868783 (AHSV-4). RT-NS3F and RT-NS3R indicate the forward and reverse primer sequences, respectively (5'-3' orientation).

Figure 7 further indicated that there was some variability within the target region of the two different AHSV-3 sequences shown. The underlined sequence is a complete match to the primer sequences. To overcome this, it was decided to either find a conserved target region amongst all three AHSV serotypes for which one primer set could be used, or to design serotype-specific primer sets for AHSV-2, AHSV-3 and AHSV-4, respectively.

To develop a primer set that could amplify a target region within the NS3 gene, genome segments 10 of the AHSV-2, AHSV-3 and AHSV-4 strains were sequenced from cDNA. cDNA was synthesised for each strain from dsRNA by a reverse transcription PCR (RT-PCR), followed by sequencing of the amplicon. Table 4 summarises the primers used for RT-PCR and sequencing. Once a good sequence read was obtained from each of the serotypes, these sequences were aligned with a bio-algorithmic software program. The sequences from the different serotypes were aligned, together with four segment 10 sequences obtained from Genbank, and a conserved target region of ~120 bp was identified (Figure 8).

Table 4: Summary of primers used for RT-PCR and sequencing of the NS3 genes of AHSV-2, -3 & -4

Primer Name	Sequence (5'-3')	Annealing Position	Tm (°C)
NS3I Forward	GTT TAA ATT ATC CCT	01-15	55
NS3II Reverse	GTA AGT CGT TAT CCC GGC	738-758	55
NS3pBam Forward	CGG GAT CCG TTT AAA TTA TCC CTTG	01-17	55
NS3pEco Reverse	CGG AAT TCG TAA GTC GTT ATC CCGG	741-748	55

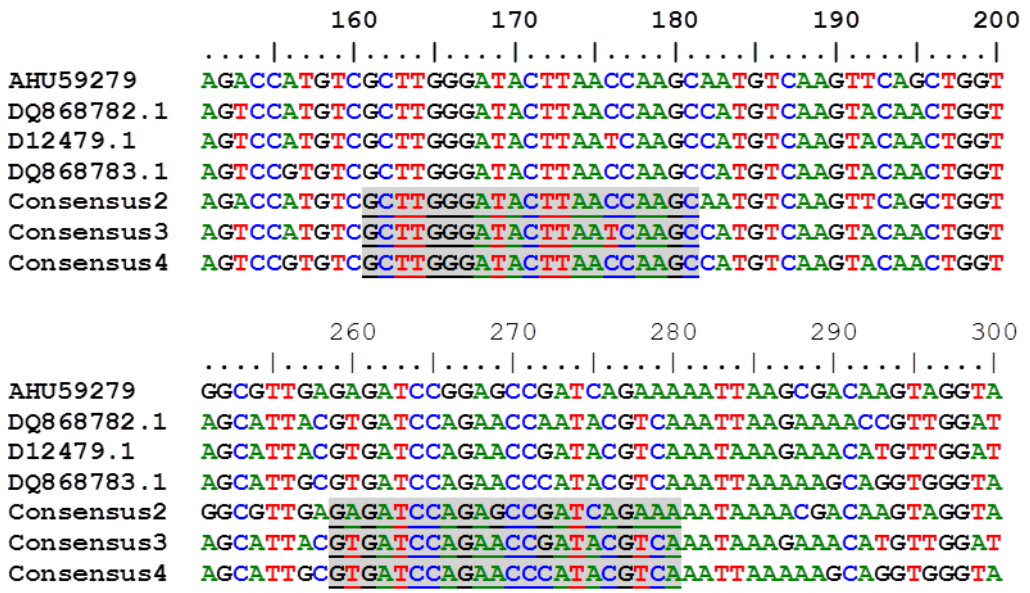

Figure 8: Sequence alignment of four Genbank sequences for segment 10 and consensus sequences obtained from sequencing experiments for AHSV-2 (Consensus2), AHSV-3 (Consensus3) and AHSV-4 (Consensus4). The highlighted regions in the bottom 3 sequences are the targeted region from which serotype-specific primer sets were designed for each AHSV serotype studied.

The identified target region was not sufficiently conserved to design one primer set that could amplify the target region amongst all three serotypes. However, three serotype-specific primer sets were developed, each set to target the identified area within the same region of each individual serotype, indicated by highlighted sequences in Figure 8 and summarised in Table 5.

Table 5: Summary of the three AHSV serotype specific primer set sequences

Serotype	Forward Primer Sequence	Reverse Primer Sequence
AHSV-2	GCT TGG GAT ACT TAA CCA AGC	TTT CTG ATC GGC TCT GGA TCT C
AHSV-3	GCT TGG GAT ACT TAA **T**CA AGC*****	T**GA** C**GT** ATC GG**T** TCT GGA TC**A** C*****
AHSV-4	GCT TGG GAT ACT TAA CCA AGC	T**GA** C**GT** AT**G** GG**T** TCT GGA TC**A** C*****

***** Underlined, bold nucleotides indicate differences to that of the AHSV-2 primer sequences

Once the serotype-specific primer sets were obtained, they were tested with a PCR experiment. The annealing temperature for each primer set was calculated to be 54°C and the PCR conditions set accordingly. Together with cDNA samples of each serotype, a Vero cell cDNA sample was also included in the experiment. This was to determine if the amplification was virus specific, rather than random amplification of a cellular origin. Amplification results were visualised using agarose gel electrophoresis. The results did not indicate efficient amplification (not shown). However, the negative control and the control with the Vero cell cDNA showed no amplification. This suggested that the primer sets developed for each serotype strain were amplifying the target regions only. The PCR experiment was repeated to obtain better amplification results for all three primer sets. This was done by testing the primer sets on newly synthesised cDNA. The cDNA samples used for the sequencing experiment were used as control samples. Success of amplification was analysed using agarose gel electrophoresis (Figure 9).

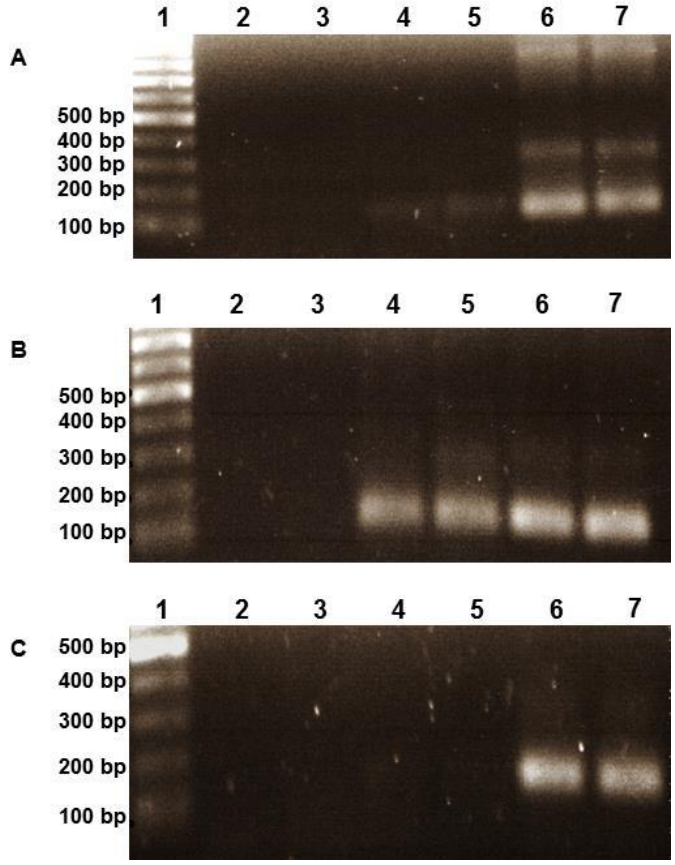

Figure 9: Agarose gel electrophoresis results showing PCR amplification of the segment 10 target regions from newly synthesised cDNA of A) AHSV-2, B) AHSV-3 and C) AHSV-4 in lanes 4 and 5 of each gel image. Lanes 6 and 7 represent amplification results from the sequencing cDNA control samples. A DNA size marker with the sizes indicated on the left (lane 1), a negative control (lane 2) and a Vero cell cDNA control (lane 3) were included in all gels.

Again results indicated that PCR amplification was not optimal, and the annealing temperature for each primer set was confirmed with a temperature gradient PCR experiment. The low and high temperature inputs were set at 50°C and 60°C, respectively. The cycler set twelve gradient temperatures accordingly but not with linear increments. The different annealing temperatures within the gradient, set by the PCR cycler, are indicated in the legend in Figure 10. Results were visualised using agarose gel electrophoresis on two sets of agarose gels (Figure 10). The first gel set was prepared with 1 × TAE buffer for AHSV-2 and AHSV-3 primer set amplification results. The second gel set was prepared using 1 × TBE buffer for better separation of the small amplicon products from all three primer sets.

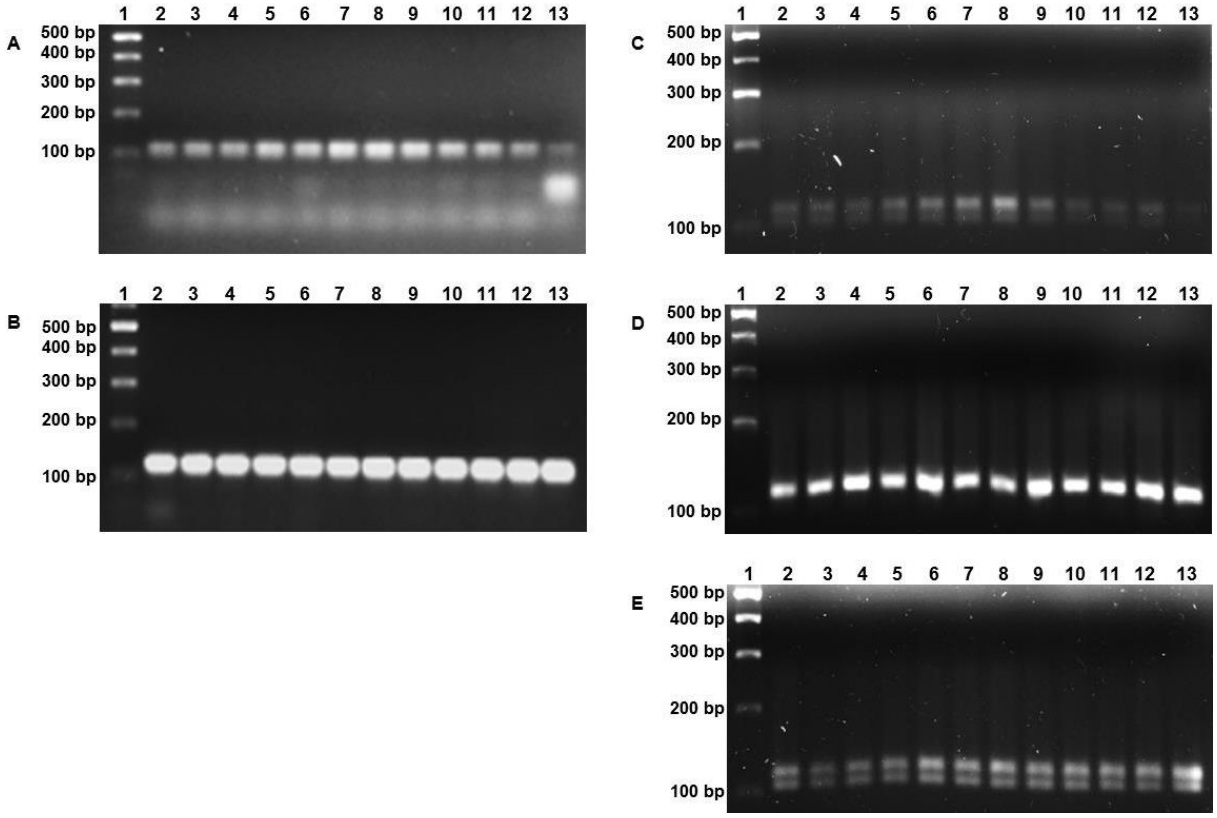

Figure 10: Amplification results of a gradient PCR showing amplification of the segment 10 target region of A and C) AHSV-2, B and D) AHSV-3 and E) AHSV-4. In all gel images lane 2 shows results at 50°C and lane 13 shows results at 60°C annealing temperatures. Lane 1 in all gel images contains a DNA size marker with the sizes indicated on the left. Gel images A and B show electrophoresis of PCR amplicons on agarose gel prepared with TAE buffer. Gel images C, D and E show electrophoresis of PCR amplicons on agarose gel prepared with TBE buffer. For all gels the annealing temperatures were: 50°C (lane 2), 50.2°C (3), 50.7°C (4), 51.6°C (5), 52.7°C (6), 54°C (7), 55.4°C (8), 56.8°C (9), 58.1°C (10), 59.2°C (11), 60°C (12), 60.4°C (13).

The results suggested that an optimal annealing temperature for the AHSV-2 specific primer set was achieved at ~55°C (lane 8, figure 10 A and C). Also, results indicated that any of the annealing temperatures tested allowed high amplification levels of AHSV-3 NS3. For quantitative real-time PCR analyses the NS3 primer sets would have to all be set at the same annealing temperature. Results for the AHSV-2- and AHSV-3-specific primer sets indicated that both these primer sets could be used at an annealing temperature of ~57°C. However, both the AHSV-2 and the AHSV-4 specific primer sets resulted in two products of different sizes being amplified. This was only visible after electrophoresis on agarose gels prepared with TBE buffer. Optimisation of the AHSV-2 and AHSV-4 primer sets was not continued due to time constraints, and it was decided that quantitative real-time PCR analyses on the NS3 gene would not be done.

3.1.2 Selection of suitable housekeeping genes for RT-qPCR analyses

In order to have a standard to which all virus specific amplification data would be normalised, two housekeeping genes primer sets were tested. The two primers sets targeted regions within the β_2-Microglobulin (β_2MG) and Glyceraldehyde-3-phosphate dehydrogenase (GAPDH) genes, respectively. Initially each primer set was tested on cDNA synthesised from total RNA extracted from uninfected Vero cells by conventional PCR, and the results visualised on an agarose gel

(Figure 11). The results indicated successful amplification of the target regions of both housekeeping genes, with no non-specific amplification or primer dimers.

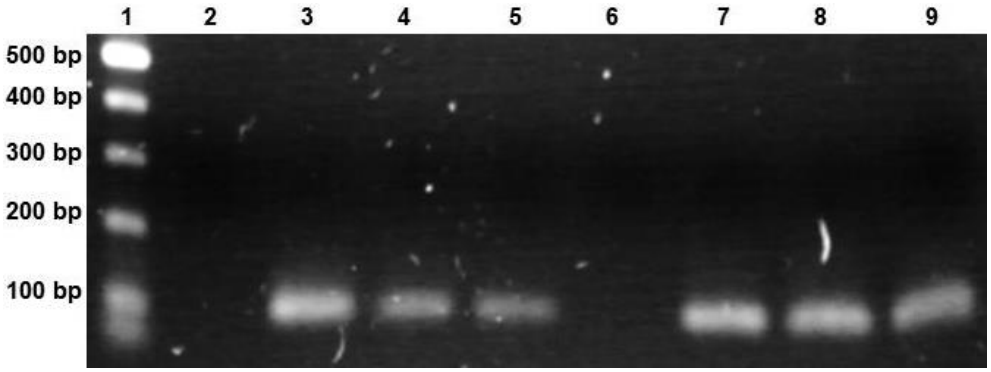

Figure 11: PCR amplification results of housekeeping genes GAPDH (lanes 3-5 and β_2MG (lanes 7-9) from uninfected Vero cells. Negative controls were included for the GAPDH primer set (lane 2) and β_2MG primer set (lane 6). Lane 1 contains a DNA size marker with the sizes indicated on the left.

To determine if the two selected housekeeping genes were suitable candidates for RT-qPCR, the amplification efficiency of the primer sets were subsequently tested using real-time PCR. For each primer set a 10-fold serial dilution (10^{-1}-10^{-4}) of cDNA from uninfected Vero cells was set up, with three technical replicates for each, and a standard curve was generated from the real-time PCR data obtained (Figure 12).

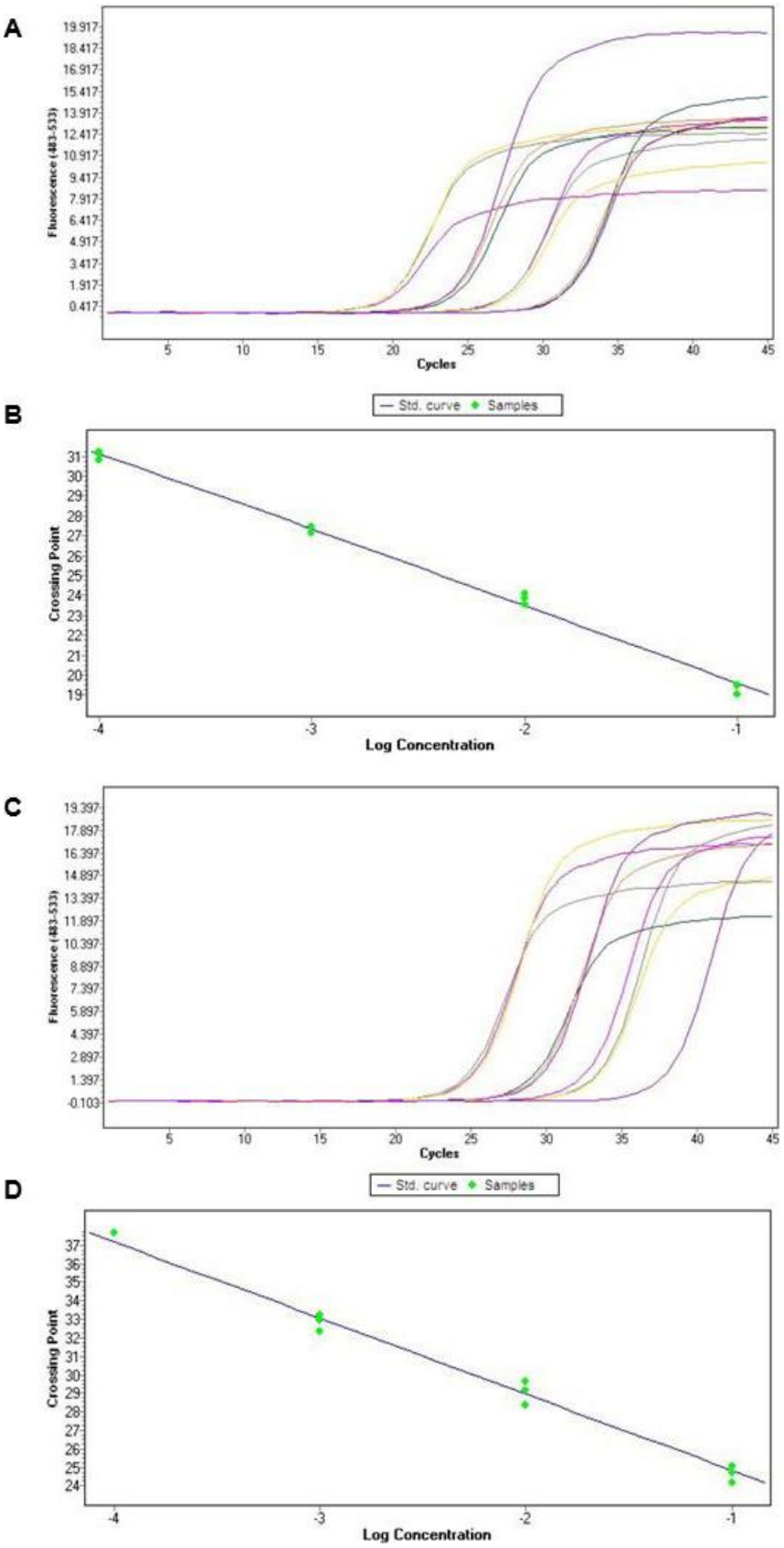

Figure 12: Real-time PCR amplification results for the A) β_2MG primer set with B) corresponding standard curve calculated, and the C) GAPDH primer set with D) corresponding standard curve calculated.

For quantitative real-time PCR analyses, a primer set should ideally have an amplification efficiency of ~2.00 (1.8-2.2, or a PCR efficiency of 90-110%). An optimal standard curve should show a slope of ~3.3, indicating that the crossing point (Cp) of each dilution factor within a dilution series is ~3.3 cycles apart. For the β_2MG primer set an amplification efficiency of 1.8 was calculated (~90%), and the standard curve had a slope of -3.89 (Figure 12A-B). Only minor differences were observed between the technical replicates of each dilution. The efficiency calculated for this primer set fell within the range of 1.8-2.2, making it sufficient for use as a reference for subsequent relative quantification analyses. For the GAPDH primer set a PCR efficiency of 1.75 was calculated (~87.5%). The corresponding standard curve showed a slope of -4.11 (Figure 12C-D). Again only small differences were observed between the technical repeats of each dilution. The efficiency calculated for this primer set fell just short of the optimum range we tried to obtain. However, an amplification efficiency of 87.5% was still considered sufficient to use as a reference for subsequent relative quantification analyses.

The products from the real-time PCR amplifications were visualized on an agarose gel (Figure 13), confirming specific amplification of a product of the correct size.

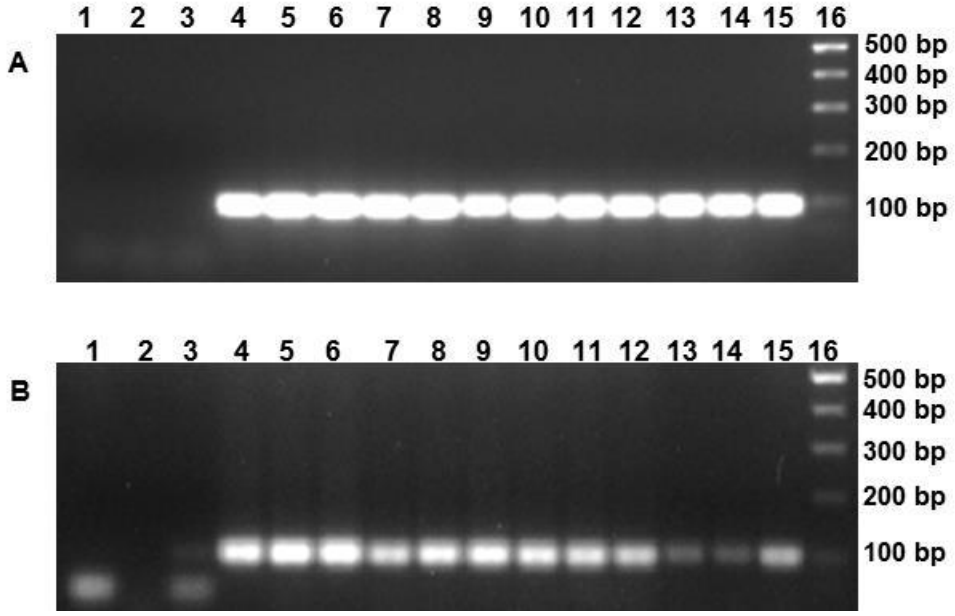

Figure 13: Electrophoresis results of the real-time PCR amplification of the A) β_2MG primer set and B) GAPDH primer set. In both gel images three technical replicates each are shown for the negative controls (lanes 1-3), with serial cDNA dilutions of 10^{-1} (lanes 4-6), 10^{-2} (lanes 7-9), 10^{-3} (lanes 10-12), and 10^{-4} (lanes 13-15). Lane 16 contains a DNA size marker with the sizes indicated on the right.

Both primer sets tested therefore showed suitable efficiency to allow use in subsequent RT-qPCR analyses, and the standard curves could be used as reference to which experimental data to be obtained from virus-specific gene amplification could be normalised.

3.1.3 Monitoring the transcriptional stability of β_2MG and GAPDH in infected mammalian cells

To determine if transcription of the selected housekeeping genes was not affected by virus infection, the primer sets were initially tested on cDNA isolated from Vero cells that were infected either with

AHSV-2, AHSV-3 or AHSV-4 and harvested 48 hours post-infection (p.i.). A conventional PCR experiment was set up the same as for the experiment done to test the primer sets on cDNA from uninfected Vero cells, and the products visualised on an agarose gel (Figure 14). Cell counts in the experiment were not normalised prior to testing the housekeeping genes. This was not essential to the experiment as only efficiency of the primers to amplify the target region within virus infected cells were considered.

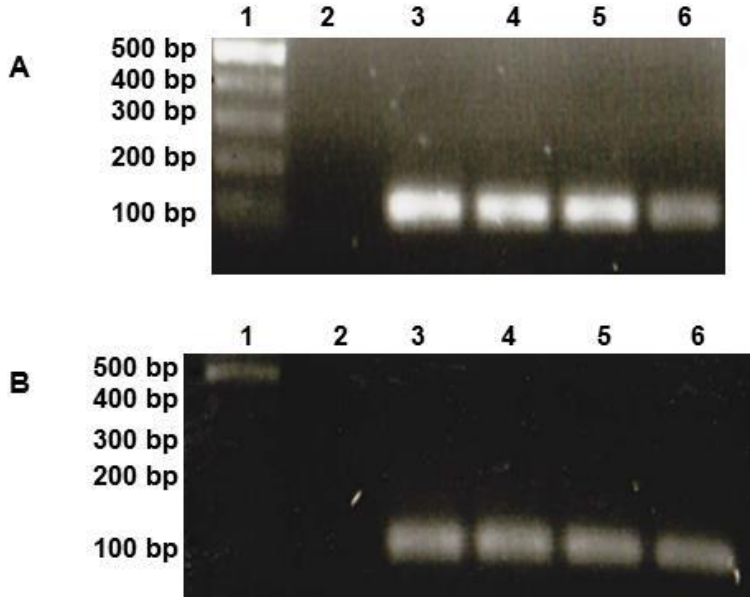

Figure 14: PCR amplification of cDNA using A) the GAPDH primer set and B) the β_2MG primer set. Lane 1 contains a DNA size marker with the sizes indicated on the left and lane 2 a negative control. cDNA was synthesised from uninfected Vero cells (lane 3) or from cells infected with AHSV-2 (lane 4), AHSV-3 (lane 5) or AHSV-4 (lane6).

Visual inspection of the electrophoresis results from the PCR on cDNA from AHSV-2- and AHSV-3-infected Vero cells, showed no significant difference in signal compared to the amplification on cDNA from uninfected Vero cells. However, amplification from AHSV-4-infected cells seemed lower, indicating that the viral infection may have affected transcription of the housekeeping genes. This was specifically obvious for GAPDH (Figure 14A). This was investigated in more detail by real-time PCR analysis.

Vero cells were mock-infected or infected with the three AHSV serotypes and harvested at 0, 2, 4, 8, 12 and 24 hours post-infection. cDNA was prepared from each sample and a real-time PCR experiment was set up with three technical replicates from each sample. The amplification data of each housekeeping gene was compared relative to the other by calculating a relative ratio for the one and then normalising the data using the relative ratio of the second. This was done for both of the selected housekeeping genes using the Light Cycler® 480 Instrument Software Applications (Chapter D, Light Cycler® 480 Operator's Manual, V1.5, Roche Diagnostics GmbH, 2008) relative quantification analyses program.

The basic relative quantification method was used, and software analyses were done based on the ΔΔCT-Method. Two analyses were performed with both housekeeping genes set as either a "*Target*" or "*Reference*". A mono-colour (SYBR Green) experiment was run and the run analysis program was set to use "*In-Run*" references for calculations with no calibrators assigned. The pairing rules for analysis was assigned as "*One to One*" where one target was paired to one reference. This

resulted in a time-to-time specific point ratio calculation where, for example, β_2MG at 0 hours p.i. was only paired with GAPDH at 0 hours p.i. and a relative ratio calculated. The Light Cycler® 480 software output analysis results for β_2MG ratios calculated relative to GAPDH are shown in Figure 15. Ratios for GAPDH calculated relative to β_2MG showed the inverse of the results in Figure 15 (not shown).

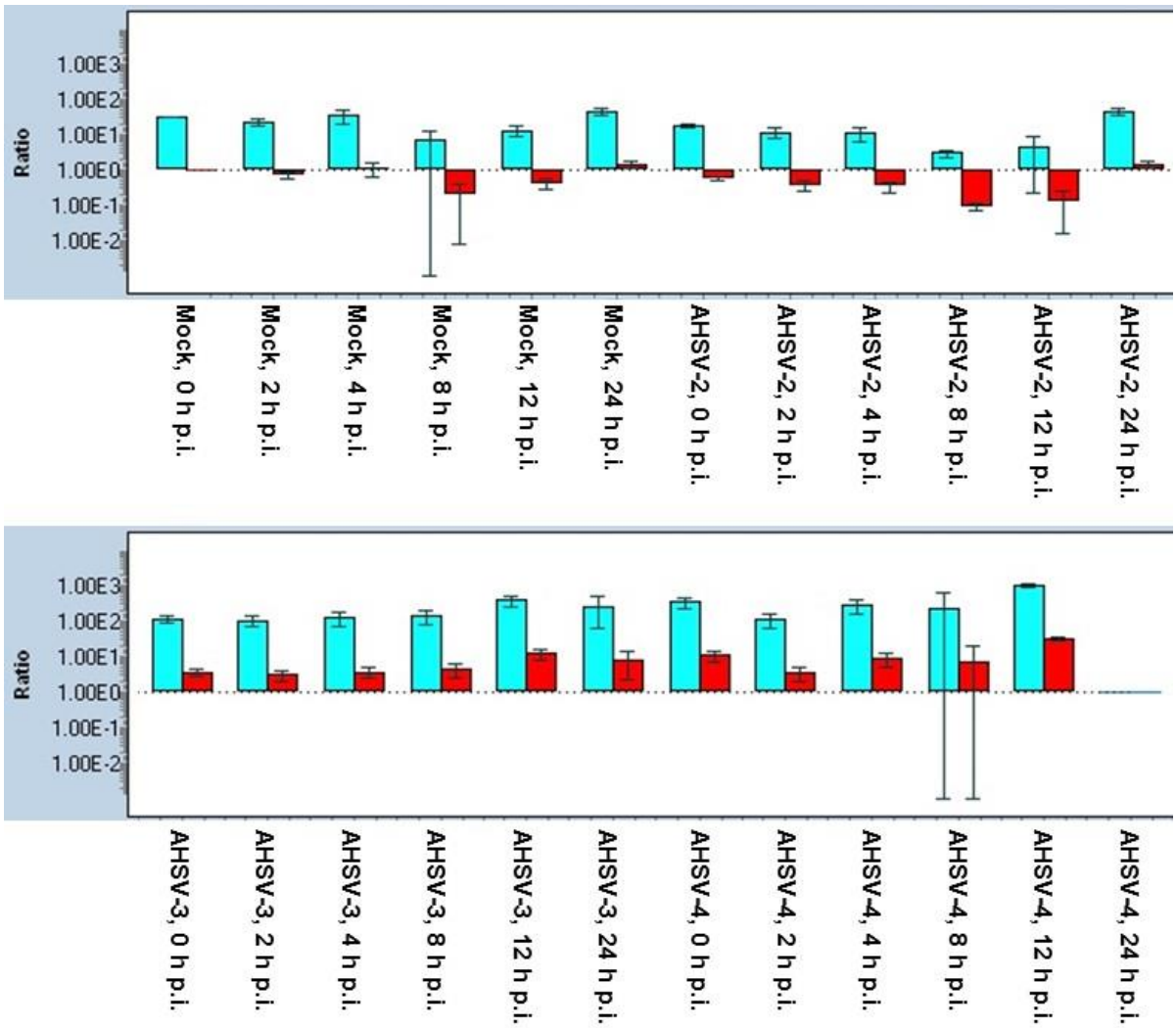

Figure 15: Relative quantification ratios calculated as *Target* over *Reference* This experiment shows the ratios for β_2MG : GAPDH. The blue bars indicate the *one-to-one* pairing ratio calculated using the crossing point concentrations. The red bars indicate the normalised quantification ratios calculated. The error bars indicate standard deviation. Samples assigned as "Mock" were unifected cells. AHSV-2, AHSV-3 and AHSV-4 assigned samples indicate that those cells were infected with the assigned virus. No data was recorded for AHSV-4-infected cells at 24 hours p.i.

To determine if transcription of the housekeeping genes of interest were stable under the test conditions (mock vs. virus-infected) at the different times post-infection, statistical analyses were run using the statistical program SPSS Statistics (IBM Corp., Version 22, 2013). Data was tested for normality using the *Shapiro-Wilk's* test followed by *Levene's test* to determine homogeneity of variance. All analyses were calculated at an alpha level of 0.05 for statistical significance. The data was found to be normally distributed and *Levene's* test for homogeneity of variance was not violated.

A Student's *t*-test was run to determine the transcriptional stability of β_2MG and GAPDH both over time, with a specific AHSV infection, and within Vero cells between different infections (mock vs.

AHSV-infected). Analyses results indicated that there was no statistical significance in mean normalised ratios between mock-infected and AHSV-infected Vero cells for each housekeeping gene investigated. Results obtained from the two different housekeeping genes were not compared to each other. Furthermore, results indicated that there was no statistical significance between the normalised ratios at different times post-infection for both these housekeeping genes. Therefore, both these housekeeping genes would be suitable to use as reference genes against which the relative quantification of viral transcripts could be measured. Due to time constraints it was decided not to continue with the real-time experiments. However, the next step would have been to optimise real-time PCR analysis of the VP7, NS1, NS2 and NS3 genes at the different times post-infection.

3.2 Host Cell Cytopathicity Monitored by Light Microscopy

Previous studies using AHSV-2, AHSV-3 and AHSV-4 showed that there was a variable degree of cytopathicity observed in mammalian host cells infected with these strains (Meiring *et al.*, 2009). Infection with AHSV-2 resulted in severe CPE, infection with AHSV-3 gave intermediate CPE and infection with AHSV-4 resulted in low CPE. Variable CPE levels were found to be non-serotype related as the CPE observed in cells infected with reassortant strains showed different CPE levels compared to those of the parental strains they originated from.

To verify these results and determine the severity of CPE on the mammalian cells at different times post-infection, in our own hands, mammalian cells were infected with each of the parental or reassortant strains at both a low and high multiplicity of infection (MOI 0.1 and 2 pfu/cell). Light microscopy images were captured of each infection at 8, 16, 24 and 48 hours post-infection (p.i.) and results are shown in Figure 16.

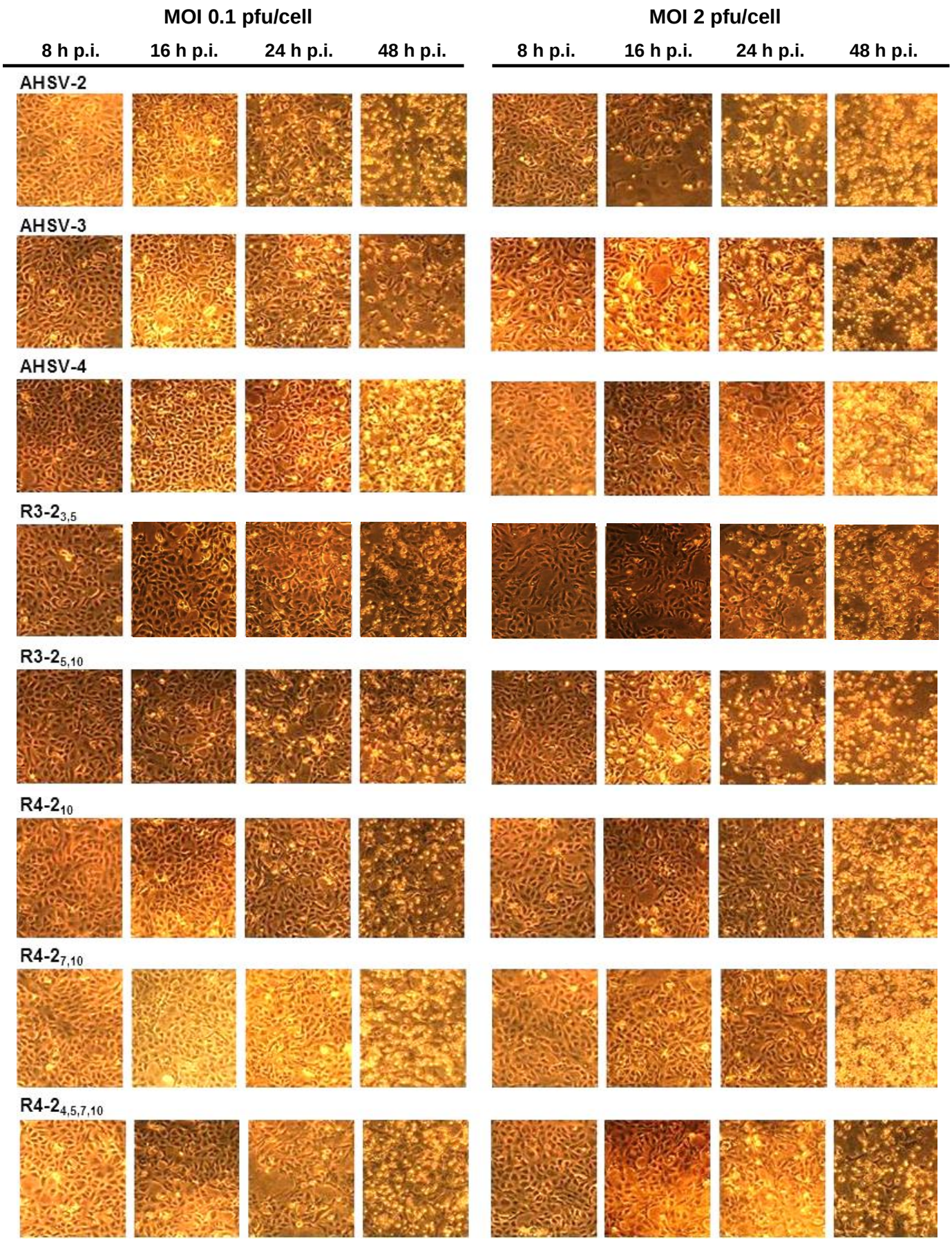

Figure 16: Microscope photos indicating the level of CPE at the indicated times post-infection from three parental AHSV serotypes and five reassortant virus strains. Results are shown for both unsynchronised infections (MOI 0.1 pfu/cell) and synchronised infections (MOI 2 pfu/cell).

The findings confirmed previous results observed. Figure 16 show the change in cell morphology as it changed due to virus infection over time post infection. Each virus strain used to infect the Vero cells indicate a different phenotype. Round loose cells are indicative of CPE whereas elongated cells with small gaps indicted healthy viable Vero cells. Results indicated that reassortant strains with a serotype 2 segment 5 and 10 combination (R3-$2_{5,10}$ and R4-$2_{4,5,7,10}$) showed the earliest and most severe onset of CPE. These effects were even more severe compared to the parental strains from which the backbone genome originated.

To investigate the underlying mechanism that could account for the observed differences in CPE, viral protein synthesis was subsequently monitored at different times post-infection.

3.3 Analyses of Viral Protein Synthesis by Immunoblot Assays

This section describes the findings of comparative investigation of virus protein synthesis amongst the different parental and reassortant virus strains. Cumulative levels of virus proteins VP7, NS1 and NS2 were monitored at various times post-infection (p.i.) using Western blot assays.

3.3.1 Optimisation of the antibody detection conditions for three AHSV proteins

In order to obtain good antibody signals for subsequent quantification, various batches of antibodies that were available in-house were tested for their specificity and strength of recognition of the three virus proteins (VP7, NS1, NS2) being studied. Each antibody was tested at various dilutions to find the optimal conditions for use in Western blot analyses. Briefly, cell lysates from AHSV-3-infected Vero cells were separated by SDS-PAGE, transferred to a nitrocellulose membrane and incubated with the various primary antibodies overnight. Antibody signals were subsequently detected using HRP-conjugated Protein A.

Results confirmed that the different primary antibodies tested were suitable for use in the subsequent studies. This was decided based on the highest possible dilution that still produced a strong enough antibody signal sufficient for quantification. Figure 17 shows examples of one blot each of the anti-VP7 (A), anti-NS1 (B) and anti-NS2 (C) antibodies. In each Western blot shown, a single band was observed corresponding to the expected sizes of each of the virus proteins targeted. These expected sizes are 38 kDa for VP7, 62 kDa for NS1 and 42 kDa for NS2.

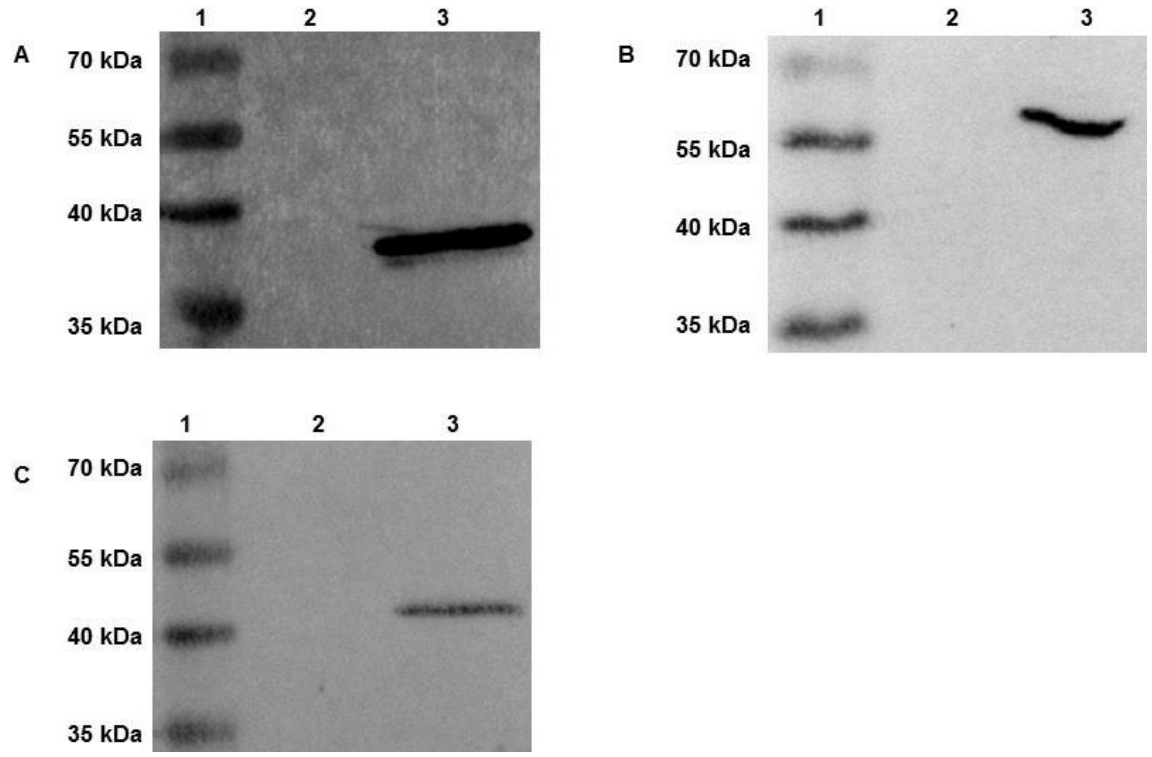

Figure 17: Western blot analyses using anti-VP7 (A), anti-NS1 (B) or anti-NS2 (C) antibodies. Each blot shows a protein size marker with the sizes indicated on the left (lane 1), a mock-infected sample (lane 2) and AHSV-3-infected cells (lane 3).

The primary antibodies used for detection of virus VP7, NS1 and NS2 were all raised against the respective proteins of AHSV-9. For subsequent use in Western blot analyses experiments, we had to determine if all the primary antibodies detected the cognate virus proteins of AHSV-2, AHSV-3 and AHSV-4 with the same specificity. This was investigated by quantifying and comparing the antibody signals and Coomassie stain intensities using a quantitation analysis software tool.

Briefly, crude cell lysates of Vero cells infected with AHSV-2, AHSV-3 or AHSV-4, under identical conditions, were subjected to subcellular fractionations to separate the samples into soluble and particulate fractions. The virus proteins under investigation were expected mainly in the particulate fraction and samples from this fraction were analysed using immunoblot assays. Bands from each resulting Western blot were quantified as volume intensity signals using Image Lab (Beta 3D, V2.0, Bio-Rad Laboratories, 2009) imaging software. The relative ratios of the three samples were calculated using the signal from each serotype and dividing it by the signal obtained for AHSV-4, randomly assigned as the reference strains. Figure 18 shows the results obtained from comparative quantitative analyses.

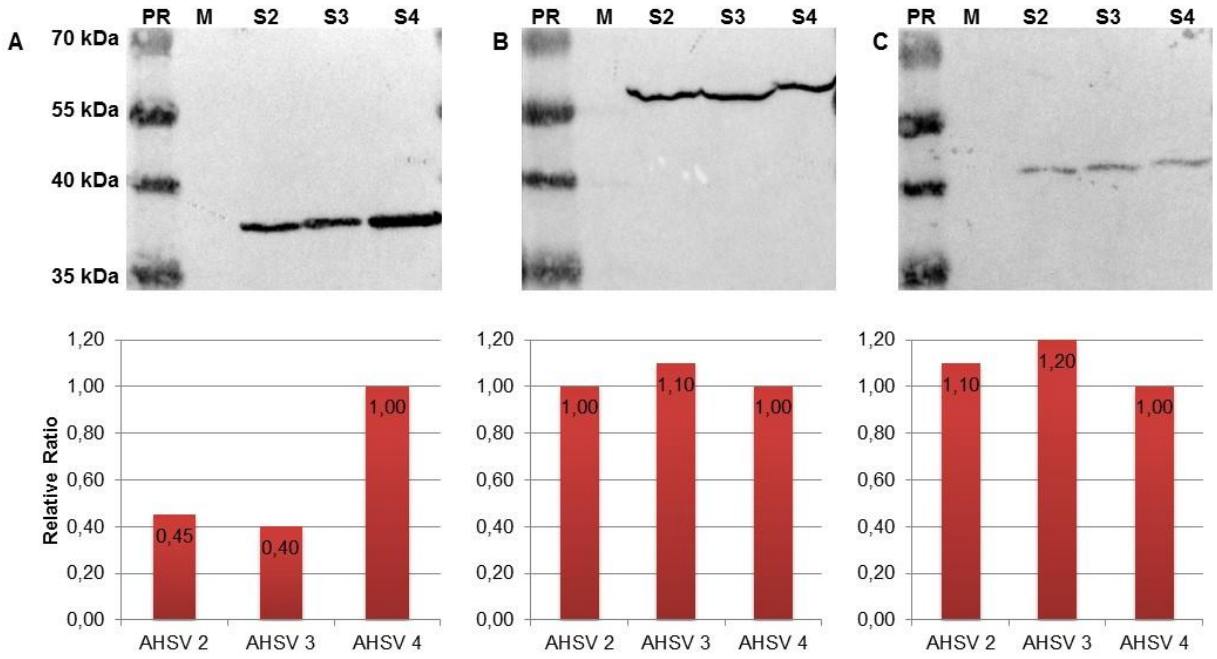

Figure 18: Western blot analysis results with corresponding quantification results showing A) VP7, B) NS1 and C) NS2, respectively, from AHSV-2, AHSV-3 and AHSV-4. Each blot shows a protein size marker (PR) with the sizes indicated on the left and a mock (M)-infected sample.

Relative quantification results indicated that for the NS1 and NS2 proteins of AHSV-2, AHSV-3 and AHSV-4 a 1:1:1 protein synthesis ratio was observed. However results for VP7 indicated that a ratio close to 1:1:2 was prevalent for protein synthesis levels between AHSV-2, AHSV-3 and AHSV-4.

To determine if the more than two fold higher levels of AHSV-4 VP7 compared to AHSV-2 or AHSV-3 was due to differences in antibody recognition efficiency or actually represented differences in protein concentration, a Coomassie-stained SDS-PAGE gel was used for quantification. A technical replicate experiment was done using the same sample material used for Western blot analyses. A sample of the particulate fraction was subjected to SDS-PAGE, stained in Coomassie brilliant blue and subsequently destained overnight. The bands on the SDS-PAGE gel indicating VP7 were quantified using the same imaging software tool and relative ratios were calculated. SDS-PAGE and quantitation results indicated approximately similar relative ratios of AHSV-2 and AHSV-3 compared to AHSV-4 (results not shown).

Our results indicated that a similar trend was observed when comparing relative quantifications ratios for both Coomassie-staining and antibody-labelling analyses. It appears that for VP7 protein synthesis, there was about equal levels of protein synthesised from AHSV-2 and AHSV-3 but twice the level from AHSV-4. This was first observed after antibody labelling (with Western blot analysis) and confirmed by SDS-PAGE results observed with Coomassie staining. In the case of NS1 and NS2, the Coomassie staining indicated equal levels of proteins present for all three serotypes (not shown), corresponding to the results from the immunoblots. We concluded that these antibodies raised against the AHSV-9 proteins detected the cognate AHSV-2, AHSV-3 and AHSV-4 proteins with similar specificity and were therefore acceptable for use in our subsequent experimental analyses.

3.3.2 Detection of VP7, NS1 and NS2 protein levels by Western blot

To study the virus protein levels at the different times post-infection, Vero cells were infected with the 8 different AHSV strains under investigation. Cells were either infected at a low multiplicity of infection (MOI) of 0.1 pfu/cell, or at a high MOI of 2 pfu/cell, which would result in a synchronised infection. In all instances cells were harvested at 8, 16 and 24 hours post-infection (h p.i.), and in the case of the low MOI infections a late harvest time point of 48 h p.i. was also included. This was not done for the high MOI infections, as cells already showed severe CPE prior to this time point. Also, cells were not harvested at 0 hours post infection as no CPE is expected at this time point and virus protein levels were only compared within a specific time post infection and not between the different time points. Virus protein levels were compared relative to each other at each specific time post infection by using the housekeeping protein levels for each time point to normalise the data. For each AHSV strain, three biological replicates (BR) were done for both MOI conditions and all harvest times. With each biological replicate a mock infection was included as control.

A small sample of the harvested cells was kept for titrations, the remaining sample was used for protein analysis. Proteins were separated on a 12% SDS-PAGE gel and subsequently transferred to a nitrocellulose membrane. The membrane was then reacted with a specific antibody against a housekeeping gene product or against viral proteins (VP7, NS1 or NS2).

In order to accurately compare results from different infections, the data had to be standardised. Two housekeeping gene proteins, Lamin A and β-Actin, were initially investigated to use as a reference to which the protein data could be normalized. SDS-PAGE and Western blot analyses were done using the anti-Lamin A and anti-β-Actin antibodies to determine if adequate antibody signals are observed. Both antibodies were tested individually according to the manufacturer's recommendations. No Lamin A signals were detected (not shown), even when the anti-Lamin A antibody was used at undiluted concentrations. However, satisfactory β-Actin signals were produced and thus only anti-β-Actin antibodies were used in the subsequent experiments. Furthermore, as dual labeling of the same membrane with e.g. anti-VP7 and anti-β-Actin proved to be problematic, triplicate blots were done using only anti- β-actin, and the average values of the quantified signals used.

For each biological replicate, time point and antibody the Western blot was evaluated. If not acceptable, one or two additional technical replicates (TR) were done. Antibody signals on the Western blots were quantified using Image Lab (Beta 3D, V2.0, Bio-Rad Laboratories, 2009) imaging software. Visual inspection of each blot was used as basis to decide if it was suitable for quantification. Blots where a region of the gel appeared to have poorly transferred onto the membrane due to technical problems, were discarded. Blots that were of suitable quality to allow for quantification are indicated in the table with a "✓" and blots that were not quantified are marked with a "×". Quantified blots from which the data was used to generate graphs are indicated by an asterisk (marked "*"). In some instances where there were multiple suitable TRs for a specific BR, these values were first averaged, and then used as a single data point for that BR.

Table 6 summarizes all the Western blot analyses done using the anti-β-Actin antibody and Table 7 summarizes all the Western blot assays done for virus proteins. Following this, data points from the different BR were averaged to obtain a value for a specific time point and MOI. Results of these blots are shown and the quantification data, that was adjusted relative to the signal of a housekeeping gene protein, as explained below.

Table 6: Summary of Western blots done for housekeeping protein β-Actin

Virus Protein Detected	MOI 0.1 pfu/cell			MOI 2 pfu/cell	
	Time of Harvest	Biological Replicate	Technical Replicates	Biological Replicate	Technical Replicates
β-Actin	8 hours p.i.	**NOT DONE**		BR 1	TR **1***(✓), TR **2**(✓)
				BR 2	TR **1***(✓)
				BR 3	TR **1***(✓), TR **2**(×)
	16 hours p.i.	BR 1	TR **1***(✓)	BR 1	TR **1***(✓)
		BR 2	TR **1***(✓)	BR 2	TR **1***(✓)
		BR 3	TR **1***(✓)	BR 3	TR **1***(✓)
	24 hours p.i.	BR 1	TR **1** (×), TR **2**(✓)	BR 1	TR **1***(✓)
		BR 2	TR **1***(✓), TR **2**(×)	BR 2	TR **1***(✓)
		BR 3	TR **1** (×), TR **2***(✓)	BR 3	TR **1***(✓), TR **2**(✓)
	48 hours p.i.	BR 1	TR **1***(✓)	**NOT DONE**	
		BR 2	TR **1***(✓)		
		BR 3	TR **1***(✓)		

✓: Indicating Western blots that were quantified ×: Indicating Western blots that were not quantified

****: Western blots of which quantification data was used for statistical analyses. Where more than one technical replicate from a biological replicate was used, the average of the different data sets were calculated***

Table 7: Summary of Western blot analyses to study virus protein expression

Virus Protein Detected	MOI 0.1 pfu/cell			MOI 2 pfu/cell	
	Time of Harvest	Biological Replicate	Technical Replicates	Biological Replicate	Technical Replicates
VP7	8 hours p.i.	BR 1	TR **1**(×), TR **2**(×), TR **3***(✓)	BR 1	TR **1** (×), TR **2**(✓)
		BR 2	TR **1**(×), TR **2**(×), TR **3***(✓)	BR 2	TR **1***(✓)
		BR 3	TR **1**(×), TR **2**(×), TR **3***(✓)	BR 3	TR **1***(✓)
	16 hours p.i.	BR 1	TR **1***(✓)	BR 1	TR **1***(✓)
		BR 2	TR **1***(✓)	BR 2	TR **1***(✓)
		BR 3	TR **1***(✓)	BR 3	TR **1***(✓), TR **2***(✓)
	24 hours p.i.	BR 1	TR **1***(✓), TR **2***(✓)	BR 1	TR **1** (✓), TR **2***(✓)
		BR 2	TR **1***(✓), TR **2***(✓), TR **3**(✓)	BR 2	TR **1** (✓), TR **2***(✓)
		BR 3	TR **1** (×), TR **2** (✓), TR **3**(×)	BR 3	TR **1***(✓)
	48 hours p.i.	BR 1	TR **1** (×), TR **2**(✓)	**NOT DONE**	
		BR 2	TR **1***(✓)		
		BR 3	TR **1***(✓)		
NS1	8 hours p.i.	BR 1	TR **1**(×), TR **2**(×)	BR 1	TR **1**(×)
		BR 2	TR **1**(×), TR **2**(×)	BR 2	TR **1**(×), TR **2**(✓)
		BR 3	TR **1**(×), TR **2**(×)	BR 3	TR **1**(×)
	16 hours p.i.	BR 1	TR **1***(✓)	BR 1	TR **1** (×), TR **2***(✓)
		BR 2	TR **1** (×)	BR 2	TR **1** (×), TR **2***(✓)
		BR 3	TR **1***(✓)	BR 3	TR **1***(✓)
	24 hours p.i.	BR 1	TR **1***(✓), TR **2** (×), TR **3***(✓)	BR 1	TR **1**(×), TR **2***(✓)
		BR 2	TR **1***(✓), TR **2***(✓), TR **3***(✓)	BR 2	TR **1**(×), TR **2***(✓)
		BR 3	TR **1** (✓), TR **2** (×), TR **3***(✓)	BR 3	TR **1**(×)
	48 hours p.i.	BR 1	TR **1***(✓)	**NOT DONE**	
		BR 2	TR **1***(✓), TR **2***(✓)		
		BR 3	TR **1***(✓), TR **2***(✓)		
NS2	8 hours p.i.	BR 1	TR **1** (×), TR **2** (✓), TR **3***(✓)	BR 1	TR **1***(✓)
		BR 2	TR **1***(✓), TR **2***(✓), TR **3** (✓)	BR 2	TR **1***(✓)
		BR 3	TR **1** (×), TR **2***(✓), TR **3** (✓)	BR 3	TR **1***(✓)
	16 hours p.i.	BR 1	TR **1** (×), TR **2***(✓)	BR 1	TR **1***(✓)
		BR 2	TR **1***(✓)	BR 2	TR **1** (✓)
		BR 3	TR **1***(✓), TR **2** (×)	BR 3	TR **1***(✓)
	24 hours p.i.	BR 1	TR **1***(✓), TR **2** (×)	BR 1	TR **1***(✓)
		BR 2	TR **1***(✓), TR **2** (×)	BR 2	TR **1***(✓)
		BR 3	TR **1***(✓), TR **2***(✓)	BR 3	TR **1** (✓), TR **2***(✓)
	48 hours p.i.	BR 1	TR **1** (×), TR **2***(✓)	**NOT DONE**	
		BR 2	TR **1***(✓)		
		BR 3	TR **1***(✓)		

✓, ×, *: Refer to Table 3.3

3.3.3 Protein levels expressed from the housekeeping gene, β-Actin, at different times

Protein synthesis levels of the housekeeping gene protein, β-Actin, were first analysed at different times. Figures 19 and 20 shows examples of one Western blot from each time point corresponding to the infections done at an MOI of 0.1 and 2 pfu/cell, respectively. A graph representing the combined data from the relevant biological repeats is shown for each time point.

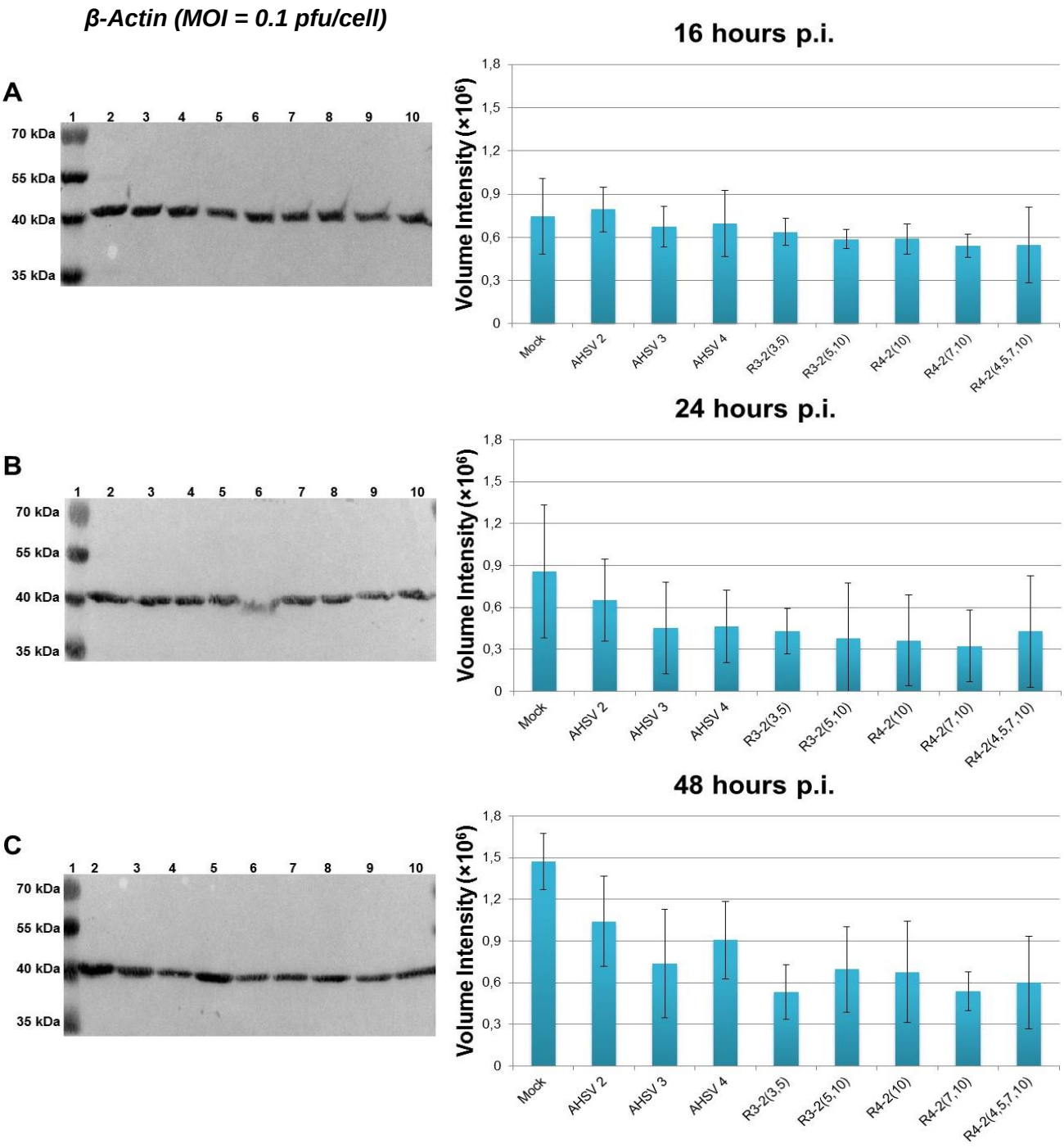

Figure 19: β-Actin protein levels in Vero cells. Cells were mock-infected, or infected with AHSV at an MOI of 0.1 pfu/cell, and harvested at A) 16 h p.i., B) 24 h p.i. or C) 48 h p.i. A representative Western blot is shown on the left. In each blot Lane 2 contains a mock-infected sample, Lanes 3-5 the parental serotypes and Lanes 6-10 the reassortant virus strains in the same order as on the graphs. The graphs shown on the right, represent the average volume intensity values obtained from the quantification of multiple blots as detailed in Table 3. Error bars indicate the standard deviation.

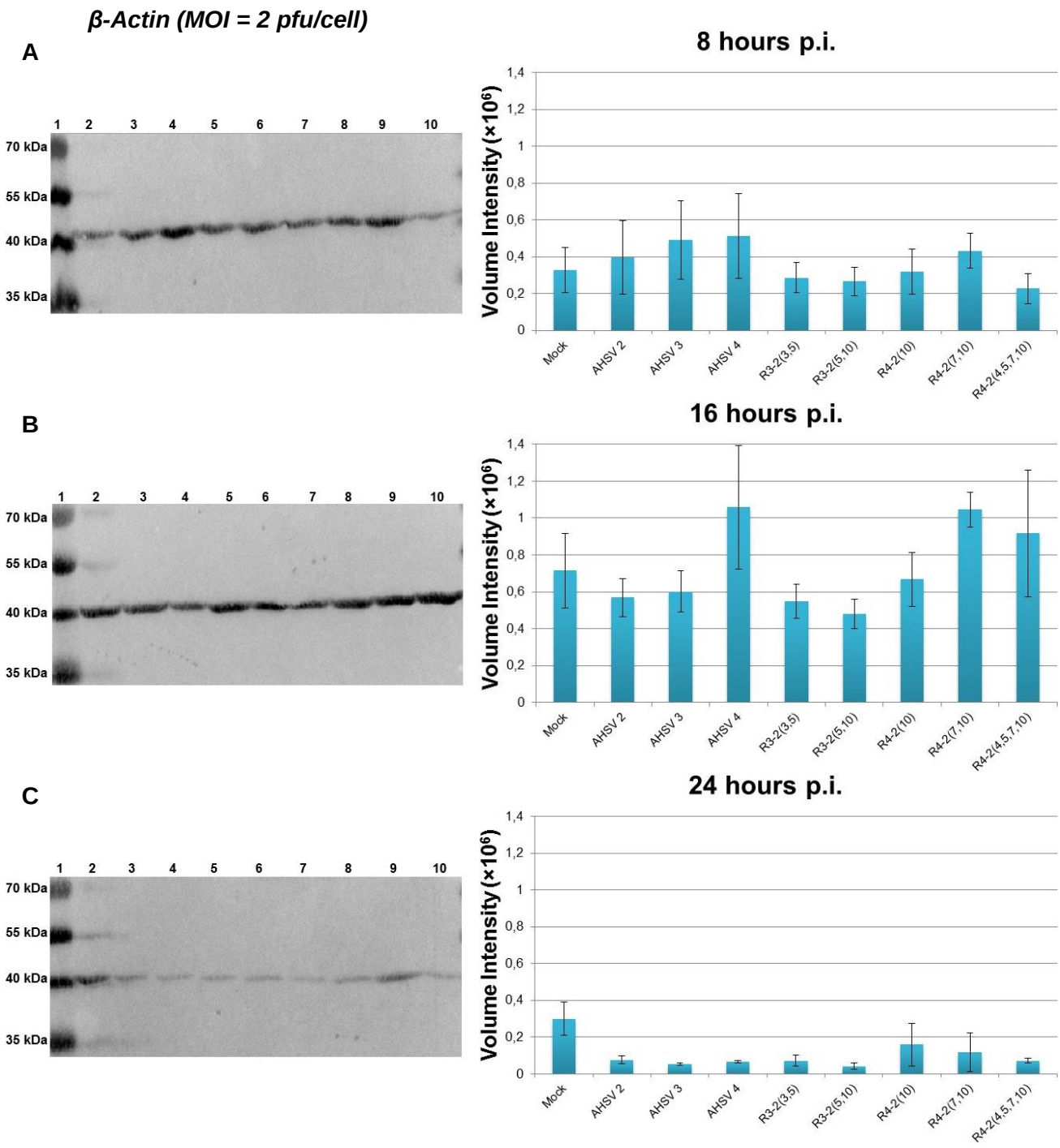

Figure 20: β-Actin protein levels in Vero cells. Cells were mock-infected, or infected with AHSV at an MOI of 2 pfu/cell, and harvested at A) 8 h p.i., B) 16 h p.i. and C) 24 h p.i. A representative Western blot is shown on the left. In each blot Lane 2 contains a mock-infected sample, Lanes 3-5 the parental serotypes and Lanes 6-10 the reassortant virus strains in the same order as on the graphs. The graphs shown on the right, represent the average volume intensity values obtained from the quantification of multiple blots as detailed in Table 3. Error bars indicate the standard deviation.

Based on anti-β-Actin quantification results, an adjustment factor was calculated for each virus-infected sample which would result in equalising the β-Actin signals in all samples for a specific time point. First the relative ratio of the β-Actin signal from each of the eight different virus-infected samples to the mock-infected reference was calculated, by dividing the volume intensity of β-Actin from each infection by the volume intensity of the reference. The adjustment factor was then one divided by the relative ratio. The factors determined for each time point are given in Table 8.

Table 8: Adjustment factors* calculated from β-Actin at each time point within each infection trial

	MOI = 0.1 pfu/cell			MOI = 2 pfu/cell		
	16 h p.i.	24 h p.i.	48 h p.i.	8 h p.i.	16 h p.i.	24 h p.i.
AHSV-2	0,9376370	1,3165756	1,4140288	0,8281856	1,2571010	3,9260977
AHSV-3	1,1037702	1,8941026	1,9940571	0,6697954	1,1883624	5,5406680
AHSV-4	1,0691549	1,8508565	1,6264083	0,6368838	0,6759230	4,5719880
R3-2$_{3,5}$	1,1672524	1,9950634	2,7665802	1,1455226	1,3004346	4,2221366
R3-2$_{5,10}$	1,2654080	2,2480424	2,1196097	1,2340434	1,4944992	7,4626036
R4-2$_{10}$	1,2625920	2,3531559	2,1745624	1,0258605	1,0710717	1,8888090
R4-2$_{7,10}$	1,3724262	2,6428776	2,7316550	0,7578145	0,6838097	2,5411565
R4-2$_{4,5,7,10}$	1,3651763	1,9990257	2,4554126	1,4394748	0,7801803	4,2125610

***** To calculate the adjustment factors, the mock-infected sample data, at each time point, was used as reference

3.3.4 Virus protein levels for VP7, NS1 and NS2 at different times

Figures 21-23 show the Western blot results of VP7, NS1 and NS2 for the three parental AHSV serotypes and five reassortant strains used to infect Vero cells at a MOI of 0.1 pfu/cell. Figures 24-26 show the results of VP7, NS1 and NS2 from Vero cells infected at a MOI of 2 pfu/cell. Virus protein levels for the different strains were compared to each other within each time post infection and not between the two infection experiments. In each case one Western blot is shown, with the corresponding graph indicating both the average volume intensity values calculated from the repeat experiments, and the adjusted values based on the β-Actin signal for that sample at that time point. Where a reassortant strain indicated statistical significant difference to the parental strains, a 2, 3 or 4 above the light blue bar on each corresponding graph specifies to which parental strains it differs. The average virus protein signals were adjusted by the factor calculated from the β-Actin data set of the same time post-infection. This would compensate for the fact that the same number of cells were not necessarily used in each lane of the gel, partly as a result of differences in the CPE caused by the different viruses. Because of the high level of CPE observed after 24 hours p.i. in cells infected at an MOI of 2 pfu/cell, virus protein levels were not monitored beyond this point. Furthermore, virus protein levels were not monitored at 0 hours p. i. as no CPE is expected. Also, because no antibody signals were detected for β-Actin at 8 hours post-infection for the unsynchronised infection (MOI 0.1 pfu/cell), our data for VP7, NS1 and NS2 at the same time point post-infection, was not adjusted.

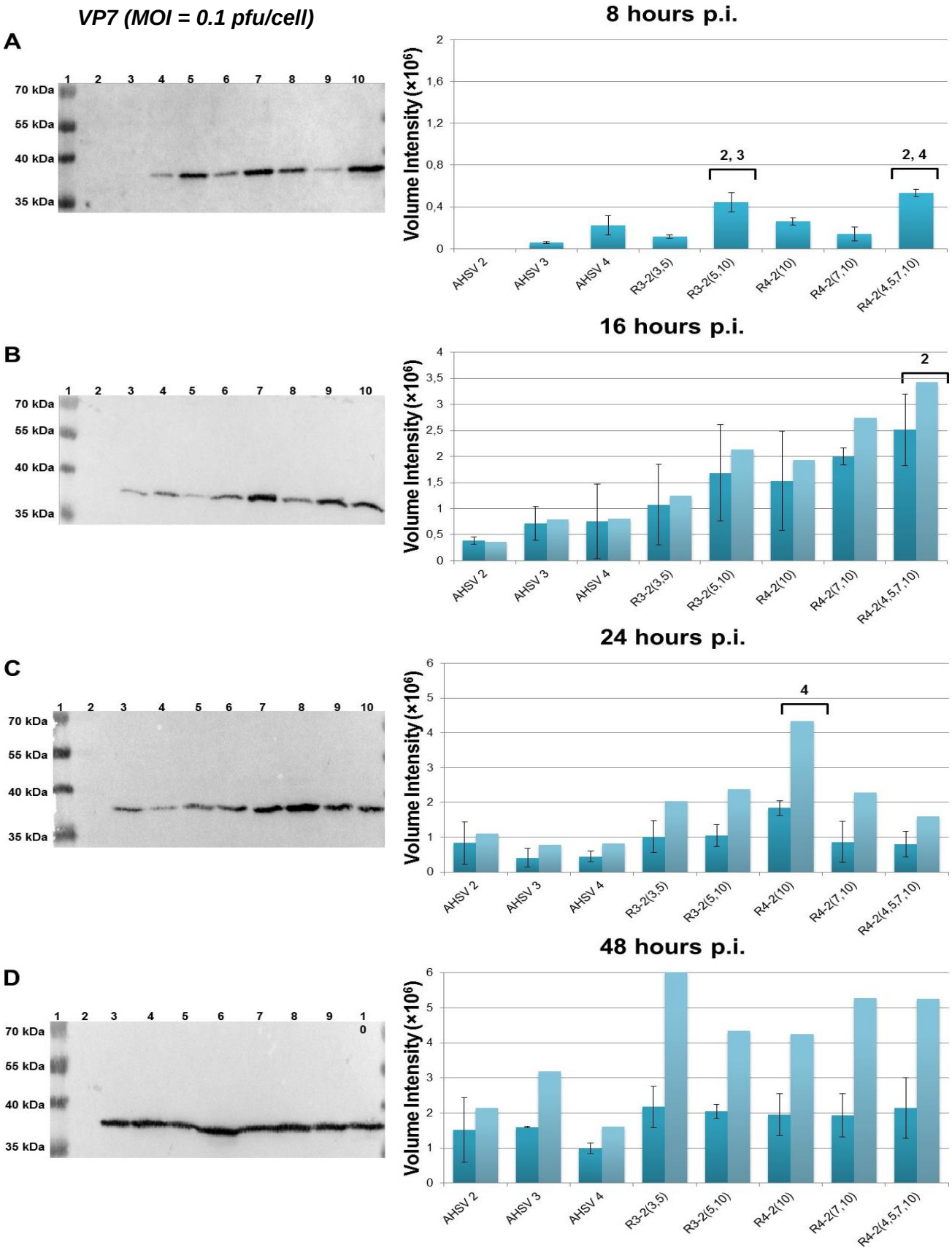

Figure 21: VP7 protein levels in Vero cells. Cells were mock-infected, or infected with AHSV at an MOI of 0.1 pfu/cell, and harvested at A) 8 h p.i., B) 16 h p.i., C) 24 h p.i. and D) 48 h p.i. A representative Western blot reacted with anti-VP7 antibody is shown on the left. In each blot Lane 2 contains a mock-infected sample, Lanes 3-5 the parental serotypes and Lanes 6-10 the reassortant virus strains in the same order as on the graphs. The graphs shown on the right, represent the average volume intensity values (dark blue bars), and the adjusted values (light blue bars). Error bars indicate the standard deviation. Numbers above bars indicate statistical significant difference to that parental strain.

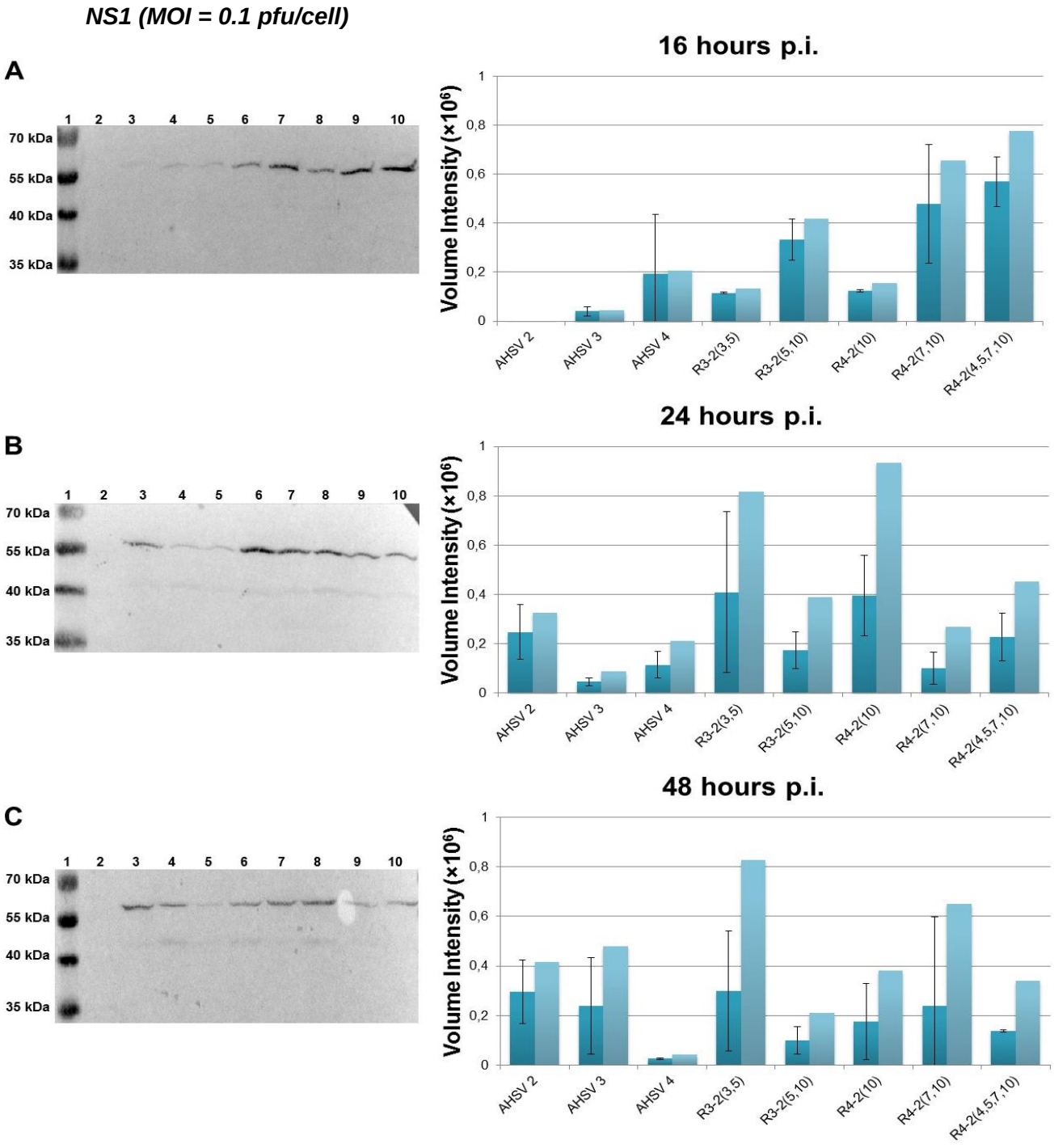

Figure 22: NS1 protein levels in Vero cells. Cells were mock-infected, or infected with AHSV at an MOI of 0.1 pfu/cell, and harvested at A) 16 h p.i., B) 24 h p.i. and C) 48 h p.i. A representative Western blot reacted with anti-NS1 antibody is shown on the left. In each blot Lane 2 contains a mock-infected sample, Lanes 3-5 the parental serotypes and Lanes 6-10 the reassortant virus strains in the same order as on the graphs. The graphs shown on the right, represent the average volume intensity values (dark blue bars), and the adjusted values (light blue bars). Error bars indicate the standard deviation. No NS1 proteins were detected at 8 hours post-infection.

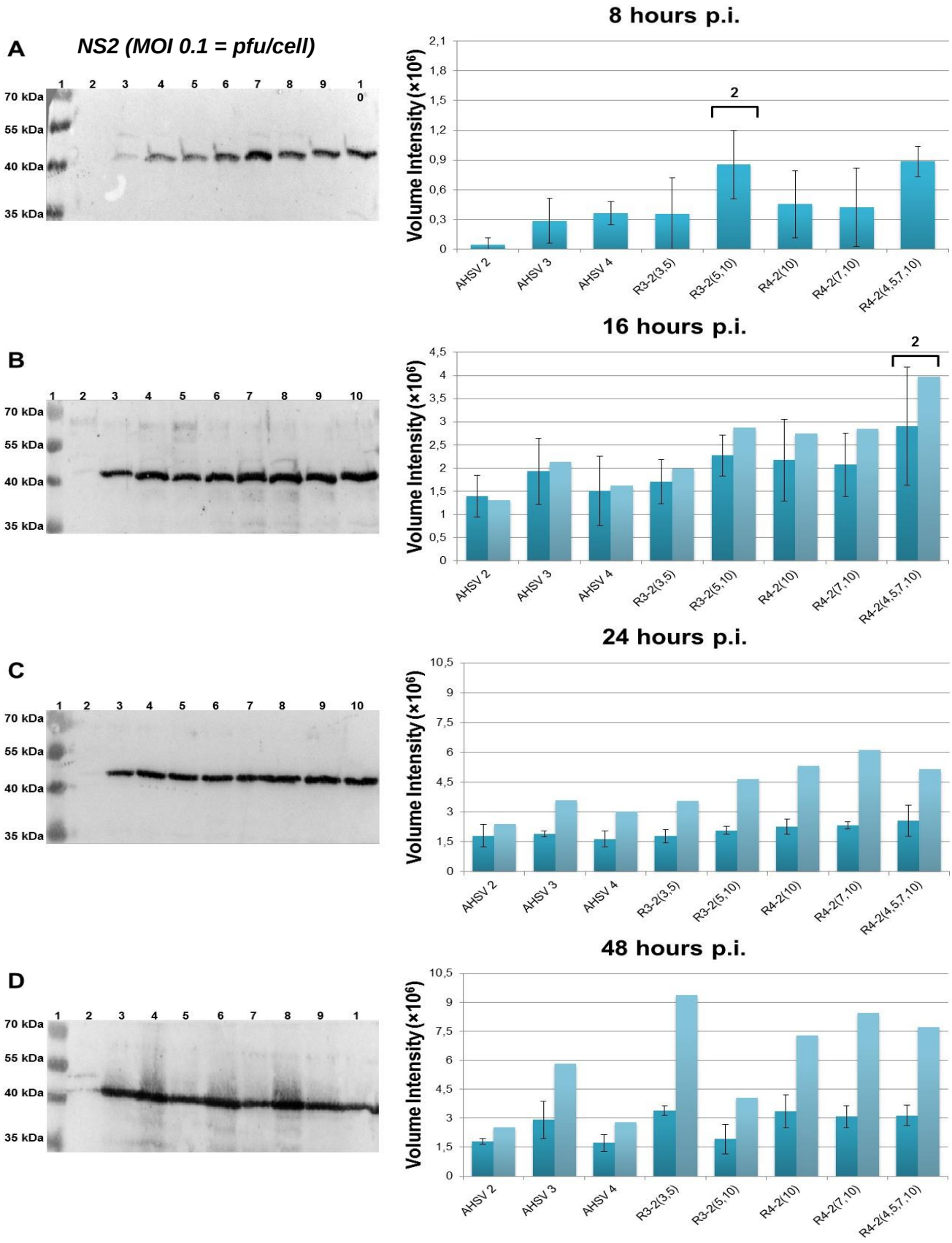

Figure 23: NS2 protein levels in Vero cells. Cells were mock-infected, or infected with AHSV at an MOI of 0.1 pfu/cell, and harvested at A) 8 h p.i., B) 16 h p.i., C) 24 h p.i., and D) 48 h p.i. A representative Western blot reacted with anti-NS2 antibody is shown on the left. In each blot Lane 2 contains a mock-infected sample, Lanes 3-5 the parental serotypes and Lanes 6-10 the reassortant virus strains in the same order as on the graphs. The graphs shown on the right, represent the average volume intensity values (dark blue bars), and the adjusted values (light blue bars). Error bars indicate the standard deviation. Numbers above bars indicate statistical significant difference to that parental strain.

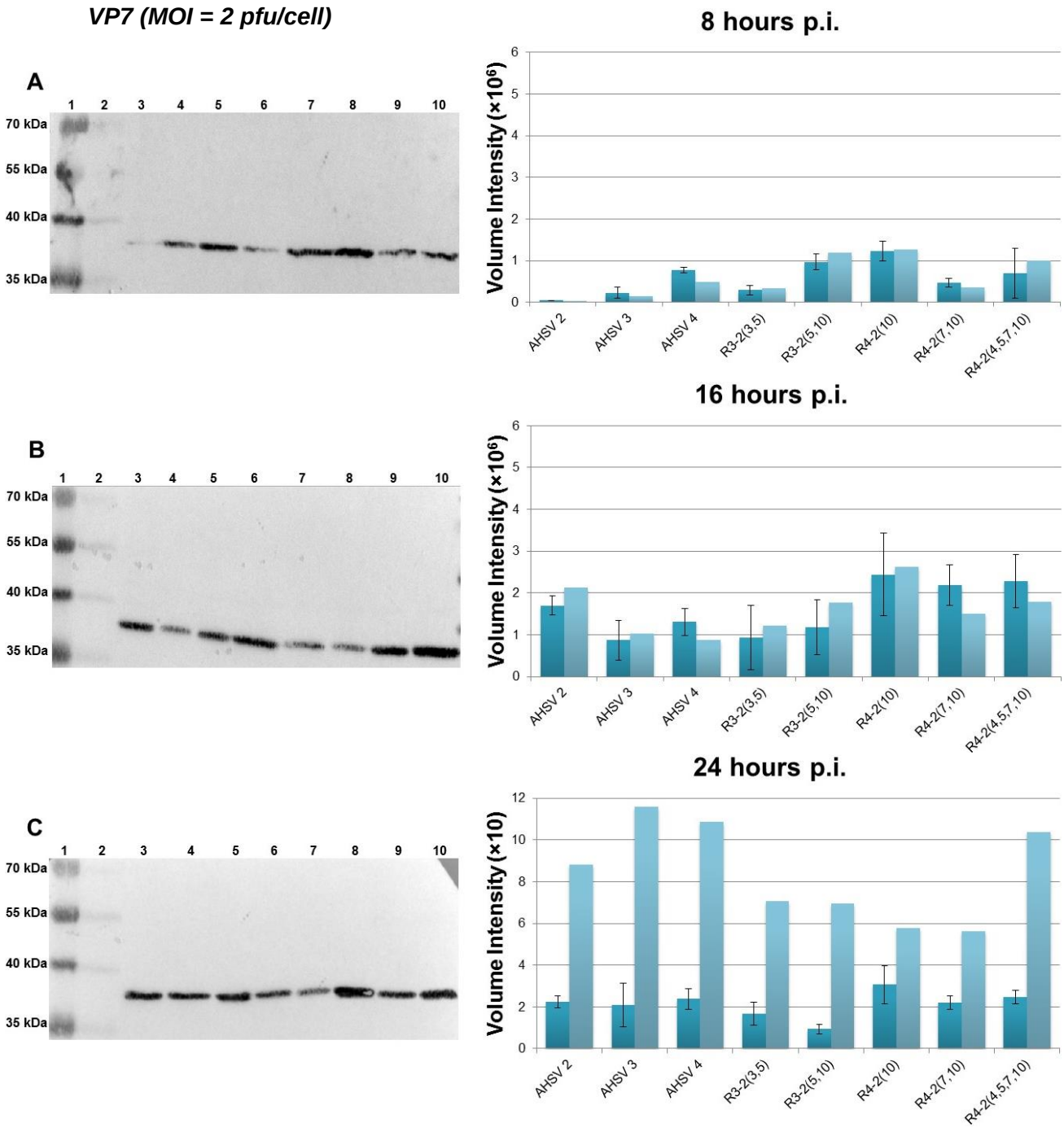

Figure 24: VP7 protein levels in Vero cells. Cells were mock-infected, or infected with AHSV at an MOI of 2 pfu/cell, and harvested at A) 8 h p.i., B) 16 h p.i. and C) 24 h p.i. A representative Western blot reacted with anti-VP7 antibody is shown on the left. In each blot Lane 2 contains a mock-infected sample, Lanes 3-5 the parental serotypes and Lanes 6-10 the reassortant virus strains in the same order as on the graphs. The graphs shown on the right, represent the average volume intensity values (dark blue bars), and the adjusted values (light blue bars). Error bars indicate the standard deviation.

NS1 (MOI = 2 pfu/cell)

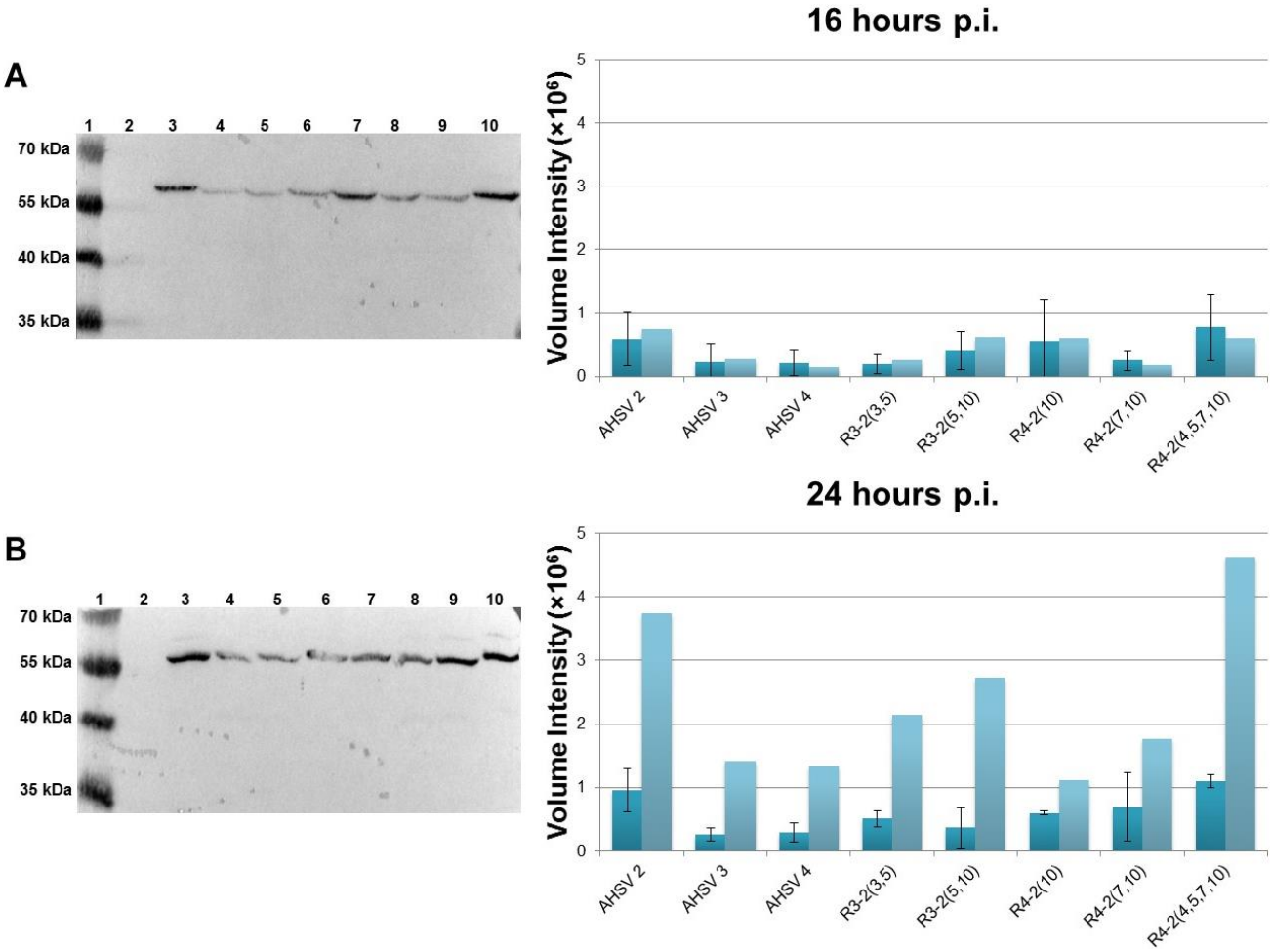

Figure 25: NS1 protein levels in Vero cells. Cells were mock-infected, or infected with AHSV at an MOI of 2 pfu/cell, and harvested at A) 16 h p.i. and B) 24 h p.i. A representative Western blot reacted with anti-NS1 antibody is shown on the left. In each blot Lane 2 contains a mock-infected sample, Lanes 3-5 the parental serotypes and Lanes 6-10 the reassortant virus strains in the same order as on the graphs. The graphs shown on the right, represent the average volume intensity values (dark blue bars), and the adjusted values (light blue bars). Error bars indicate the standard deviation. Again, no NS1 proteins were detected at 8 hours post-infection.

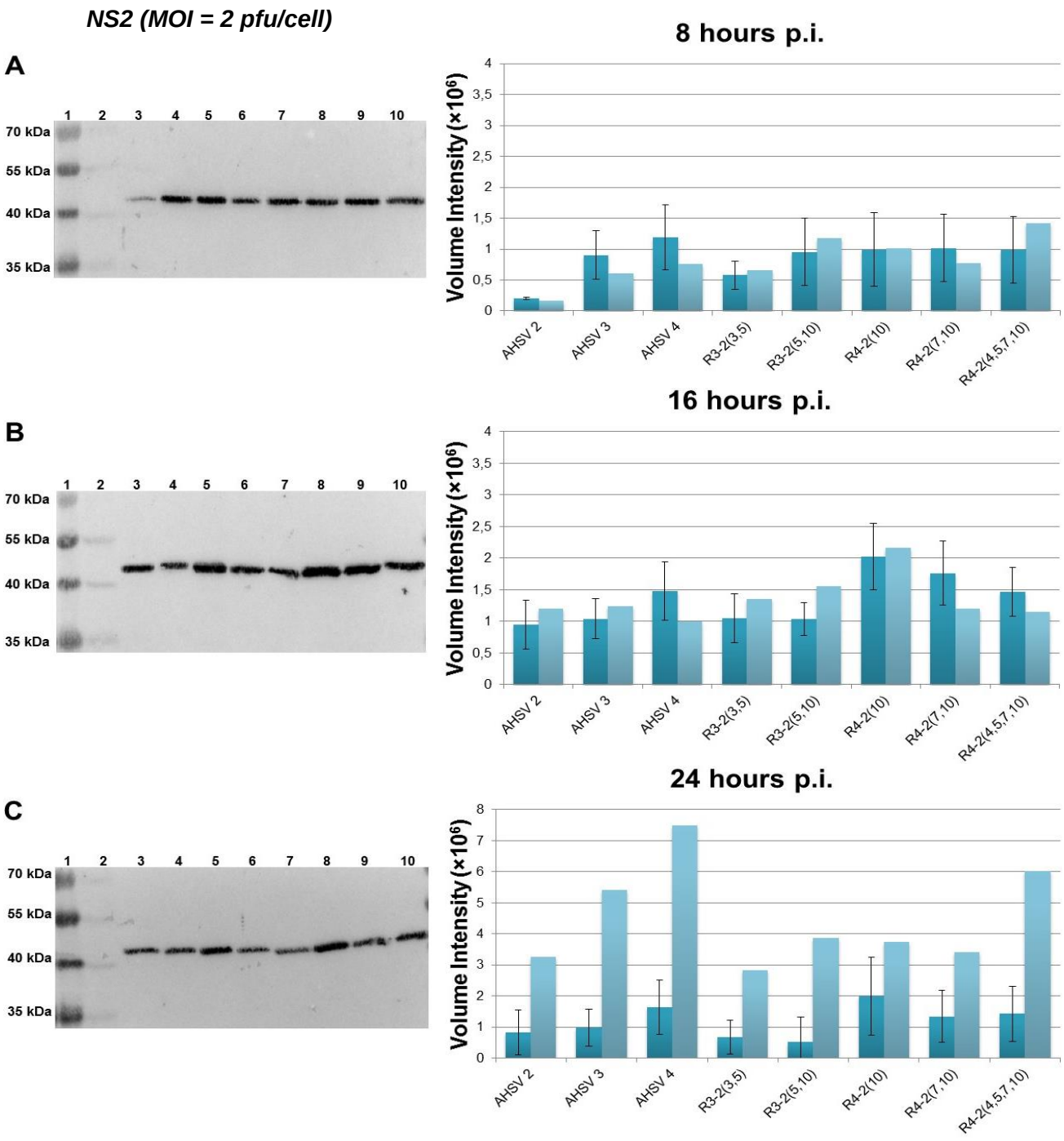

Figure 26: NS2 protein levels in Vero cells. Cells were mock-infected, or infected with AHSV at an MOI of 2 pfu/cell, and harvested at A) 8 h p.i., B) 16 h p.i. and C) 24 h p.i. A representative Western blot reacted with anti-NS2 antibody is shown on the left. In each blot Lane 2 contains a mock-infected sample, Lanes 3-5 the parental serotypes and Lanes 6-10 the reassortant virus strains in the same order as on the graphs. The graphs shown on the right, represent the average volume intensity values (dark blue bars), and the adjusted values (light blue bars). Error bars indicate the standard deviation.

3.3.5 Statistical analyses of VP7 and NS2 immunoblot data

Variability in the protein levels between the different AHSV strains are suggested and this was evident from Figures 21-26. To determine if there were statistically significant differences in the protein expression levels, our data was subjected to statistical analyses using the statistical program SPSS Statistics (IBM Corp., Version 22, 2013). In each case we only compared the data between the three parental and five reassortant strains for one virus protein at a specific time point, and not across the time trial or between the two infection experiments. It was decided to only use the data for VP7 and NS2 to continue investigations, as NS1 Western blot signals were weak and our data deemed unreliable. Although AHSV NS1 protein is expressed at very high levels within infected cells, it is suggested that the antibodies used to detect NS1 proteins, could not detect the proteins with high efficiency. Furthermore, statistical analyses were done using the volume intensity data and not the adjusted values (dark blue and light blue bars, respectively, Figures 21-26) as variance and standard deviation could not be calculated from the adjusted values.

One-way ANOVA is used to determine the equality of means of the different data sets examined for each of the three virus proteins monitored. This was considered an applicable model for testing our data. Each virus protein monitored at a specific time p.i. was considered a categorical explanatory variable. Further, each categorical explanatory variable had $\boldsymbol{k}$ levels which were the eight different AHSV strains studied. The analysis was run to determine if there were significant differences between the observed protein levels of a reassortant virus strain and the parental strains it originated from. For example, the anti-VP7 signal obtained for R3-$2_{3,5}$ at 8 hours p.i. for MOI 0.1 was compared to the corresponding signals of AHSV-2 and AHSV-3. A group ($\boldsymbol{i}$) was defined as the set of biological replicate data points, where $N \geq 3$, for a virus protein measured (indicated as volume intensity), for an AHSV strain monitored, at each specific time point for the unsynchronised and synchronised infections. For instance, the different volume intensity signals observed ($\boldsymbol{j}$) for AHSV-2 VP7, 16 hours p.i at MOI 0.1, used for calculating an average (see Figure 21B, dark blue bar), were considered a group.

Each group was first assessed using the *Shapiro-Wilks* test to determine normality of the data. All groups, within each of the original data sets, were found to be at least approximately normally distributed ($p > \alpha_{0.05}$). Furthermore, no outliers in the data sets were identified based on assessment from the box plots. Homogeneity of variances of the groups within each data set was then evaluated by *Levene's* Test for Equality of Variances. If homogeneity of variances was violated ($p < \alpha_{0.05}$), the one-way ANOVA analysis was run using the *Welch-Satterthwaite* correction.

To obtain a quantitative outcome, the ANOVA *F* statistic ratio, indicating the ratio between *explained variance* and *error*, was calculated. The "*Between*" variation, or *explained variance*, describe variation amongst the different groups ($\boldsymbol{i}$) for each categorical explanatory variable. This was designated as the "sum of squares between groups" ($SS_{Between}$), and calculated as the sum of the squared deviations from the mean for each level ($\boldsymbol{k}$). The "*Within*" variation, or *error variance*, describe the variation ($SS\boldsymbol{i}$) between the different biological replicates ($\boldsymbol{j}$) within a single group ($\boldsymbol{i}$) which are then summated for all virus strains ($\boldsymbol{k}$). This was designated as the "sum of squares within groups" (SS_{Within}).

Variance amongst the individual measurements ($\boldsymbol{j}$) for each specific virus strain ($\boldsymbol{k}$) between different groups ($\boldsymbol{i}$) within a data set, were indicated as the "mean square between groups" ($MS_{Between}$). This was calculated by dividing the $SS_{Between}$ by the between-groups "degrees of freedom" (*df*, $\boldsymbol{k} - 1$). Similarly, variance of the biological replicates of protein levels measured ($\boldsymbol{j}$) within a single group ($\boldsymbol{i}$),

and summated for all virus strains ($\boldsymbol{k}$), was defined as the "mean square within groups (MS_{Within}) and was calculated by dividing SS_{Within} by the within-groups *df* ($\boldsymbol{N-k}$). The *F* statistic was then calculated as the ratio between $MS_{Between}$ and MS_{Within}. Table 9 shows a summary of the calculations done for the one-way ANOVA analyses.

Table 9: Summary of the calculations done for the one-way ANOVA analyses

Group	Sum of Squares	*df*	Mean Squares	*F* statistic
Between	$SS_{Between} = \sum_{i=1}^{k} n_i\left(\bar{Y}_i - \bar{\bar{Y}}\right)^2$	*k* - 1	$MS_{Between} = \frac{SS_{Between}}{k-1}$	$F = \frac{MS_{Between}}{MS_{Within}}$
Within	$SS_i = \sum_{j=1}^{n_i}\left(Y_{ij} - \bar{Y}_i\right)^2$ $SS_{Within} = \sum_{i=1}^{k} SS_i$	*N* - *k*	$MS_{Within} = \frac{SS_{Within}}{N-k}$	
Total	$SS_{Between} + SS_{Within}$	*N* - 1		

In the equation for $SS_{Between}$ (Table 9), $\bar{\boldsymbol{Y}}_{\boldsymbol{i}}$ is the sample mean for a group ($\boldsymbol{i}$), and $\bar{\bar{\boldsymbol{Y}}}$ is the grand mean of the total data set. The total sample size for a data set is indicated by $\boldsymbol{N}$ and the sample size of each group ($\boldsymbol{i}$) indicated by $\boldsymbol{n}$. In the equation for $SS\boldsymbol{i}$ (Table 9), $\boldsymbol{Y_{ij}}$ indicate an individual observation ($\boldsymbol{j}$) made for a specific group ($\boldsymbol{i}$). Analyses results indicated that there were statistically significant differences between certain groups at early time points in the time trial. These results are summarised in Table 10, where *SS* is the "Sum of Squares", *df* the "degrees of freedom", *MS* the "Mean Squares", *F* is the "*F* statistic ratio" calculated for the ANOVA, and the *P-value* our level of significance at $\alpha_{0.05}$.

Table 10: One-way ANOVA analyses results from immunoblot assays on infected mammalian cells

Data Set	Source	*SS*	*df*	*MS*	*F*	*P-value*	***P-value*
VP7, 8 h pi (MOI 0.1)	*Between*	5.542E+11	6	9.237E+10	27.433	0.000	
	Within	4.714E+10	14	3.367E+09			
	Total	6.014E+11	20				
VP7, 16 h pi (MOI 0.1)	*Between*	1.099E+13	7	1.570E+12	3.607	0.016	
	Within	6.967E+12	16	4.354E+11			
	Total	1.796E+13	23				
VP7, 24 h pi (MOI 0.1)	*Between*	4.165E+12	7	5.951E+11	3.642	0.015	
	Within	2.615E+12	16	1.634E+11			
	Total	6.780E+12	23				
NS2, 8 h pi (MOI 0.1)	*Between*	2.162E+12	7	3.088E+11	5.223	0.001	
	Within	1.419E+12	24	5.913E+10			
	Total	3.581E+12	31				
NS2, 16 h pi (MOI 0.1)	*Between*	4.860E+12	7	6.943E+11	1.218	0.349	
	Within	9.119E+12	16	5.700E+11			
	Total	1.398E+13	23				
*****NS2, 24 h pi (MOI 0.1)	*Between*	2.231E+12	7	3.187E+11	1.383	0.257	0.205
	Within	5.530E+12	24	2.304E+11			
	Total	7.761E+12	31				
*****VP7, 8 h pi (MOI 2)	*Between*	2.280E+12	7	3.257E+11	5.287	0.016	0.013
	Within	4.928E+11	8	6.160E+10			
	Total	2.773E+12	15				
*****VP7, 16 h pi (MOI 2)	*Between*	9.587E+12	7	1.370E+12	3.278	0.014	0.034
	Within	1.003E+13	24	4.178E+11			
	Total	1.961E+13	31				
VP7, 24 h pi (MOI 2)	*Between*	8.092E+12	7	1.156E+12	3.239	0.024	
	Within	5.711E+12	16	3.569E+11			
	Total	1.380E+13	23				
NS2, 8 h pi (MOI 2)	*Between*	2.061E+12	7	2.945E+11	1.361	0.287	
	Within	3.462E+12	16	2.164E+11			
	Total	5.524E+12	23				
°*NS2, 16 h pi (MOI 2)	*Between*	2.203E+12	7	3.147E+11	1.846	0.204	0.658
	Within	1.364E+12	8	1.705E+11			
	Total	3.566E+12	15				
NS2, 24 h pi (MOI 2)	*Between*	5.419E+12	7	7.741E+11	1.102	0.408	
	Within	1.124E+13	16	7.027E+11			
	Total	1.666E+13	23				

° *Levene's* test was not calculated, *N* too low (*N* = 2)

***** Homogeneity of Variances was violated and the *Welch-Satterthwaite* correction was made

****** Corrected *p*-value using the *Welch-Satterthwaite* correction

Levene's test for homogeneity of variances was not significant for the VP7 (MOI 2) at 8 hours p.i. [*Levene F*(7,8) = 4.292E+15, $p = 0.000$] and 16 hours p.i. [*Levene F*(7,24), $p = 0.024$], and NS2 (MOI 0.1) at 24 hours p.i. [*Levene F*(7,24), $p = 0.008$] data sets. The *Welch-Satterthwaite* correction was made to these ANOVA analyses to decrease the probability of making a *Type I error* of incorrectly rejecting H_0. The calculated p-value after this correction was made is shown in Table 10. *Levene's* test could not be run for the NS2, 16 hours p.i. (MOI 2) data set because *N* was too low. For this data set the *Welch-Satterthwaite* correction was also calculated as there was no indication that the assumption for homogeneity of variances was not violated. Results after correction for assumed violation of the assumption are shown in Table 10. For comparison, results of the one-way ANOVA analyses for these data sets are shown in Table 10.

Where the ANOVA *F* statistic was significant ($p < \alpha_{0.05}$), a *post-hoc* multiple comparisons test was done. *Tukey's Honestly Significant Difference (HSD) post-hoc* multiple comparisons test were done to "unpack" the *F-statistic* and to determine which specific groups indicated statistically significant difference thereby contributing to the one way ANOVA results that were significant ($p < \alpha_{0.05}$). For all data sets where homogeneity of variances were not true, the *Games-Howell post-hoc* multiple comparisons test were done. An alpha level of 0.05 was used for all analyses. Statistically significant differences in mean VP7 and NS2 protein levels were reported only if they were observed between the reassortant viruses and parental strains and not between the reassortant strains. Results between the mean VP7 and NS2 protein levels of the reassortant virus strains and their parental origins are summarized in Table 11.

Table 11: Summary of the *post-hoc* multiple comparisons test on virus protein levels that revealed statistically significant difference

Data Set	*Post-Hoc* Analysis	Statistically Significant Difference			
		Reassortant Virus	AHSV-2	AHSV-3	AHSV-4
VP7, 8 h pi (MOI 0.1)	*Tukey HSD*	R3-$2_{5,10}$	Yes	Yes	×
VP7, 8 h pi (MOI 0.1)	*Tukey HSD*	R4-$2_{4,5,7,10}$	Yes	×	Yes
VP7, 16 h pi (MOI 0.1)	*Tukey HSD*	R4-$2_{4,5,7,10}$	Yes	×	No
VP7, 24 h pi (MOI 0.1)	*Tukey HSD*	R4-2_{10}	No	×	Yes
NS2, 8 h pi (MOI 0.1)	*Tukey HSD*	R3-$2_{5,10}$	Yes	No	×
NS2, 8 h pi (MOI 0.1)	*Tukey HSD*	R4-$2_{4,5,7,10}$	Yes	×	No

The *Tukey HSD post-hoc* multiple comparisons test indicated no statistically significant difference in mean VP7 or NS2 protein levels between the three parental strains at any time point in either of the infection experiments (MOI 0.1 and MOI 2 pfu/cell). Furthermore, statistically significant differences between reassortant viruses and parental strains were only observed for infections done at MOI 0.1 pfu/cell. Results indicated that there is significantly higher R3-$2_{5,10}$ and R4-$2_{4,5,7,10}$ mean VP7 protein levels synthesised up to 8 hours p.i. compared to their parental strains. At 16 hours p.i. R4-$2_{4,5,7,10}$

indicated significantly higher mean VP7 levels to AHSV-2 only and at 24 hours p.i. R4-2_{10} indicated significantly higher mean VP7 levels compared to AHSV-4 only (Table 11). The R3-$2_{5,10}$ and R4-$2_{4,5,7,10}$ reassortant virus strains showed significantly higher mean NS2 protein synthesis levels, at 8 hours p.i., but only to AHSV-2 (Table 11). No statistical significance was observed at 16 or 24 hours p.i. for the reassortant viruses mean NS2 protein levels when compared to the parental strains. Because differences in mean VP7 and NS2 levels between the different reassortant virus strains were not of any importance to our investigation, none of these results are presented here.

3.4 Analyses of Viral Protein Synthesis by Pulse Labelling

The previous section described results when monitoring accumulated virus proteins levels, from infected mammalian cells, up to the ends of the specified time points post-infection. This section will describe results from monitoring the same eight virus strains, within infected mammalian cells, but considered virus protein levels synthesised only at precise time intervals post-infection. This was monitored using radioactive pulse labelling assays. These results were then compared to the accumulated protein levels.

3.4.1 Optimising virus infections and pulse labelling in mammalian cells

To obtain reliable results from pulse labelling experiments, certain variables of these experiments had to be optimised first. These variables were i) the volume of Tris-HCl buffer in which to resuspend virus particles for infection of mammalian cells; and ii) the optimal minimum volume of growth medium to sustain the infected cells. These variables were tested at different volumes and in combination with each other, to determine the minimal total volume in which to obtain optimal virus adsorption and infection. Four different experiments (A-D) were set up, each testing a different combination of variables (i) and (ii), and are summarised in Table 12. For these initial experiments, all Vero cells were infected at an MOI of 5 pfu/cell using AHSV-2, AHSV-3, AHSV-4 and three reassortant strains (R4-2_{10}, R4-$2_{7,10}$, and R4-$2_{4,5,7,10}$). A multiplicity of infection higher than 2 pfu/cell, as in previous experiments, were chosen to ensure a synchronised infection. Furthermore, all experiments were conducted in a single 48 well plate where all wells were seeded to form a monolayer with a cell concentration of ~9×10^4 cells per well.

Table 12: Preparation of four experiments A-D indicating different volumes of variables tested in combination to each other

Experiment	Growth Medium (µl)	*Tris-HCl Buffer (µl)	Total Volume (µl)
A	15	10	25
B	15	45	60
C	15	200	215
D	215	0	215

*** Tris-HCl buffer already contained the virus particles and were diluted with additional Tris-HCl (where applicable) to make up the total volumes indicated for each experiment**

In experiment A, cells were infected with the virus stocks (10 µl) without further Tris-HCl buffer added. In experiments B and C, the virus stocks used for infection, were diluted with additional Tris-HCl buffer to a volume of 45 µl or 200 µl respectively. In experiment D no additional Tris-HCl buffer was added; however, the virus stocks were diluted using growth medium.

Depletion of cellular methionine (Met) was accomplished by incubating cells in Met-free growth medium for one hour at 11 hours p.i. The depletion step ensured that the cells would incorporate labelled Met rather than cellular Met during pulse labelling. After depletion, ^{35}S-Met was added to the cells for 3 hours (12-15 h p.i.) and cells were harvested after 15 hours p.i. As per manufacturer's instructions, a concentration of 5 µCi/ml labelled isotopes were added to infected cells. Proteins from crude cell lysates were then separated using SDS-PAGE. Gels were subsequently dried and exposed overnight onto an imaging-screen (BioRad) for visualisation. Figure 27 shows the results obtained from the four different experiments done.

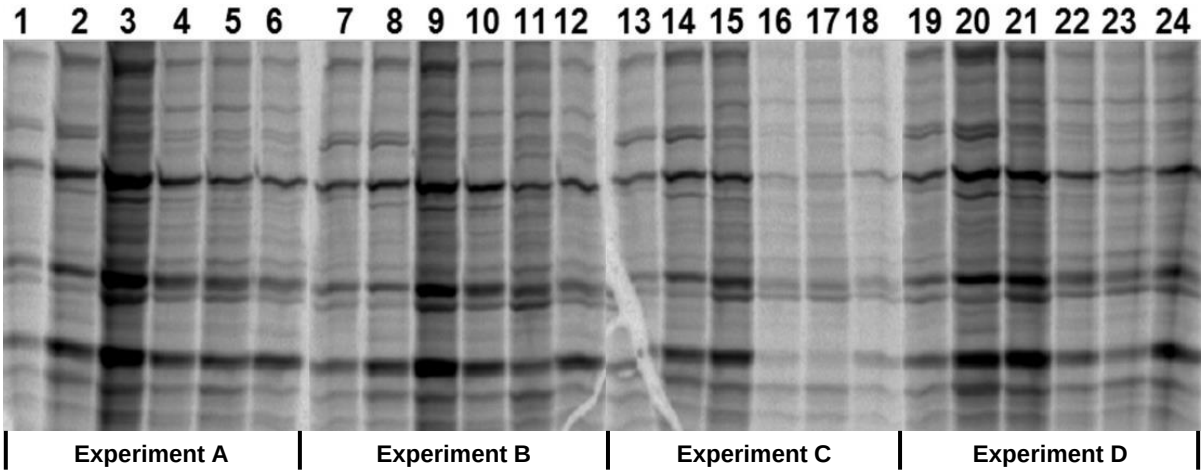

Figure 27: Pulse labelling results for the four different optimisation experiments. Visualisation of bands from an overnight exposure onto an autorad-screen. Lanes 1-6 show results for experiment A, Lanes 7-12 show results for experiment B, Lanes 13-18 results for experiment C and Lanes 19-24 for experiment D. In all experiments the lanes were loaded in the order: AHSV-2, AHSV-3, AHSV-4, R4-2$_{4,5,7,10}$, R4-2$_{7,10}$ and R4-2$_{10}$.

Pulse labelling results indicated that optimal virus adsorption can occur in a small volume and that large volumes of added Tris-HCl buffer appeared to reduce adsorption efficiency. This was clear when inspecting the results for experiment A and comparing this to experiments B and C. When substituting the added Tris-HCl buffer with growth medium to obtain a larger cell inoculum volume (experiment D) the results did not differ much from that of experiment A. A larger volume of growth medium might increase the volume-to-area ratio and it was decided to do all subsequent cell infection experiments in a small inoculum volume with no added Tris-HCl buffer. Thus, all subsequent experiments were conducted using similar conditions as in experiment A with a total volume of 25 µl. Results further suggested that adding the radio-labelled isotope at a concentration of 5 µCi/ml, were optimal for monitoring subsequent protein synthesis.

3.4.2 Monitoring time-specific virus protein synthesis using ^{35}S-Methionine pulse labelling

Time-specific synthesis of VP7, NS1 and NS2 were monitored in infected Vero cells at 5-8, 13-16 and 21-24 hours post-infection. Cells were infected at an MOI of 5 with the three parental strains (AHSV-2, AHSV-3 and AHSV-4) and five reassortant strains (R3-2$_{3,5}$, R3-2$_{5,10}$, R4-2$_{10}$, R4-2$_{7,10}$ and R4-2$_{4,5,7,10}$) studied. For each specific time point two biological replicate experiments were prepared due to limited availability of the ^{35}S-Met. After infection, cells were depleted from cellular Met by incubating cells in a Met-free medium. Cells were depleted from cellular Met for an hour, either 4-5

hours, 12-13 hours or 20-21 hours post-infection. Subsequently, depleted cells were labelled with ^{35}S-Met for 3 hours, either at 5-8 hours, 13-16 hours or 21-24 hours post-infection and harvested immediately after pulse labelling. Figure 28 illustrates the results obtained from exposing SDS-PAGE gels onto autrorad screens for visualisation of proteins containing the incorporated radioactively labelled Met. One biological replicate from each labelling experiment is shown.

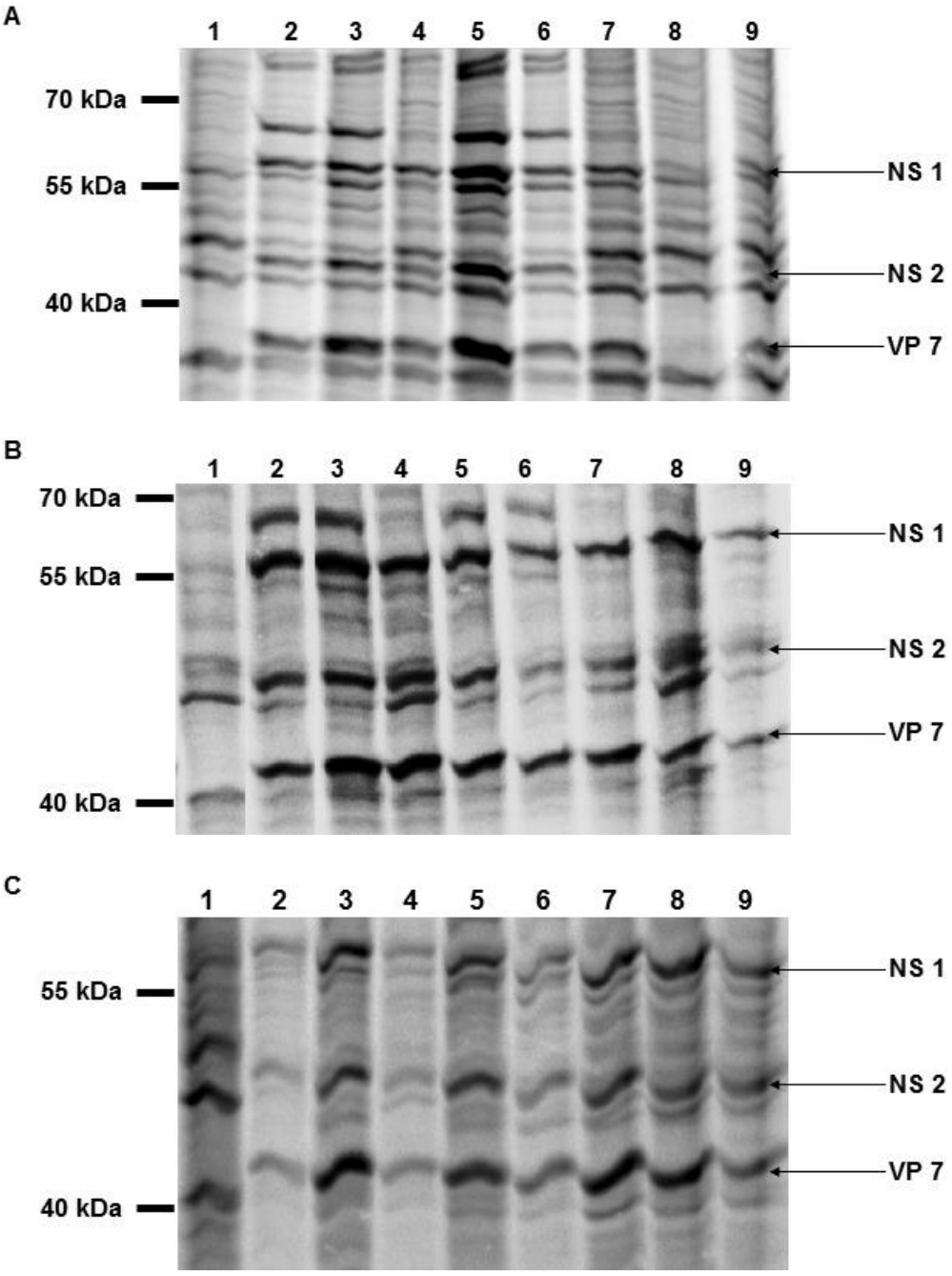

Figure 28: Pulse labelling results from infected cells labelled at A) 5-8 hours p.i., B) 13-16 hours p.i. and C) 21-24 hours p.i. Visualisation of labelled proteins from overnight exposure. Position of the protein marker is indicated on the left. Protein bands for VP7, NS1 and NS2 are indicated with arrows on the right. For each image, samples were loaded in the order: L1: Mock-infected sample, L2: AHSV-2, L3: AHSV-3, L4: AHSV-4, L5: R3-2$_{3,5}$, L6: R3-2$_{5,10}$, L7: R4-2$_{10}$, L8: R4-2$_{7,10}$, L9: R4-2$_{4,5,7,10}$.

Again these images were subject to relative quantification of the VP7, NS1 and NS2 bands (indicated with arrows to right of Figure 28) using the Image Lab imaging software. As described for the Western blots in the previous section, a unit for volume intensity was assigned to each band of interest from each of the autorad images. Where more than one replicate for a specific virus strain was available for quantification, an average and standard deviation was calculated. Figure 29 shows these averaged values for the VP7, NS1 and NS2 virus proteins, during the three time intervals.

Figure 29: VP7, NS1 and NS2 protein synthesis levels during A) 5-8, B) 13-16 and C) 21-24 hours p.i. for the different AHSV strains studied. Pulse labelling, using ^{35}S-Met, were done at the three time intervals indicated. At 5-8 and 21-24 hours p.i., more than one replicate for each set of data was available to calculate average volume intensities and error bars are shown, indicating standard deviation. Numbers above bars indicate statistical significant difference to that parental strain.

3.4.3 Statistical analyses of VP7, NS1 and NS2 pulse labelling data

Statistical analyses were done on the data, as presented in the previous section, using the statistical program SPSS Statistics (IBM Corp., Version 22, 2013). Analyses were done the same way as for the data obtained from immunoblot experiments on infected mammalian cells. A data set was again defined as the set of values calculated for the synthesised levels of VP7, NS1 or NS2 for each of the eight different virus strains at each time point investigated. In most data sets groups had $N = 2$, thus the test for Normality of data could not be run. Furthermore, *Levene's* test for Homogeneity of Variances were not run if $N < 3$. Subsequently, all one-way ANOVA analyses were calculated with the *Welch-Satterthwaite* correction, at an alpha level of 0.05. Table 13 summarises the ANOVA analyses results. Again, *SS* is the "Sum of Squares", *df* the "degrees of freedom", *MS* the "Mean Squares", *F* is the "*F*-statistic ratio" calculated for the ANOVA, and the *P-value* the level of significance at $\alpha_{0.05}$.

Table 13: Summary of ANOVA analyses results from pulse labelling assays on infected Vero cells

Data Set	Source	*SS*	*df*	*MS*	*F*	*P-value*	***P-value*
ᐞVP7 (5-8 h p.i.)	*Between*	1.671E+14	7	2.388E+13	0.813	0.589	0.316
	Within	4.697E+14	16	2.936E+13			
	Total	6.368E+14	23				
*°VP7 (13-16 h p.i.)	*Between*	4.836E+13	7	6.909E+12	×	×	×
	Within	0.000	0	×			
	Total	4.836E+13	7				
*ᐞVP7 (21-24 h p.i.)	*Between*	1.305E+14	7	1.864E+13	4.333	0.028	0.045
	Within	3.442E+13	8	4.303E+12			
	Total	1.649E+14	15				
ᐞNS1 (5-8 h p.i.)	*Between*	5.351E+13	7	7.644E+12	0.732	0.648	0.202
	Within	1.671E+14	16	1.011E+13			
	Total	2.206E+14	23				
*ᐞNS1 (13-16 h p.i.)	*Between*	4.550E+13	7	6.500E+12	2.281	0.135	0.192
	Within	2.279E+13	8	2.849E+12			
	Total	6.829E+13	15				
NS1 (21-24 h p.i.)	*Between*	5.245E+13	7	7.493E+12	4.879	0.004	-
	Within	2.457E+13	16	1.536E+12			
	Total	7.702E+13	23				
ᐞNS2 (5-8 h p.i.)	*Between*	5.467E+13	7	7.810E+12	0.913	0.521	0.250
	Within	1.368E+14	16	8.553E+12			
	Total	1.915E+14	23				
*°NS2 (13-16 h p.i.)	*Between*	9.934E+12	7	1.419E+12	×	×	×
	Within	0.000	0	×			
	Total	9.934E+12	7				
*ᐞNS2 (21-24 h p.i.)	*Between*	1.485E+13	7	2.122E+12	0.884	0.558	0.476
	Within	1.921E+13	8	2.401E+12			
	Total	3.407E+13	15				

***** *Shapiro-Wilk's* test was not calculated because *N* too low (*N* = 2)

° *Levene's* test was not calculated because *N* too low (*N* = 2)

ᐞ Homogeneity of Variances was violated and the *Welch-Satterthwaite* correction was made

****** Corrected *p*-value using the *Welch-Satterthwaite* correction

Where *Levene's* test for Homogeneity of Variances were significant ($p < \alpha_{0.05,}$), the *Welch-Satterthwaite* correction was made. This was done for the data sets indicated with "ᐞ" and results are indicated in Table 13.

If the ANOVA analyses were calculated with the *Welch-Satterthwaite* correction and results were significant ($p < \alpha_{0.05}$), the *Games-Howell post-hoc* multiple comparisons test was run. However, if the one-way ANOVA analyses were not corrected, the *Tukey HSD post-hoc* multiple comparisons test was run where ANOVA results were significant. *Post-hoc* analyses test were done to determine

which groups indicated statistically significantly differences in time specific mean protein levels. Differences were only reported if it was observed between a reassortant virus strain and its corresponding parental strains. Furthermore, mean synthesised VP7, NS1 and NS2 protein levels were compared between the parental and reassortant virus strains at a specific time point only and not across a time trial experiment. Table 14 shows results from the *post-hoc* multiple comparisons tests done.

Table 14: Results from *post-hoc* multiple comparisons test from pulse labelling assays on infected Vero cells

Data Set	*Post-Hoc* Analysis	Statistically Significant Difference			
		Reassortant Virus	**AHSV-2**	**AHSV-3**	**AHSV-4**
VP7 (21-24 h p.i.)	***Tukey HSD*	R4-2_{10}	Yes	×	No
NS1 (21-24 h p.i.)	*Tukey HSD*	R3-$2_{3,5}$	Yes	No	×
NS1 (21-24 h p.i.)	*Tukey HSD*	R4-2_{10}	Yes	×	No
NS1 (21-24 h p.i.)	*Tukey HSD*	R4-$2_{7,10}$	Yes	×	No

* *Tukey HSD post-hoc* multiple comparison results considered even though *Welch-Satterthwaite* correction made

Statistically significant differences were observed for mean VP7 and NS1 protein levels synthesized 21-24 hours p.i. ANOVA analyses results for VP7 protein synthesis (21-24 hours p.i.) were significant; however, the *Games-Howell post-hoc* analysis indicated no differences in mean VP7 levels synthesised. In contrast, the *Tukey HSD post-hoc* test indicated a significantly higher level of mean R4-2_{10} VP7 and NS1 synthesised 21-24 hours p.i. when compared to AHSV-2. Similarly, reassortant virus R3-$2_{3,5}$ and R4-$2_{7,10}$ indicated a significantly higher level of mean NS1, synthesised 21-24 hours p.i., when compared to AHSV-2. However, no statistical significant difference were observed in the mean VP7 or NS1 protein levels when compared to the “backbone” parent. Furthermore, statistically significant differences were observed for mean VP7 and mean NS1 protein levels synthesised from parental strains (not shown in Table 14). Results indicated that AHSV-3 mean VP7 and NS1 levels, synthesised at 21-24 hours p.i., were significantly higher compared to AHSV-2. Similarly, mean NS1 levels synthesised from AHSV-4, 21-24 hours p.i., were significantly higher compared to AHSV-2. Notably, statistically significant differences between groups were only observed at late time intervals, when CPE levels are already very high for most of the AHSV strains studied.

3.5 Analyses of Virus dsRNA Production in Infected Mammalian Cells

Double-stranded RNA (dsRNA) levels are an indication of genome segment packaging and replication into newly assembled core particles. This section reports findings observed from monitoring virus dsRNA levels, isolated from AHSV-infected mammalian cells.

3.5.1 Optimising total RNA isolation and virus dsRNA purification

To monitor newly synthesised virus dsRNA levels within infected mammalian cells, TRIzol® RNA isolation and LiCl precipitation were optimised. Vero cells were infected at an MOI of 2 using the eight different AHSV strains under investigation. Infected cells were harvested once ~90% CPE was observed and subjected to total RNA isolation using TRIzol® reagent (Invitrogen, Life Technologies) following the manufacturer's instructions. This was followed by LiCl precipitation to separate dsRNA from all other RNA species in the sample. Subsequently polyacrylamide gel electrophoresis (PAGE) was done to separate the dsRNA segments from each virus strain, shown in Figure 30.

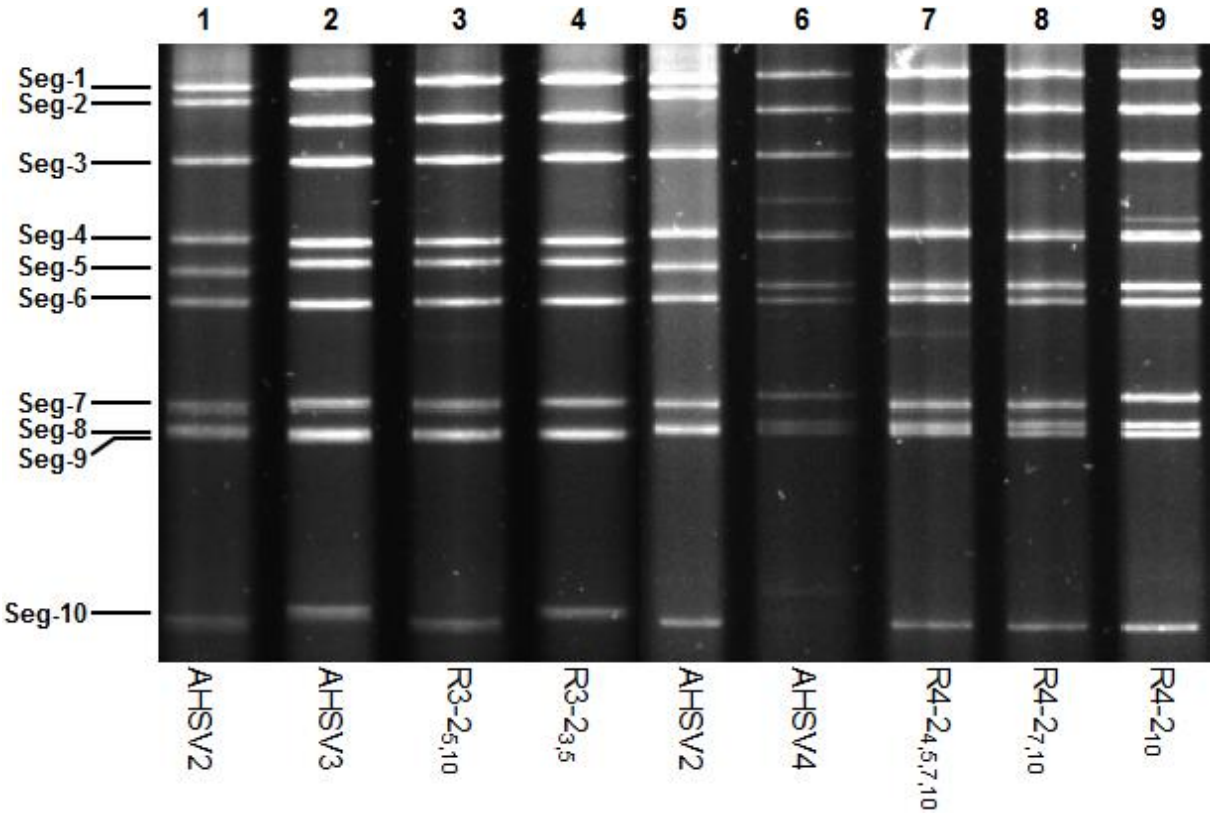

Figure 30: RNA PAGE results showing the three parental strains, Lanes 1 and 5: AHSV-2, Lane 2: AHSV-3, Lane 6: AHSV-4 and Lanes 3, 4, 7, 8 and 9: the five reassortant strains. The genome segments are indicated to the left of the image.

Results indicated that TRIzol® total RNA extraction and LiCl precipitation were successful and yielded adequate amounts of dsRNA for subsequent quantification.

3.5.2 Monitoring virus dsRNA levels

Levels of newly synthesised virus dsRNA was monitored from infected Vero cells as an indication of successful core formation and packaging. To investigate this, two experiments were set up using the eight AHSV strains under investigation in this study. Vero cells were either infected with virus at an MOI of 0.1 or an MOI of 2 and two biological replicates of each were done. Infected cells were harvested at 24 hours p.i. (MOI 2) or 48 hours (MOI 0.1), dsRNA isolated and separated by electrophoresis. Figure 31 shows a representative PAGE from each experiment.

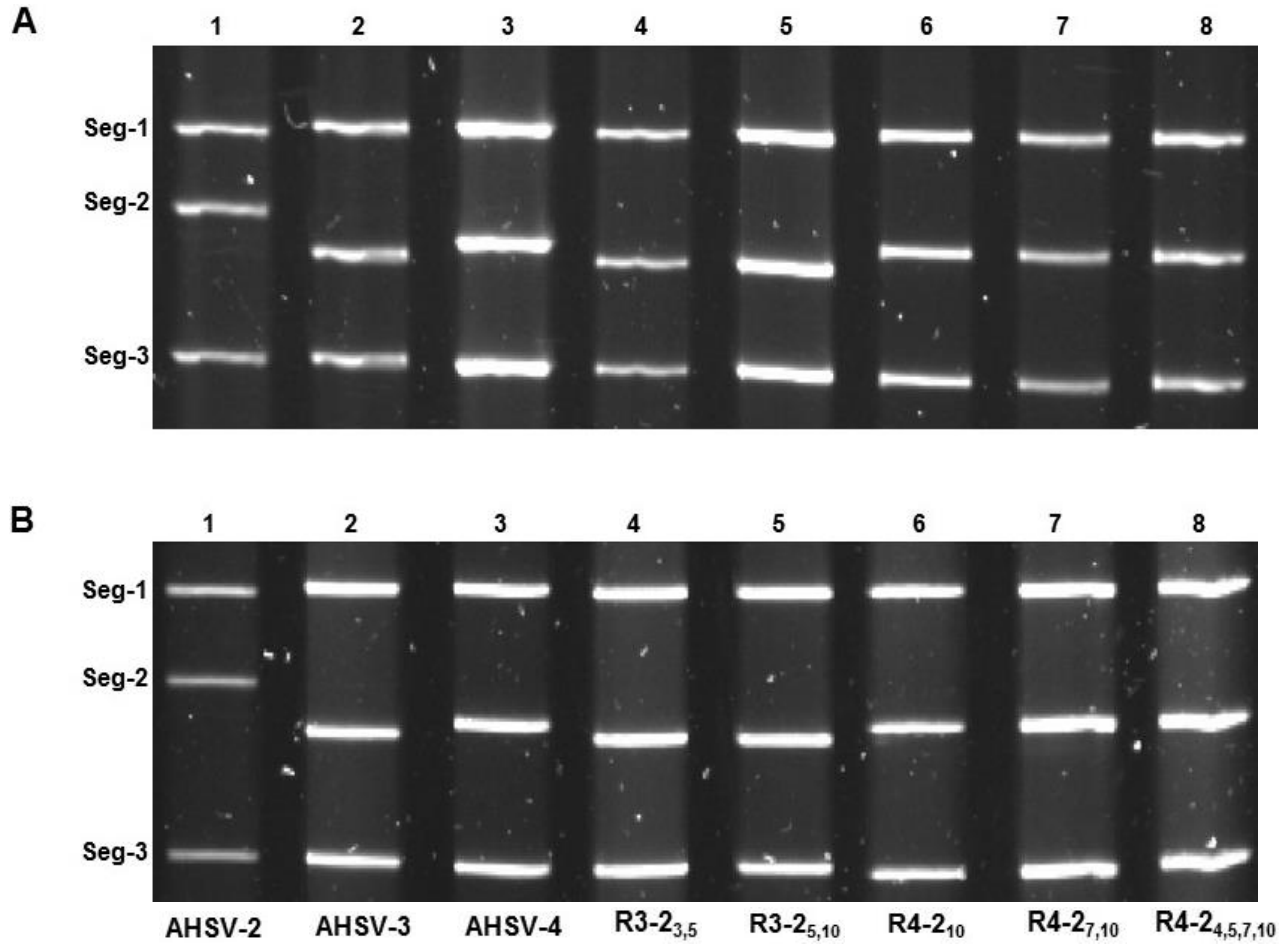

Figure 31: RNA PAGE results showing virus dsRNA levels at: A) 24 hours p.i. from Vero cells infected at an MOI of 2 pfu/cell and B) 48 hours p.i. from Vero cells infected at an MOI of 0.1 pfu/cell. AHSV-2, AHSV-3 and AHSV-4 were loaded in Lanes 1-3, respectively. The reassortant virus strains were loaded in the order: R3-2$_{3,5}$, R3-2$_{5,10}$, R4-2$_{10}$, R4-2$_{7,10}$ and R4-2$_{4,5,7,10}$ in Lanes 4-8. Only genome segments 1-3 are shown, indicated to left of image.

All genome segments are synthesised in equal ratios and it was decided to quantify segment 3 of each virus strain using the Image Lab imaging software tool. The average was calculated from the volume intensity values obtained from the two biological replicates. Figure 32 shows the data for the different AHSV strains at 24 hours p.i. (MOI 2 pfu/cell) and 48 hours p.i. (MOI 0.1 pfu/cell).

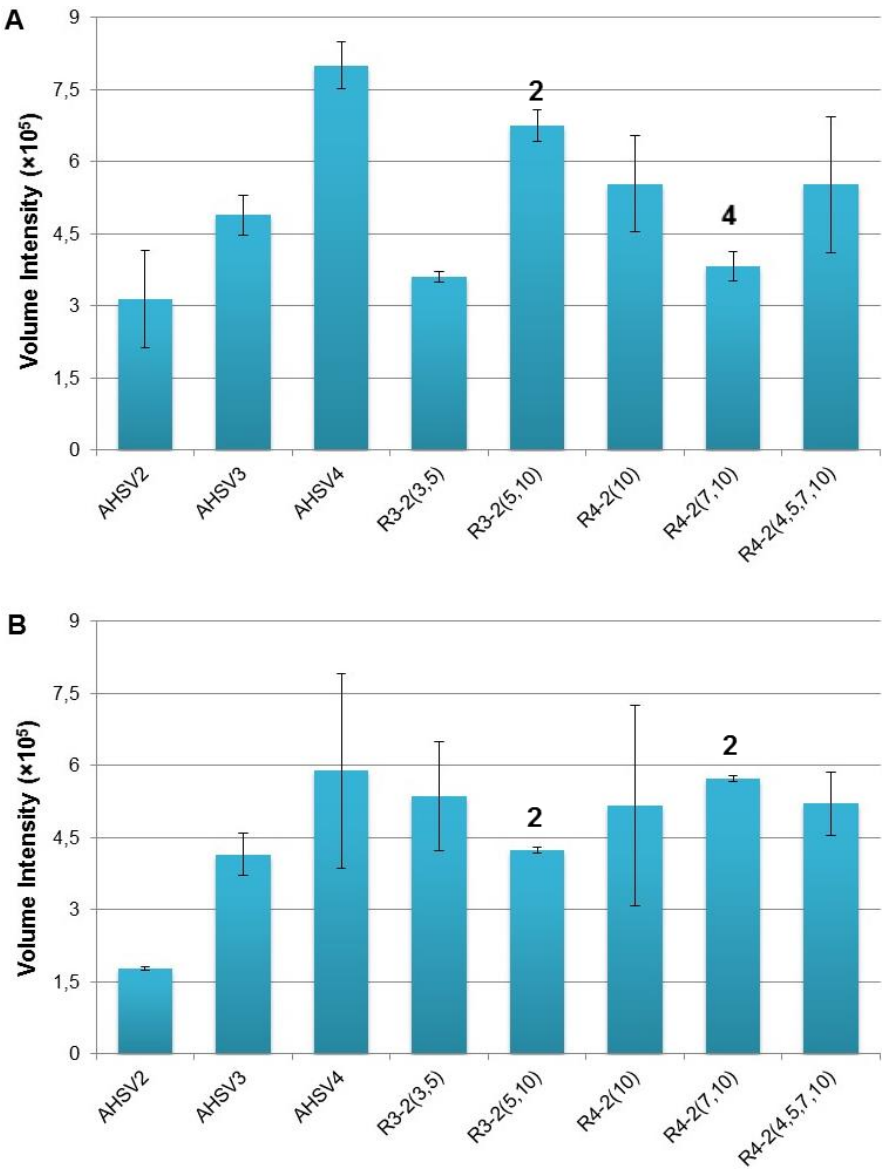

Figure 32: Averaged volume intensity values of A) virus dsRNA levels for Seg-3 at 24 hours p.i., cells were infected at an MOI of 2 pfu/cell. B) Virus dsRNA levels at 48 hours p.i., cells were infected at an MOI of 0.1 pfu/cell. Error bars indicate standard deviation. Numbers above bars indicate statistical significant difference to that parental strain.

3.5.3 Statistical analyses of AHSV segment 3 dsRNA levels at 24 and 48 hours p.i.

Statistical analyses test were run in SPSS Statistics (IBM Corp., Version 22, 2013) as previously explained and the same statistical analyses were run as outlined (section 3.3.5). Again, an alpha level of 0.05 was used for all statistical analyses and the *Welch-Satterhwaite* correction was made if *Leven's* test was significant ($p < \alpha_{0.05}$). Furthermore, the *Games-Howell post-hoc*, instead of the *Tukey HSD post-hoc* multiple comparisons test was run if the *Welch-Satterhwaite* correction were made. Table 15 shows the ANOVA analyses results for virus dsRNA levels at 24 and 48 hours p.i. *SS* is the "Sum of Squares", *df* the "degrees of freedom", *MS* the "Mean Squares", *F* is the "F-statistic ratio" calculated for the ANOVA, and the *P-value* our level of significance at $\alpha_{0.05}$.

Table 15: One-way ANOVA results from virus dsRNA levels at 24 and 48 hours p.i. monitored in infected Vero cells

Data Set	Source	*SS*	*df*	*MS*	*F*	*P-value*	***P-value*
*dsRNA 24 h p.i. (MOI 0.1)	*Between*	3.857E+11	7	5.511E+10	9.451	0.003	0.013
	Within	4.664E+10	8	5.831E+9			
	Total	4.324E+11	15				
*dsRNA 48 h p.i. (MOI 2)	*Between*	2.477E+11	7	3.538E+10	2.732	0.091	0.000
	Within	1.036E+11	8	1.295E+10			
	Total	3.513E+11	15				

***** Homogeneity of Variances was violated and the *Welch-Satterthwaite* correction was made

****** Corrected *p*-value using the *Welch-Satterthwaite* correction

Results for *Levene's* test was significant for both the 24 hours p.i. [F(7,8) = 3.633E+15, $p = 0.000$] and 48 hours p.i [F(7,8) = 3.041E+16, $p = 0.000$] data sets. Subsequently, for both one-way ANOVA analyses run, the *Welch-Satterthwaite* correction was made and results shown in Table 15. Results after correction indicated that there were significant differences in mean Seg-3 dsRNA levels of certain reassortant viruses and the parental strains they were compared to, for both data sets. However, the *Games-Howell post-hoc* analysis showed differences in group means only at 48 hours p.i. Again the *Tukey HSD post-hoc* analyses was run on the 24 hours p.i. data. Again, only reassortant viruses and their corresponding parental strains showing statistically significant differences in mean dsRNA levels were identified. These results are shown in Table 16.

Table 16: Summary of the *post-hoc* multiple comparisons test on virus dsRNA levels from infected Vero cells

Data Set	*Post-Hoc* Analysis	Statistically Significant Difference			
		Reassortant Virus	AHSV-2	AHSV-3	AHSV-4
dsRNA (24 h p.i.)	**Tukey HSD*	R3-$2_{5,10}$	Yes	No	×
dsRNA (24 h p.i.)	**Tukey HSD*	R4-$2_{7,10}$	No	×	Yes
dsRNA (48 h p.i.)	*Games-Howell*	R3-$2_{5,10}$	Yes	No	×
dsRNA (48 h p.i.)	*Games-Howell*	R4-$2_{7,10}$	Yes	×	No

***** *Tukey HSD post-hoc* multiple comparison results considered even though homogeneity of variances was violated

Result indicated that with a synchronised infection (MOI 2) reassortant virus R3-$2_{5,10}$ showed significantly higher mean dsRNA levels at 24 hours p.i. compared to the AHSV-2. On the contrary, reassortant virus R4-$2_{7,10}$ indicated significantly lower mean Seg-3 dsRNA levels at 24 hours p.i. when compared to AHSV-4. At a low MOI (0.1) both these reassortant virus strains showed significantly higher mean dsRNA levels at 48 hours p.i. when compared to AHSV-2.

3.6 Analyses of Virus Yield through Titration

This section report our findings observed through monitoring yield of new infectious AHSV particles assembled within infected mammalian cells. Yield was assayed through titration and plaque assays. These results will be used to investigate a possible correlation between synthesised virus protein levels, viral dsRNA levels and the quantity of new infectious particles observed in infected mammalian cells.

3.6.1 Assaying virus yield from infected mammalian cells following an unsynchronised and synchronised infection

To investigate yield of new infectious AHSV particles, a 200 µl sample from each infection from the time trial experiments (section 3.3.4) was kept aside for titration. Samples were taken from all three biological replicates of each virus infection during the initial harvesting step for both the MOI 0.1 and MOI 2 experiments. Based on results from the previous sections, it was decided to only titrate samples from the late times from each experiment. Thus, samples from infected cells (MOI of 2 pfu/cell) harvested 24 hours p.i., and samples from infected cells (MOI of 0.1 pfu/cell) harvested 48 hours p.i. were used.

Serial dilutions of each sample to be titrated were prepared up to 10^{-6}. For each sample, and all three biological replicates of each, the last three dilutions of each were used to infect BSR cells. Infected cells were then covered with a thin layer of agarose and incubated. Plaques were subsequently stained for counting and the averages from three biological replicates calculated for each of the eight AHSV strains studied. Figure 33 shows results obtained.

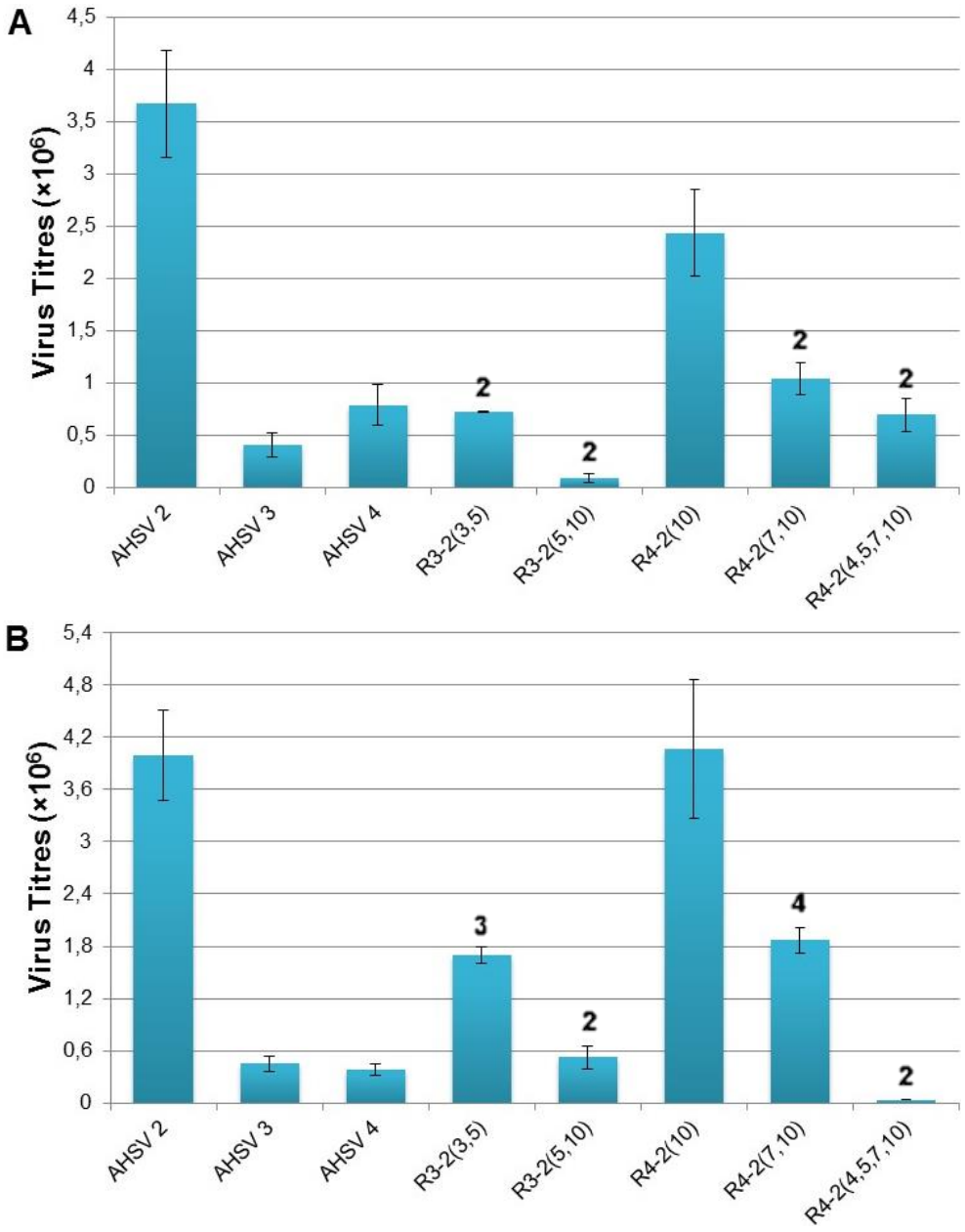

Figure 33: Titration results shown for yield of newly assembled infectious AHSV particles at A) 24 hours p.i. for a synchronous infection (MOI 2 pfu/cell) and B) 48 hours p.i. for an unsynchronous infection (MOI 0.1 pfu/cell). The graphs represent the average of three biological replicates for each strain at the two time points. Error bars indicate standard deviation. Numbers above bars indicate statistical significant difference to that parental strain.

Titrations in this study were performed to monitor the total virus yield only. Total virus yield was obtained by combining the collected cell pellet and supernatant fraction. An additional step however, would be to compare the levels of new progeny virus between the released and cell associated fractions of each of the AHSV strains investigated. Similarly to compare the virus yield of new infectious particles from the different strains investigated at different times post infection. However, due to time constraints, these experiments were not done.

3.6.2 Statistical Analyses of virus yield results at 24 and 48 hours p.i.

To determine if a differences exist in the mean level of newly assembled infectious particles between the different AHSV strains, statistical analyses test were run on the data as shown. Data was analysed using the statistical analysis program SPSS Statistics (IBM Corp., Version 22, 2013). All statistical analyses test were run as explained previously (section 3.3.5) and an alpha level of 0.05 used. Again, if results for ***Levene's*** test was significant ($p < \alpha_{0.05}$) the one-way ANOVA analyses was run with the *Welch-Satterthwaite* correction. *Post-hoc* multiple comparisons were done if the ANOVA results were significant ($p < \alpha_{0.05}$). If the ANOVA analysis was run using the *Welch-Satterthwaite* correction, the *Games-Howell post-hoc* multiple comparisons test was run. Alternatively, the *Tukey HSD post-hoc* multiple comparisons test was considered if the *Welch-Satterthwaite* correction was not calculated. Table 17 show results from the statistical analyses test done.

Table 17: One-way ANOVA results from virus titrations at 24 and 48 hours p.i. to monitor yield of newly assembled infectious AHSV particles

Data Set	Source	*SS*	*df*	*MS*	*F*	*P-value*	***P-value*
*****24 h p.i. (MOI 2)	*Between*	3.042E+17	7	4.346E+16	64.410	0.000	0.000
	Within	1.080E+16	16	6.747E+14			
	Total	3.150E+17	23				
*****48 h p.i. (MOI 0.1)	*Between*	5.504E+17	7	7.863E+16	64.419	0.000	0.000
	Within	1.953E+16	16	1.221E+15			
	Total	5.700E+17	23				

***** Homogeneity of Variances was violated and the *Welch-Satterthwaite* correction was made

****** Corrected *p*-value using the *Welch-Satterthwaite* correction

The *Welch-Satterthwaite* correction was calculated for both data sets as results for ***Levene's*** test were significant. ANOVA results for the virus yield 24 hours p.i., after correction, was $F(7,6.044) = 77.767$, $p = 0.000$ and $F(7,6.004) = 146.336$, $p = 0.000$ for virus yield 48 hours p.i. Subsequently, the *Games-Howell post-hoc* multiple comparisons analyses were run for both data sets. Table 18 show results for statistically significant differences observed between reassortant and parental AHSV strains.

Table 18: Summary of the *post-hoc* multiple comparisons test results on virus titrations at 24 and 48 hours p.i.

Data Set	*Post-Hoc* Analysis	Statistically Significant Difference			
		Reassortant Virus	AHSV-2	AHSV-3	AHSV-4
24 h p.i.	*Games-Howell*	R3-$2_{3,5}$	Yes	No	×
24 h p.i.	*Games-Howell*	R3-$2_{5,10}$	Yes	No	×
24 h p.i.	*Games-Howell*	R4-$2_{7,10}$	Yes	×	No
24 h p.i.	*Games-Howell*	R4-$2_{4,5,7,10}$	Yes	×	No
48 h p.i.	*Games-Howell*	R3-$2_{3,5}$	No	Yes	×
48 h p.i.	*Games-Howell*	R3-$2_{5,10}$	Yes	No	×
48 h p.i.	*Games-Howell*	R4-$2_{7,10}$	No	×	Yes
48 h p.i.	*Games-Howell*	R4-$2_{4,5,7,10}$	Yes	×	No

Post-hoc multiple comparison analyses showed that reassortant strains R3-$2_{3,5}$, R3-$2_{5,10}$, R4-$2_{7,10}$ and R4-$2_{4,5,7,10}$ showed statistically significant difference in mean yield of newly assembled particles released compared to only one of the two parental strains. From the synchronised infection (MOI 2 pfu/cell) it was observed that up to 24 hours p.i., a lower mean yield of new virus particles for R3-$2_{3,5}$, R3-$2_{5,10}$, R4-$2_{7,10}$ and R4-$2_{4,5,7,10}$ were produced, compared to AHSV-2. However, from the unsynchronised infection (MOI 0.1 pfu/cell) it was observed that R3-$2_{5,10}$ and R4-$2_{4,5,7,10}$ produced a significant lower mean yield of new virus particles up to 48 hours p.i. compared to AHSV-2. Reassortant strains R3-$2_{3,5}$ and R4-$2_{7,10}$, showed a significantly higher mean yield of new virus particles produced up to 48 hours p.i., compared to AHSV-3 and AHSV-4 respectively. In both graphs in Figure 33 it appears as though the mono-reassortant strain, R4-2_{10}, produced significantly higher mean yields at 24 and 48 hours p.i. compared to AHSV-4. However, statistical analyses indicated that strain R4-2_{10} did not differ from AHSV-2 and AHSV-4. This could be due to a large variance and standard deviation calculated between the 3 biological replicates for the mono-reassortant strain.

3.7 Monitoring Virus Protein Synthesis, Virus dsRNA and Virus Yield in Infected Insect Cells

African horsesickness virus infections in insect cells have been observed to show no cytopathicity (Mirchamsy *et al.*, 1970; Osawa and Hazrati, 1965), even though new infectious particles are actively assembled and released for reinfection. Recent studies have shown that infection with AHSV in insect cells does not induce apoptosis (Stassen *et al.*, 2012), suggesting a reason for the lack of CPE. AHSV protein synthesis, virus dsRNA synthesis and virus yield in infected insect cells were

studied and compared to the corresponding results observed from infected mammalian cells (section 3.3.5, 3.5.3 and 3.6.2 respectively).

3.7.1 Analyses of viral protein synthesis by immunoblot assays

To study AHSV VP7, NS1 and NS2 protein synthesis in insect cells, KC cells (derived from the *Culicoides variipennis* midge) were infected with the eight different AHSV strains studied. Cells were infected at an MOI of 0.1 pfu/cell, and two biological replicates for each virus infection were prepared. After incubation, at 28°C for 8 days, cells were harvested and subjected to Western blot assays as described previously (section 3.3.4). Results were subsequently quantified and statistical analyses run using the software analyses tools previously described. Again, only blots with good quantifiable signals were used and where two blots were used an average of the synthesised protein levels was calculated. Figure 34 show a representative Western blot for each of the virus proteins studied and a graph illustrating the corresponding quantified protein levels.

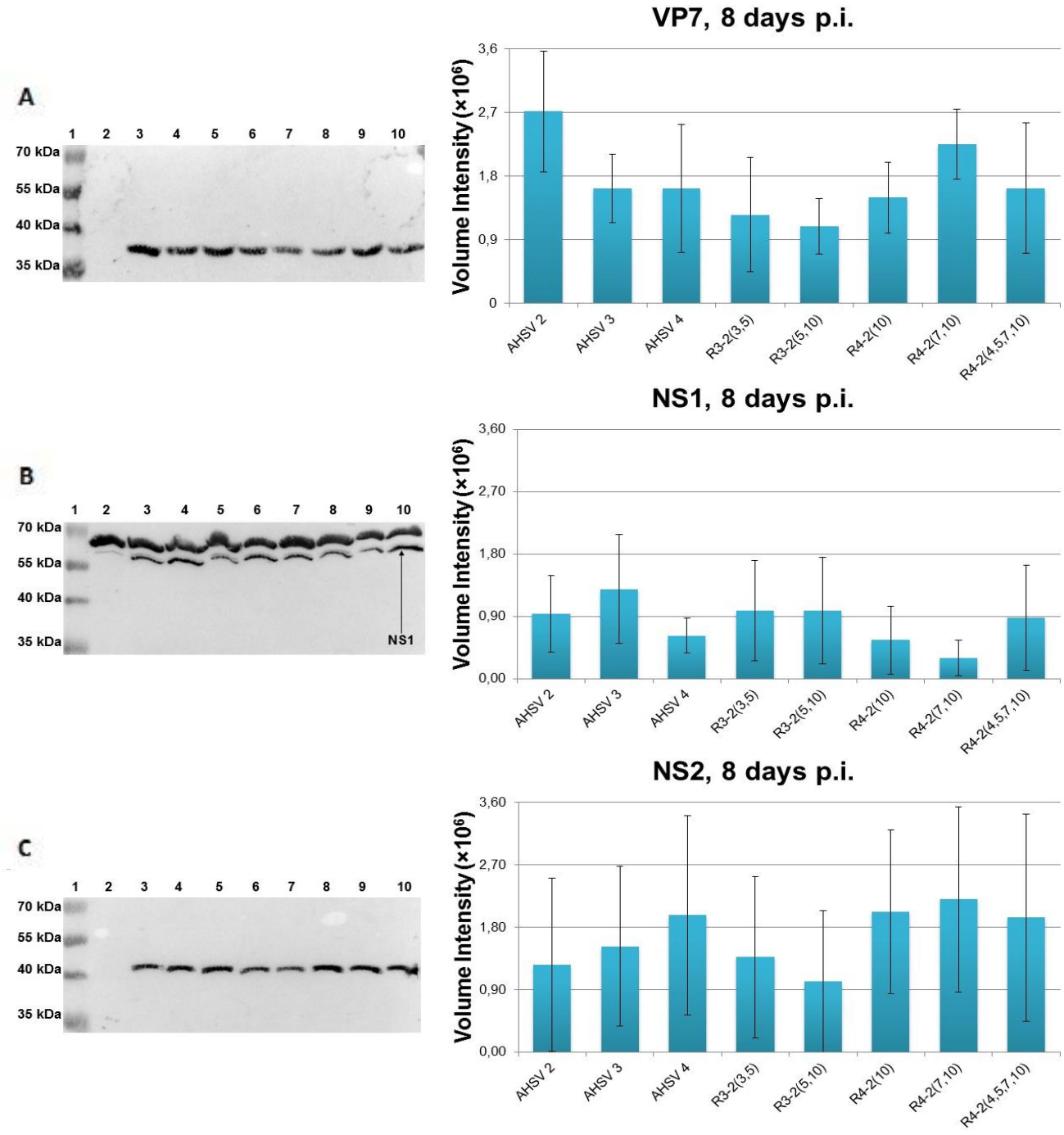

Figure 34: Results showing a representative blot for AHSV proteins studied with a corresponding graph indicating the quantified protein levels synthesised up to 8 days post-infection. For each blot a size marker (Lane 1) is indicated with sizes on the left. For each blot Lane 2 indicates the mock-infected sample and Lanes 3-10 show the AHSV results for A) VP7, B) NS1 and C) NS2. NS1 results are indicated with arrow. Results from Western blots are indicated in the same order as shown on graphs. Error bars on graphs represent standard deviations.

No housekeeping gene protein was identified for the KC cells used and due to time constraints, none was tested. The results shown in Figure 34 were not normalised before statistical analyses were run. Statistical analyses on the results were done as before using SPSS Statistics (IBM Corp., Version 22, 2013). The same analyses were run to determine if the AHSV reassortant viruses VP7, NS1 or NS2 protein levels were significantly different compared to the parental strains. One-way ANOVA analyses results are summarised in Table 19.

Table 19: Summary of the one-way ANOVA results for AHSV VP7, NS1 and NS2 protein levels from infected KC cells

Data Set	Source	*SS*	*df*	*MS*	*F*	*P-value*
VP7 (8 days p.i.)	*Between*	1.182E+13	7	1.689E+12	3.438	0.006
	Within	1.965E+13	40	4.912E+11		
	Total	3.147E+13	47			
NS1 (8 days p.i.)	*Between*	2.041E+12	7	2.915E+11	0.779	0.614
	Within	5.989E+12	16	3.743E+11		
	Total	8.029E+12	23			
NS2 (8 days p.i.)	*Between*	7.648E+12	7	1.093E+12	0.687	0.682
	Within	6.361E+13	40	1.590E+12		
	Total	7.125E+13	47			

Results for *Levene's* test for homogeneity of variances for the data sets shown in Table 19, were not significant ($p > \alpha_{0.05}$) and the *Welch-Satterthwaite* correction was not calculated. One-way ANOVA analyses results for VP7 was significant ($p < \alpha_{0.05}$) and *Tukey's HSD post-hoc* multiple comparisons were calculated. Results were considered significant if there were statistically significant differences observed between a reassortant virus and its corresponding parental strains. Table 20 show results of the *post-hoc* analysis.

Table 20: Summary of the *post-hoc* multiple comparisons test results for virus protein synthesis at 8 days p.i.

Data Set	*Post-Hoc* Analysis	Statistically Significant Difference			
		Reassortant Virus	AHSV-2	AHSV-3	AHSV-4
VP7 (8 days p.i.)	*Tukey HSD*	R3-$2_{3,5}$	Yes	No	×
VP7 (8 days p.i.)	*Tukey HSD*	R3-$2_{5,10}$	Yes	No	×

Results from the *Tukey HSD post-hoc* multiple comparisons test, indicated that reassortant viruses R3-$2_{3,5}$ and R3-$2_{5,10}$ were statistically different from the AHSV-2 parental strain only. Mean VP7 levels of these reassortant virus strains were significantly lower than AHSV-2, meassured at 8 days p.i. In comparison, R3-$2_{5,10}$ showed significant higher mean VP7 levels in mammalian cells at 8 hours p.i. (MOI 0.1 pfu/cell), compared to both AHSV-2 and AHSV-3. No significant difference in mean VP7 protein levels, measured at 8 days p.i., were observed between the three parental AHSV strains.

3.7.2 Analyses of viral dsRNA levels in infected insect cells

To monitor AHSV dsRNA levels in insect cells, KC cells were infected at an MOI of 0.1 pfu/cell with each of the 8 different virus strains studied. Two biological replicates were done and infected cells were harvested 8 days p.i. followed by sample preparation and analyses. Gels where good signals for AHSV genome segment 3 were observed, were subjected to relative quantification as previously described (see 3.5.2). Average Seg-3 dsRNA levels were calculated for virus strains where more than one gel was considered for analysis. Figure 35 show the RNA-PAGE results with a corresponding graph indicating average quantified dsRNA levels.

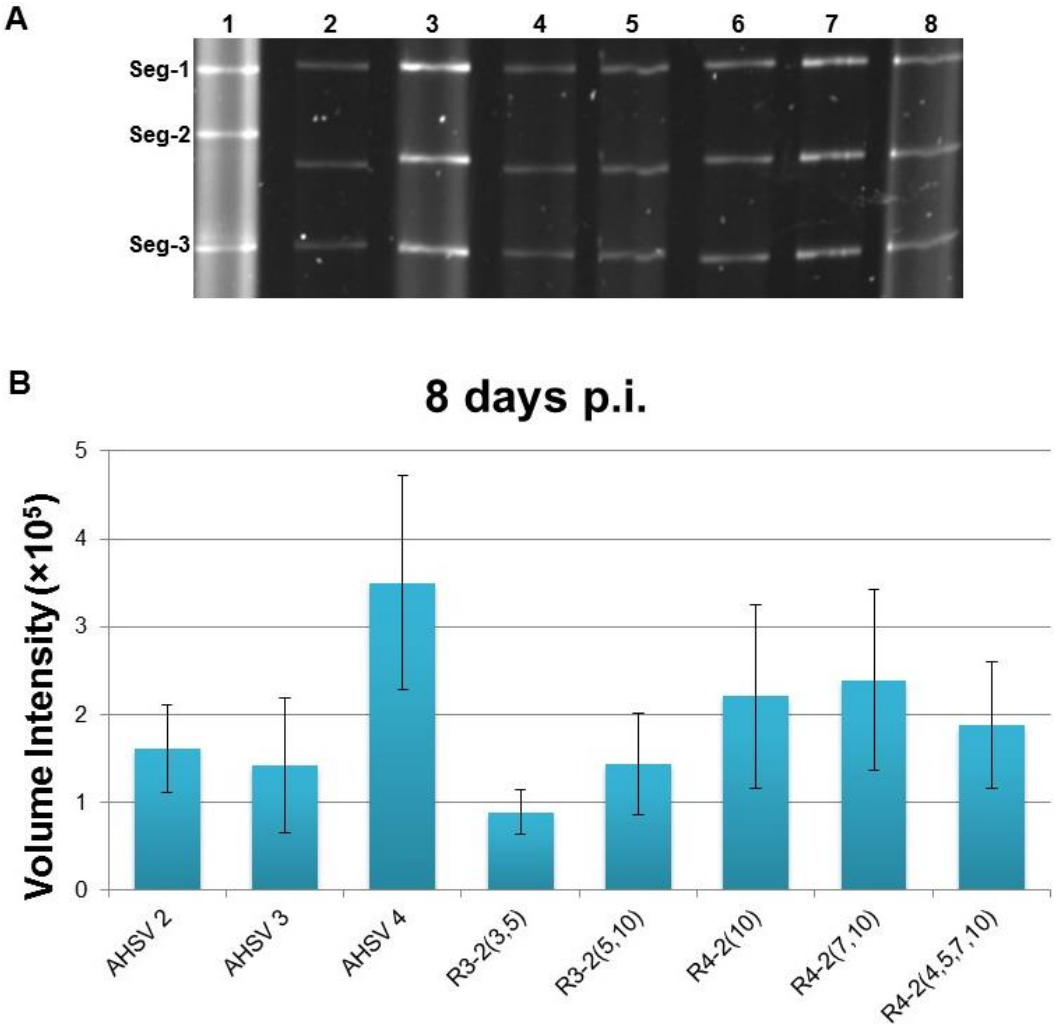

Figure 35: A) Results showing virus segment 3 dsRNA levels at 8 days p.i. in infected KC cells. Genome segments indicated to left of image. Samples on gel loaded in same order as indicated on graph. B) Average virus segment 3 dsRNA levels at 8 days p.i. for the 8 different virus strains as indicated. Error bars indicate standard deviation.

Results were subjected to statistical analyses using SPSS Statistics (IBM Corp., Version 22, 2013), and the same tests were run as described for the corresponding results obtained from monitoring AHSV dsRNA in infected Vero cells. An alpha (α) level of 0.05 was used for all statistical analyses run. One-way ANOVA analyses results are summarised in Table 21.

Table 21: Summary of one-way ANOVA results for virus dsRNA levels at 8 days p.i. in infected KC cells

Data Set	Source	*SS*	*df*	*MS*	*F*	*P-value*	***P-value*
*dsRNA (8 days p.i.)	*Between*	1.783E+11	7	2.547E+10	3.781	0.007	0.033
	Within	1.617E+11	24	6.737E+9			
	Total	3.400E+11	31				

* Homogeneity of Variances was violated and the *Welch-Satterthwaite* correction was made

****** Corrected *p*-value using the *Welch-Satterthwaite* correction

Levene's test for homogeneity of variance was significant for the data set $F(7,24) = 2.801$, $p = 0.028$ and the *Welch-Satterthwaite* correction was made. ANOVA results after correction was $F(7,9.948) = 3.638$, $p = 0.033$. ANOVA results for the data was significant ($p < \alpha_{0.05}$) and the *Games-Howell post-hoc* multiple comparisons test was run. Results indicated no statistically significant difference in mean virus Seg-3 dsRNA levels for any of the reassortant viruses when compared to their corresponding parental strains. However, results indicated that mean virus Seg-3 dsRNA levels at 8 days p.i. for AHSV-3 were significantly lower than for AHSV-4.

3.7.3 Assaying virus yield from infected insect cells through titration

To assay yield of new infectious AHSV particles in infected KC cells, 200 µl of each sample initially harvested to monitor virus protein synthesis (section 3.7.1) was kept aside for titration. Samples were taken from both biological replicates of each virus infection done. The experimental procedure as explained previously (section 3.6.1) were followed and the average yield for each of the eight AHSV strains studied, was calculated. Figure 36 shows titration results at 8 days p.i.

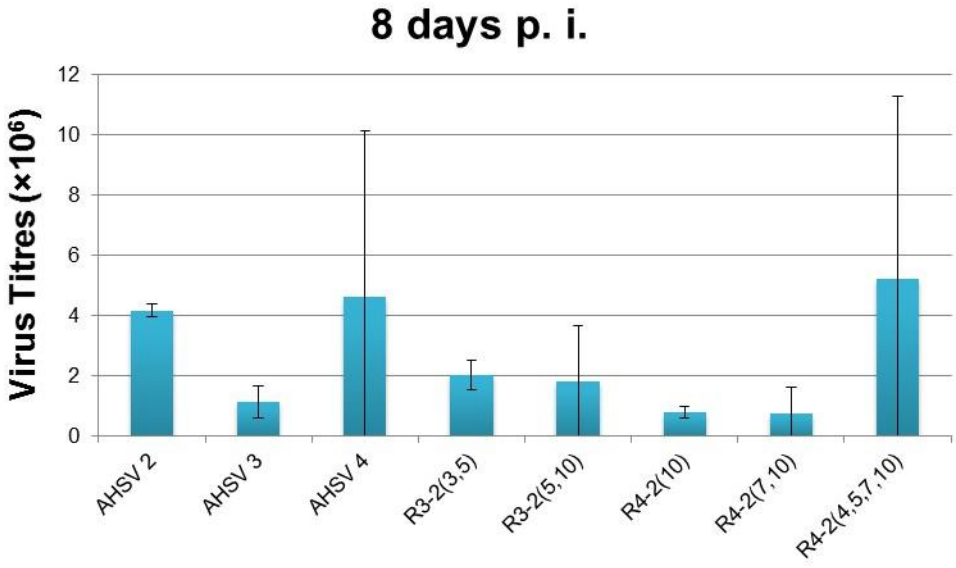

Figure 36: Titration results showing average yield of new infections AHSV particles from infected KC cells at 8 days p.i. Error bars indicate standard deviations.

Statistical analyses was run on the data shown in Figure 36 using SPSS Statistics (IBM Corp., Version 22, 2013). Data were analysed using the same statistical test as outlined for the corresponding results from monitoring virus yield in infected Vero cells (section 3.6.2). Results from the one-way ANOVA analysis are shown in Table 22.

Table 22: Summary of the one-way ANOVA results for new infectious AHSV particles from infected KC cells

Data Set	Source	*SS*	*df*	*MS*	*F*	*P-value*	***P-value*
*Yield (8 days p.i.)	*Between*	4.651E+17	7	6.644E+16	0.741	0.647	0.012
	Within	7.177E+17	8	8.971E+16			
	Total	1.183E+18	15				

* Homogeneity of Variances was violated and the *Welch-Satterthwaite* correction was made

****** Corrected *p*-value using the *Welch-Satterthwaite* correction

Results for *Leven's* test was significant ($p < \alpha_{0.05}$) and homogeneity of variances was violated, F(7,8) = 1.171E+17, $p = 0.000$. Accordingly, the *Welch-Satterthwaite* correction was made, and ANOVA results after correction was significant F(7,3.292) = 19.866, $p = 0.012$. To determine if there was significant difference in the mean yield at 8 days p.i. between reassortant viruses and their corresponding parental strains, the *Games-Howell post-hoc* analyses test was run. Results are summarised in Table 23.

Table 23: Summary of the *post-hoc* multiple comparisons test results for virus yield at 8 days p.i

Data Set	*Post-Hoc* Analysis	Statistically Significant Difference			
		Reassortant Virus	AHSV-2	AHSV-3	AHSV-4
8 days p.i.	*Games-Howell*	R4-2_{10}	Yes	×	No

Results indicated that only reassortant virus R4-2_{10} showed a significantly lower mean yield 8 days p.i. compared to AHSV-2 only. No statistically significant difference in mean yield was observed between the other reassortant viruses and their corresponding parental strains.

4 DISCUSSION AND CONCLUDING REMARKS

Currently orbiviruses are recognised as causing worldwide emerging and re-emerging disease outbreaks that have been documented since the late 1800's. Specifically African horsesickness, which can manifest in four clinically distinct forms in equid species, is of great economic importance in South Africa. AHS can present itself with varying mortality rates, and to date no known correlation exist between specific serotypes and specific clinical forms. While many studies have focused on the disease pathogenesis and viral replication kinetics of orbiviruses, our study was a direct follow up from findings observed by Meiring *et al*. (2009). In their study, varying degrees of CPE was observed in cultured mammalian cells upon infection with three different serotypes of AHSV and five reassortant strains. As the molecular basis for these differences are not yet known or fully understood, the aim of this study was to monitor different stages of the AHSV lifecycle to propose a cause for the diverse cytopathogenesis phenotypes observed. To accomplish this, systematic comparisons of gene expression studies on parental and reassortant AHSV strains were done in both a mammalian and insect tissue culture system.

This study set out to monitor different AHSV replication cycle stages that focused mainly on i) transcription, ii) translation, iii) genome segment packaging and dsRNA synthesis, and iv) virus release since little is known about the discrepancies in replication kinetics between the different strains. Earlier studies revealed that transcription of the orbivirus dsRNA segments take place simultaneously and repeatedly, although not in equimolar amounts (Bartlett *et al*., 1974; Mertens & Diprose, 2004). Correspondingly, virus proteins are translated throughout the replication cycle and detected as early as two to four hours post-infection. Translated proteins continue to accumulate throughout the replication cycle until assembly of new virus particles and cell lysis occur (Huismans & Van Dijk, 1990). To investigate a possible molecular basis for the different cytopathic phenotypes observed, we attempted to correlate quantified levels of virus mRNA, dsRNA and proteins with CPE for the eight AHSV strains studied. To compare the eight selected virus strains, we selected both a structural (VP7) and non-structural (NS2) protein that are highly expressed throughout the virus replication cycle. VP7 presents a particularly immune-dominant antigen and is highly conserved among serotypes and different orbivirus serogroups (Bremer *et al*., 1990; Mertens *et al*., 1984). Moreover as VP7 epitopes are present on the virus core, immune pressure governing its mutation is relatively low (Anthony *et al*., 2007). Non-structural proteins NS1 and NS3/NS3A were also selected as candidates, as previous studies had made important postulates regarding their specific role during the replication cycle (Owens *et al*., 2004).

While non-structural protein NS2 is responsible for the formation of the VIBs, much less is known about the function of NS1. The NS2 protein has multiple RNA binding sites and can readily recruit RNA molecules, subsequently initiating core scaffold assembly. The core particles become stable once associated with VP7 trimers (Limn & Roy, 2003). Following assembly of a stable core, the outer capsid proteins are recruited for assembly (Bhattacharya *et al.*, 2007), and will render the transcriptionally active particle inactive and primed for release (Roy, 2005). Orbivirus release from an infected cell has been observed in one of two ways, either through budding off or by lytic release. NS3/NS3A was suggested to facilitate mature virion release from infected cells (Roy, 2005), and was observed to sequester the cellular exocytosis pathway to assist in nonlytic release (Beaton *et al*., 2002). It is known that AHSV infection does not induce CPE in insect cells, and this encouraged us to conduct similar studies in an insect tissue culture system to determine and compare differences on a molecular level.

The three parental serotypes used were AHSV-2, AHSV-3 and AHSV-4. For the reassortant strains, the backbone of each reassortant consisted of six or more genome segments originating from either AHSV-3 or AHSV-4. The remainder of the genome segments were contributed by AHSV-2. Reassorted AHSV-2 genome segments were Seg-3 (VP3), Seg-4 (VP4), Seg-5 (NS1), Seg-7 (VP7) and Seg-10 (NS3/NS3A). Each reassortant strain had either one (R4-2_{10}) or a combination (R3-$2_{3,5}$, R3-$2_{5,10}$, R4-$2_{7,10}$ or R4-$2_{4,5,7,10}$) of these reassorted genome segments. Our initial observations on the degree of CPE induced by these strains in mammalian cells correlated with the results of Meiring and colleagues (2009). Observations at 24 hours post-infection indicated AHSV-2 as having the most severe and AHSV-4 as having the least severe cytopathogenic phenotypes. AHSV-3 infection resulted in an intermediately severe CPE. Reassortant strain R3-$2_{5,10}$ showed more severe CPE than AHSV-2, strains R4-2_{10} & R4-$2_{7,10}$ showed less CPE than AHSV-4, and R3-$2_{3,5}$ and R4-$2_{4,5,7,10}$ gave intermediate phenotypes resembling AHSV-3.

For many decades PCR has been widely used as a qualitative assay for detecting the presence or absence of specifically virus mRNA transcripts. However, development of real-time qPCR has offered many advantages over conventional end-point PCR to study low abundance nucleic acid species and its potential to quantify target nucleic acids accurately (Bustin *et al*., 2009). While quantification capabilities of end-point PCR proved limiting, real-time quantitative PCR is an amplification-and-analysis single-step method with no subsequent sample manipulation (Al-Khatib & Carr, 2003). Important advantages of real-time qPCR include high sensitivity and specificity of the assay, high throughput and reproducibility capabilities, and the ability to quantify viral mRNA levels (Al-Khatib & Carr, 2003; Bustin *et al*., 2009). These advantages led to the development of various uses for this application. These uses including nucleic acid and microbial quantification, biomarker discovery and validation, cancer risk assessment, gene dosage determination and detection of extremely low copy targets for forensic investigation (Bustin *et al*., 2009).

The use of real-time qPCR assays are grouped into two main focus aims, namely research or diagnostic applications (Bustin *et al*., 2009), and numerous real-time qPCR studies of orbiviruses have focused on the latter. These studies aimed to develop a rapid, analytically sensitive assay for detection and identification of specific virus serotypes. For AHSV, real-time PCR assays have been developed that proved both virus-species-specific and type-specific without non-target amplification of serotypes previously reported to cross-react on neutralisation tests. These included studies by Rodriguez-Sanchez *et al*. (2008), designing an assay that targeted AHSV segment 5 (NS1); Fernández-Pinero *et al*. (2009) who developed a TaqMan-MGB real-time reverse transcription-PCR assay targeting a highly conserved region of genome segment 7 (VP7); Quan *et al*. (2010), developing a duplex real-time RT-PCR assay that targeted both the VP7 and NS2 genes; Monaco *et al*. (2011) who designed a duplex FAM-labelled TaqMan-MGB real-time RT-PCR assay targeting genome segment 8 (NS2); Bachanek-Bankowska *et al*. (2014) who developed both a serogroup-specific assay targeting genome segments 1 (VP1) and 3 (VP3) and a type-specific assay targeting segment 2 (VP2); and Weyer *et al*. (2015) that designed three triplex real-time RT-PCR assays for qualitative molecular typing targeting VP2. These studies proved the sensitivity and reliability of real-time PCR, displaying specificity to reference and field strains of all 9 AHSV serotypes.

Similar studies have also been done for BTV and EEV. The molecular diagnosis of BTV is especially complex because of high genetic variability between the 26 different serotypes. Real-time RT-PCR assays were developed for rapid and sensitive diagnosis of BTV of all 26 serotypes. Among these studies were assays developed by Toussaint *et al*. (2007), targeting BTV segments 1 and 5; Anthony *et al*. (2007), targeting genome segment 7 (VP7) and Shaw *et al*. (2007), targeting genome segment

1. Real-time RT-PCR assays using TaqMan-MGB probes were developed recently that detected either all 26 BTV serotypes by targeting genome segment 9 (Maan *et al*., 2015), or targeted the VP2 encoding genomic sequence to discriminate between 22 BTV serotypes (Feng *et al*., 2015). A similar assay, using TaqMan-MGB probes, was developed to detect the serogroup specific orbivirus EEV. The real-time RT-PCR assay targeted genome segment 7 (VP7) with 81% efficiency (Rathogwa *et al*., 2014).

For our systematic analysis of the AHSV replication cycle, the focus of our study at the virus transcription and replication level was to investigate differences in levels of AHSV mRNA transcribed. The initial aim was to monitor AHSV VP7, NS1, NS2 and/or NS3/NS3A transcript levels at 0, 2, 4, 8, 12 and 24 hours post-infection for the eight strains studied. According to the MIQE (Minimum Information for Publication of Quantitative Real-Time PCR Experiments) guidelines, one of the checkpoints is to determine and evaluate suitable internal controls (Bustin *et al*., 2009). Suitable housekeeping genes, to use as internal controls for quantitative gene expression studies, were tested for expression stability. Available primers for the β_2M and GAPDH housekeeping genes for mammalian Vero cells were evaluated for our studies according to the guidelines from previous studies (Svobodová *et al*., 2008; Vandesompele *et al*., 2002). Standard curve analyses indicated that quantitative reliability and PCR efficiency for both housekeeping genes were suitable for gene expression studies in mammalian cells. A primer amplification efficiency of 90% and 87.5% respectively was calculated for β_2M and GAPDH, and considered appropriate for our analyses. Segment-specific primers were optimised for VP7, NS1 and NS2 using conventional PCR analyses. For the NS3 gene, regions for primer binding were identified and suitable primers for all three parental strains were designed, however only AHSV-2 NS3 and AHSV-3 NS3 primers were optimised successfully. The different NS3 primer sets could however not be optimised to the same conditions, and subsequent gene expression studies monitoring NS3 mRNA levels would prove difficult to standardise and compare. Consequently this meant that AHSV strains would have to be assayed separately for Seg-10 expression, necessitating the decision to eliminate NS3 from further gene expression studies.

Due to time constraints, only limited real-time qPCR analyses were done. Future steps would be to optimise the real-time PCR assays using the suitable segment-specific primers identified. Although postulated that relative quantification of virus mRNA levels could potentially indicate a correlation between the cytopathogenic phenotypes observed in infected mammalian cells and the relative mRNA levels, our hypothesis remains inconclusive. However, a similar study by Shmulevitz *et al*. (2012) provides solid motivation for future investigations along this line in our own studies. They identified two reassortant human reovirus strains (T3v1 and T3v2) that showed increased replication efficiency compared to the highly oncolytic serotype 3 Dearing (T3wt). They suggested that reassortment of genome segments introduced these new characteristics compared to strain T3wt. Detailed examination of the virus replication steps demonstrated that both these reassortant strains achieved a strategy to enhance virus infection, leading to higher levels of early virus transcription. These findings could suggest that reassortment of AHSV genome segments, leading to increased cytopathogenesis in infected mammalian cells, achieve a similar strategy for superior replication. We are hopeful that we would indeed observe similar results with future real-time qPCR analyses.

Although similar phenotypic differences are not observed in AHSV-infected insect cells, it should not deter our efforts to improve our understanding of the AHSV replication kinetics, specifically in the vector host. However, to approach this, identification of suitable housekeeping genes is vital for use as internal calibrators for gene expression studies in the KC (*Culicoides*-derived) insect cell line. Investigation for putative housekeeping genes and their expression stability in the planthopper,

Delphacodes kuscheli, infected with the *Mal de Río Cuarto virus* (MRCV), of the *Fijivirus* genus from the *Reoviridae* family, has been done (Maroniche *et al*., 2011). The study concluded that the most suitable housekeeping gene for use as internal controls in quantitative gene expression studies (real-time qPCR) are the genes encoding polyubiquitin C (UBI), ribosomal protein S18 (RPS18) and actin (ACT). Therefore, this study suggest value in testing these housekeeping genes in KC insect cells as potential suitable internal controls.

Early studies done to investigate the orbivirus proteins aimed to identify and characterise the different proteins, and assign each to a segment of the virus genome. Initial studies done by Bremer (1976) investigated the physico-chemical structure of AHSV and compared it to other members of the *Reoviridae* family. Studies by Huismans (1979) focussed on the protein synthesis of BTV *in vitro*, whereas studies by Van Dijk & Huismans (1988) looked at *in vitro* transcription of BTV mRNA and compared the molar ratio of these species to the corresponding ratios of proteins synthesised. Grubman & Lewis (1992) identified and characterised the structural and non-structural AHSV proteins, and allocated coding assignments to genome segments. Later Van Staden *et al*. (1995) investigated the translation of AHSV genome segment 10 *in vitro*. This was followed by a number of studies looking at non-structural proteins such as Uitenweerde *et al*. (1995) that investigated the NS2 protein of BTV, AHSV and EHDV to characterise its structure and ssRNA-binding ability. Stoltz *et al*. (1996) investigated the subcellular localisation *in vitro* of AHSV NS3 protein, and Maree & Huismans (1997) characterised the AHSV NS1 tubular structures, *in vitro* in insect cells. Van Staden *et al*. (1998) thereafter characterised the AHSV NS1 and NS3 non-structural proteins *in vitro*. Studies following these aimed at more in-depth investigation to characterise and formulate their role in the orbivirus replication cycle. Van Niekerk *et al*. (2001a) focussed on AHSV NS3 to determine its cytotoxicity and membrane association affinity and localisation. Han & Harty (2004) investigated the viroporin-like properties of BTV NS3 protein, while Wirblich *et al*. (2006) further explored BTV NS3 role in the virus release pathway and the mobilisation of the ESCRT-I Protein Tsg101. Later Roy (2008a) reviewed the different virus proteins, using functional mapping to demonstrate proposed functions of each protein, showing their integrated part in the structure, biochemistry, assembly and replication of BTV. A study by Meiring *et al*. (2009), utilising both parental and reassortant AHSV strains, indicated the role of AHSV NS3 in membrane permeability and virus release. More recently studies have been done to detect and identify a fourth non-structural orbivirus protein NS4 (Belhouchet *et al*., 2011). Although extensive research has been done one the different AHSV proteins to propose their function in the AHSV replication cycle, we have only focused our efforts on AHSV VP7, NS1 and NS2.

With monitoring AHSV protein synthesis, we aimed at studying aspects of viral replication kinetics of AHSV parental and reassortant strains *in vitro*. Our findings implied that reassortment of AHSV genome segments could potentially affect the *in vitro* CPE phenotypes in Vero cells. Our aim was to monitor protein synthesis using two methods, i) Western blot assays, to monitor accumulated protein levels, and ii) pulse labelling with ^{35}S-methionine, to monitor time-specific protein synthesis. Levels of three AHSV proteins, VP7, NS1 and NS2, were monitored at the end of 8, 16, and 24 hours for a synchronised (MOI 2 pfu/cell) infection. Similar experiments were done for an unsynchronised (MOI 0.1 pfu/cell) infection with an additional observation point at the end of 48 hours post-infection. Pulse labelling experiments were done at intervals of 5-8, 13-16 and 21-24 hours post-infection. Resulting data from these experiments were quantified and statistically analysed.

Our results indicated reassortants R3-$2_{5,10}$ and R4-$2_{4,5,7,10}$ showed statistically significant higher VP7 protein levels synthesised during early AHSV replication in Vero cells than the parental strains. This correlates with their ability to induce more severe CPE than their backbone parents. This was in

agreement with results of Shaw *et al*. (2013), indicating that major differences in the replication cycle *in vitro*, from reassortment between BTV-1 and 8, can be observed at early time points post-infection. Our study did not indicate similar results for the two non-structural proteins (NS1 & NS2) studied, and the differences were only observed when studying total VP7 protein levels at various times post-infection throughout the replication cycle. Results for time-specific (*de novo*) protein synthesis showed no significant differences for any of the pulse labelled intervals. However, Shmulevitz and colleagues (2012) showed that the rates of protein expression were equivalent between the reovirus wild type (T3wt) strain and the reovirus variant strains (T3v1 & T3v2). This was evident from both virus protein accumulation by Western blot analyses and *de novo* synthesis by ^{35}S-met pulse labelling. They hypothesised that, compared between all three strains studied, the rate of virus protein expression was equivalent per infectious particle.

Additionally, results from our own study appear to be in line with the findings by Coetzee and colleagues (2014). Their study suggested that reassortment could potentially result in phenotypic differences *in vitro*. Similarly to observation from our study, the only correlation found was between reassortment and the rate of CPE induced. However, as there was no further evidence to support this correlation, the study did suggest that this could perhaps be due to limitations in an *in vitro* model such as Vero cells, as compared to the *in vivo* conditions. This may indicate why our own study did not substantiate results between the two different methods used to monitor virus proteins synthesised. A specific pattern or mechanism for this observations has not been explicitly identified, through our own study or that by Coetzee *et al*. (2014). It is suggested that certain reassortment combinations lead to changes in the cytopathic phenotypes *in vitro*.

The same study done by Coetzee *et al*. (2014) aimed at investigating *in vitro* properties of BTV reverse genetics-generated parental, reassortant and attenuated field isolate control strains 1, 6 and 8. Their focus was to investigate the potential effect genetic reassortment had on the different *in vitro* phenotypes of BTV in Vero cells. To study the different virus phenotypes, they monitored parameters including virus replication kinetics and the rate at which the viruses induced CPE. These parameters were chosen based on similar studies done to investigate potential indicators suggested to cause changes in virulence *in vivo* (Baumgartner *et al*., 1991; DeMaula *et al*., 2001; Dortmans *et al*., 2011; Freistadt & Eberle, 1996; Slosaris *et al*., 1989; Tscherne & Garcia-Sastre, 2011).

Using electrical impedance assays, measured as CI_{50} values, their study indicated that most BTV reassortant strains showed different CPE induction rates compared to the parental strains. They concluded that reassortment between strains with distinct CPE induction rates resulted in “variable and unpredicted” new phenotypes. Where reassortment occurred between the highly pathogenic strain (rgP8) and less pathogenic strain (rgP1), increased CPE rates were observed. These strains indicated a more severe CPE induction rate compared to the rgP1 strain. Additionally, these strains contained genome Seg-5 & 8, in combination with other segments, heterologous to the backbone genome, i.e. originating from rgP8 [rgR1-8(5,8), rgR1-8(2,5,), rgR5,6,8), rgR1-8(5,7,8) & rgR1-8(5,8,10)]. Reassortment between rgP6 and rgP8, containing a mono-reassortment [rgR6-8(10)], indicated a delay in the onset of CPE. Likewise, a study by Shaw *et al*. (2013) investigating reassortment between BTV 1 and 8, serologically unrelated. With the aid of reverse genetics, their findings suggested that reassortment is a plastic event, at least between strains 1 and 8. They theorised that no “inherent or structural barriers” prevent or favour the reassortment of any combination of genome segments. Moreover, they suggested that the ability of potential replication mechanisms could be influenced by the interaction of gene products from specific reassortment combinations.

Our results, observed from monitoring protein synthesis with Western blot assays, suggested probable interaction between the products of AHSV-2 Seg-5 and 10. If heterologous relative to the backbone genome, this reassortment combination produced a more severe cytopathic phenotype compared to AHSV-2. It may be hypothesised that the interaction between AHSV NS1 and NS3, when originating from the same parental strain, may play a role in the rate of onset of CPE. Consequently influencing the severity of cytopathicity *in vitro*, at least between AHSV-2, 3 and 4.

It further stands to argue that only certain combinations reassort and that there seems to be a potential higher affinity between specific genome segments, or their protein products, evident from our results. A similar hypothesis was proposed from a study by Ramig *et al*. (1989), showing that not all BTV genome segments reassort with equal affinity, when studying reassortment between BTV-10 & 17. This was first indicated by Graham *et al*. (1987), and confirmed by Kobayashi *et al*. (1995), who proposed evidence for non-random segregation of different genome segments. These studies demonstrated various degrees of compatibility between rotavirus strains. However, in their study Shaw and colleagues (2013) revealed with reverse genetics that there is pronounced plasticity between all different genome segments, at least between BTV strains 1 and 8. Furthermore, they showed that earlier evidence which suggests that BTV VP2 and VP5 of a particular serotype will preferentially reassort together, is in fact not the case. Their results indicated no evidence of structural constrains that hinder any reassortment combinations to be packaged into a BTV core particle. Moreover, they suggested that reassortment is the rule rather than the exception when different strains cocirculate.

All other reassortant strains (R3-$2_{3,5}$, R4-2_{10} and R4-$2_{7,10}$), when monitoring protein synthesis levels of VP7 and NS2 showed significant difference to only one of the two parental strains they originate from. Thus, indicating either a lesser or more severe cytopathic phenotype when compared to the backbone parent (AHSV-3 or -4) but never showing a more severe cytopathic phenotype compared to AHSV-2. These results were considered not significant. However, statistical significant difference observed between the VP7 levels of R4-2_{10} and AHSV-4, suggested R4-2_{10} attained a delayed onset of CPE when compared to AHSV-4. Results were confirmed with light microscopy. This indicated a lower level of CPE at 24 hours post-infection even for a synchronised infection (MOI 2 pfu/cell). This implied that mono-reassortment of AHSV-2 Seg-10 may have an effect on the time of onset of cytopathicity levels observed. Similar findings in the study by Coetzee and colleagues (2014) suggested that a mono-reassortment [rgR6-8(10)], caused delayed onset of CPE. Where Seg-10 was heterologous to the backbone genome, the time of CPE induction was delayed when compared to both parental strains.

To determine if a correlation existed between the level of AHSV dsRNA synthesised, virus yield and the different cytopathogenic phenotypes observed, we monitored these parameters in Vero cells. Synthesised AHSV dsRNA levels were monitored, at 24 and 48 hours post-infection, in a synchronised (MOI 2 pfu/cell) and unsynchronised (MOI 0.1 pfu/cell) infection respectively. Similarly, virus yield was measured by virus titrations at 24 and 48 hours post-infection, under the same infection conditions. In KC cells both the AHSV dsRNA levels and virus yields were measured at 8 days post-infection. All ten AHSV dsRNA genome segments, one copy of each, are packaged within the virus core particle and not found freely in the cytoplasm of infected cells. Therefore, virus dsRNA levels were monitored as an indication of successful core packaging and virus production to express accurate levels of virus particles present within the infected cells. In comparison, titration assays were done to monitor virus yield of infectious particles only, thus indicating the effectiveness of virus

release. Results were compared for infected Vero cells and KC cells, since insect cells exhibit no observable CPE and non-lytic virus release is prominent.

Monitoring and analyses of AHSV dsRNA, as well as the yield in both infected mammalian and insect cells, indicated no correlation to our previous results. There was statistically significant difference between some reassortant strains and one of their parental strains but never to both. This was again only observed for virus genome segments 3 (VP3) of the different strains monitored. Furthermore, when comparing results for dsRNA levels and virus yield monitored, from the two different infection experiments (MOI 0.1 or 2 pfu/cell), observations did not correlate. It was apparent that the specific phenotypic changes from reassortant virus R3-$2_{5,10}$ and R4-$2_{4,5,7,10}$, with at least Seg-5 &10 of AHSV-2, did not affect dsRNA levels or virus yield for either infection experiment. Similarly, Shmulevitz and colleagues (2012) suggested that dsRNA synthesis were equivalent for the control strain (T3wt) and their reovirus variants (T3v1 & T3v2). This indicated correlating dsRNA levels within newly assembled reovirus core particles for all three strains studied. However, in contrast to our own observations, Smulevitz *et al*. (2012) observed higher titres for the reovirus variant strains compared to the control strain. They suggested that novel reovirus variants can achieve the ability to become more infectious compared to wild type reovirus strains. They showed that variant strains with enhanced potency, resulted in correlating higher titres per infected cell after each round of infection. Also, in a previous study by Smith *et al.* (2006) reovirus yield was shown to increase 10 to 100 fold in the presence of eukaryotic transcription factor eIF2. The study hypothesised that phosphorylation of eIF2 facilitate reovirus replication, by creating a competitive advantage for reovirus transcripts for the limited cellular translational components. These observations propose a valuable reference for future *in vitro* studies to investigate host cell interactions with the different AHSV reassortant strains.

It is suggested that the replication kinetics during later stages, as was monitored with dsRNA synthesis and yield, were not affected regardless of the reassortment combination. However, this could be a result of the cell culture model used, as previously suggested (Coetzee *et al*., 2014). Another explanation is that more stringent parameters to monitor late stages of AHSV replication is necessary. In their study, Shaw and colleagues (2013) suggested that the use of classic forward genetics techniques have severe limitations. They implied that a great shortfall of using electrophoresis to study the genome of members of the Reoviridae family in the past, relied on the migration properties of each segment. Segments that co-migrate could not be clearly distinguished, restricting the observation for total diversity between genome segments. Observations from plaque assays however, have suggested that a reassortment of at least Seg-8 had a detrimental effect on plaque formation. From their study Shaw *et al*. (2013) indicated that reassortant BTV-1_{8NS2} had significantly smaller plaques compared to the BTV-1 parent and reassortant BTV-8_{1NS2}. These results suggest merit for monitoring plaque formation of our own AHSV reassortant strains in future studies to determine if our reassortment combinations has the same effect on plaque phenotypes.

The same studies in infected insect cells indicated significant difference observed for virus yield only between the mono-reassortant strain (R4-2_{10}) and AHSV-2, of which the parental strain levels were higher. AHSV release from insect cells has been shown to be non-lytic and virus infection does not cause apoptosis (Stassen *et al*., 2012). Hence, differences observed between AHSV-2 and R4-2_{10} cannot be attributed to the mono-reassortant achieving a delayed onset of CPE. Although this was suggested from our observations studying AHSV protein synthesis in mammalian cells, the function of a heterologous Seg-10 appears to have a different function *in vitro* in KC cells.

A recent study of BTV RNA by Feenstra and colleagues (2016) has suggested insight into the packaging signals of Seg-10. Their findings suggested that the Seg-10 RNA elements are conserved

among different orbiviruses. BTV chimeras demonstrated that CPE could still be induced if the virus contains a Seg-10 from EEV or EHDV that expressed functional NS3. In contrast, CPE could not be induced when the BTV chimera expressed NS3 from AHSV. Moreover, the exchange of BTV NS3 did not retain functionality in KC cells as all three chimeric viruses indicated significantly lower virus release in infected cells. Although NS3/NS3a is not essential for virus replication *in vitro* (Van Gennip *et al*., 2014) it has been suggested that RNA elements in the BTV Seg-10 ORF is (Feenstra *et al*., 2014). Likewise, it has been hypothesised from the study by Feenstra and colleagues (2016) that the RNA inserts studied, might contain packaging signals or form structures enabling RNA packaging.

Although similar studies with reassortant AHSV strains, studying the replication kinetics of the virus *in vitro*, in insect cells, have not been published, one study is of note. A study by Mills *et al*. (2015), implicated the use of virus dsRNA to establish RNAi used as a tool for studies on the orbivirus insect vector, *Culicoides sonorensis*. The study suggested that regulation of apoptosis could be the fundamental response that cause persistent virus infection in the insect vector. Their aim was to target the IAP1 protein, a key regulator of apoptosis (Hay *et al*. 1995; Tenev *et al*., 2007). It has been shown that IAP1 functions in persistent viral infections of insect cells and play a role in antiviral defences, as reviewed by Clarke & Clem (2003). Mills and colleagues (2015) observed an accelerated mortality rate when adult female midges were injected with an IAP1 orthologue, ds*CsIAP1*. These results were in line with that observed in hemipterans (Walker & Allen, 2011) and mosquitoes (Wang *et al*., 2012). These studies suggested that an accelerated mortality rate, a conserved phenotype observed between these studies, can be ascribed to the inoculation of long dsRNAs that trigger RNA interference. Winston *et al.* (2002) and Bronkhorst & Van Rij (2014) has suggested the use of RNAi as an antiviral immune response to influence virus replication in insect vectors. Additionally, Mills *et al*. (2015) indicated that RNAi has great potential as use for gene function analyses in *C. sonorensis.*

Our study has demonstrated that reassortment does affect *in vitro* cytopathogenic phenotypes. This was first established by Meiring *et al*. (2009) and confirmed through our systematic comparisons of different stages of the AHSV life cycle. Our results supported the hypothesis by Meiring and colleagues (2009) that specific homologous reassortment combinations can result in cytopathogenic phenotypes superior than the more severe parental strain. This phenotype was specifically observed for recombinant strains with at least a Seg-5 & 10 combination donated from the genome of the cytopathogenically more severe parental strain.

Moreover, we have shown that the replication kinetics for the different reassortment progeny studied, only showed changes in early replication stages, and only in infected mammalian cells. Even though certain reassortant strains did achieve early changes in virus replication, late virus replication stages indicated indistinguishable results. This suggested that no specific steps during subsequent replication stages were more efficient, indicated by the parameters in this study monitoring replication kinetics. We have also shown that replication kinetics, from all strains investigated, in insect cells appear to be unchanged, at least during the replication steps monitored. This suggested that the cause for superior *in vitro* cytopathogenic strains in mammalian cells, but not in insect cells, grants merit for further investigation of host cell interactions and responses.

The AHSV reassortant strains investigated in our study were all rescued through natural coinfection in Vero cells Meiring *et al*., 2009). However, success has recently been achieved with reverse genetics of AHSV strains to produce modified strains maintaining unique mutations or specific reassortment combinations (Matsuo *et al*., 2010; Vermaak *et al*., 2015). Although more research is vital to ultimately understand the replication kinetics of AHSV, this study has been an initial step towards better understanding the underlying mechanisms. Our study relied on the findings from investigating naturally produced reassortment strains through classic forward genetics. However, this practice remains extremely difficult to derive specific reassortment combinations. Furthermore the existence of specific barriers remains undetected and detailed analyses of these are challenging. Moreover, increased natural reassortment in the field is being detected, raising concerns for suitable AHSV vaccine therapies (Allison *et al*., 2012; Batten *et al*., 2008; Oberst *et al*., 1985; Oberst *et al*., 1987; Samal *et al*., 1987a; Samal *et al*., 1987b). There is no doubt however, that genome reassortment among the orbiviruses result in “supervariants” that give rise to distinctive phenotypes and properties (Shmulevitz *et al*., 2012). Although the influence of different reassortment combinations to the cumulative effect on these have not been fully characterised, the consequences of orbivirus reassortment remain relatively unpredictable for now.

REFERENCES

AL-KHATIB, K. & CARR, D. J. J. (2003) Relative quantitation of mRNA: Real-Time PCR vs. End-Point PCR. *Bio-Rad Tech Note,* Bulletin 2915.

ALBERCA, B., BACHANEK-BANKOWSKA, K., CABANA, M., CALVO-PINILLA, E., VIAPLANA, E., FROST, L., GUBBINS, S., URNIZA, A., MERTENS, P. & CASTILLO-OLIVARES, J. (2014) Vaccination of horses with a recombinant modified vaccinia Ankaravirus (MVA) expressing African horse sickness (AHS) virus major capsid protein VP2 provides complete clinical protection against challenge. *Vacc*, 32, 3670-3674.

ALEXANDER, K. A., KAT, P. W., HOUSE, J., HOUSE, C., O'BRIEN, S. J., LAURENSON, M. K., MCNUTT, J. W. & OSBURN, B. I. (1995) African horse sickness and African carnivores. *Vet Microbiol,* 47**,** 133-40.

ALLISON, A. B., HOLMES, E. C., POTGIETER, A. C., WRIGHT, I. M., SAILLEAU, C., BREARD, E., RUDER, M. G. & STALLKNECHT, D. E. (2012) Segmental configuration and putative origin of the reassortant orbivirus, epizootic hemorrhagic disease virus serotype 6, strain Indiana. *Vir*, 424, 67-75.

ANTHONY, S. J., DARPEL, K. E., BELAGANAHALLI, M. N., MAAN, N., NOMIKOU, K., SUTTON, ATTOUI, H., MAAN, S. & MERTENS, P. P. C. (2011) RNA segment 9 exists as a duplex concatemer in an Australian strain of epizootic haemorrhagic disease virus (EHDV): Genetic analysis and evidence for the presence of concatemers as a normal feature of orbivirus replication. *Vir*, 420, 164-171.

ANTHONY, S. J., DARPEL, K. E., MAAN, S., SUTTON, G., ATTOUI, H. & MERTENS, P. P. C. (2010) The evolution of two homologues of the core protein VP6 of epizootic haemorrhagic disease virus (EHDV), which correspond to the geographical origin of the virus. *Virus Genes*, 40, 67-75.

ANTHONY, S., JONES, H., DARPEL, K. E., ELLIOTT, H., MAAN, S., SAMUEL, A., MELLOR, P. S. & MERTENS, P. P. (2007) A duplex RT-PCR assay for detection of genome segment 7 (VP7 gene) from 24 BTV serotypes. *J Virol Methods*, 141, 188-197.

BACHANEK-BANKOWSKA, K., MAAN, S., CASTILLO-OLIVARES, J, NICOLA M. MANNING, J. M., MAAN, N. S., ABRAHAM C. POTGIETER, A. C., DI NARDO, A., SUTTON, G., BATTEN, C. & MERTENS, P. P. C. (2014) Real Time RT-PCR Assays for Detection and Typing of African Horse Sickness Virus. *PLOS One*, 9, 1-13.

BAKHOUM, M. T., FALL, M., FALL, A. G., BELLIS, G. A., GOTTLIEB, Y., LABUSCHAGNE, K., VENTER, G. J., DIOP, M., MALL, I., SECK, M. T., XAVIER ALLÈNE, X., DIARRA, M., GARDÈS, L., BOUYER, J., DELÉCOLLE, J.-C., BALENGHIEN, T. & GARROS, C. (2013) First record of *Culicoides oxystoma* Kieffer and diversity of species within the Schultzei group of *Culicoides* Latreille (Diptera: Ceratopogonidae) biting midges in Senegal. *PLoS One*, 8, e84316.

BANSAL, O. B., STOKES, A., BANSAL, A., BISHOP, D. & ROY, P. (1998) Membrane organization of bluetongue virus nonstructural glycoprotein NS3. *J Virol,* 72**,** 3362-9.

BARNARD, B. J. (1993) Circulation of African horsesickness virus in zebra (*Equus burchelli*) in the Kruger National Park, South Africa, as measured by the prevalence of type specific antibodies. *Onderstepoort J Vet Res,* 60**,** 111-7.

BARTLETT, N. M., GILLIES, S. C., BULLIVANT, S. & BELLAMY, A. R. (1974) Electron microscopy of Reovirus reaction cores. *J Viral*, 14, 315-326.

BATTEN, C. A., MAAN, S., SHAW, A. E., MAAN, N. S. & MERTENS, P. P. (2008) A European field strain of bluetongue virus derived from two parental vaccine strains by genome segment reassortment. *Irus Res*, 137, 56-63.

BAUMGÄRTNER, W., KRAKOWKA, S. & DURCHFELD, B. (1991) In vitro cytopathogenicity and in vivo virulence of two strains of canine parainfluenza virus. *Vet Pathol*, 28, 324-331.

BEATON, A. R., RODRIGUEZ, J., REDDY, Y. K. & ROY, P. (2002) The membrane trafficking protein calpactin forms a complex with bluetongue virus protein NS3 and mediates virus release. *Proc Natl Acad Sci U S A,* 99**,** 13154-9.

BELAGANAHALLI, M. N., MAAN, S., MAAN, N. S., BROWNLIE, J., TESH, R., ATTOUI, H. & MERTENS, P. C. (2015) Genetic characterization of the tick-borne orbivirus. *Vir*, 7, 2185-2209.

BEKKER, S., HUISMANS, H. & VAN STADEN, V. (2014) Factors that affect the intracellular localization and trafficking of African horse sickness virus core protein, VP7. *Vir*, 456-457: 279-291.

BELHOUCHET, M., MOHD JAAFAR, F., FIRTH, A. E., GRIMES, J. M., MERTENS, P. P. & ATTOUI, H. (2011) Detection of a fourth orbivirus non-structural protein. *PLoS One*, 6, e25697.

BHATTACHARYA, B., NOAD, R. J. & ROY, P. (2007) Interaction between Bluetongue virus outer capsid protein VP2 and vimentin is necessary for virus egress. *Virol J,* 4**,** 7.

BHATTACHARYA, B. & ROY, P. (2008) Bluetongue Virus Outer Capsid Protein VP5 Interacts with Membrane Lipid Rafts via a SNARE Domain. *J Virol,* 82**,** 10600-10612.

BHATTACHARYA, B. & ROY, P. (2013) Cellular phosphoinositides and the maturation of bluetongue virus, a non-enveloped capsid virus. *Vir J*, 10, 1-11.

BOYCE, M., CELMA, C. C. & ROY, P. (2012) Bluetongue virus non-structural protein 1 is a positive regulator of viral protein synthesis. *Virol J*, 9, 178.

BOYCE, M., MCCRAE, M. A., BOYCE, P. & KIM, J. T. (2016) Inter-segment complementarity in orbiviruses: a driver for co-ordinated genome packaging in the *Reoviridae*? *J Gen Virol*,97, 1145-1157.

BOYCE, M., WEHRFRITZ, J., NOAD, R. & ROY, P. (2004) Purified recombinant bluetongue virus VP1 exhibits RNA replicase activity. *J Virol,* 78**,** 3994-4002.

BREMER, C. W. (1976) A gel electrophoretic study of the protein and nucleic acid components of African horsesickness virus. *Onderstepoort J Vet Res,* 43**,** 193-9.

BREMER, C. W., HUISMANS, H. & VAN DIJK, A. A. (1990) Characterization and cloning of the African horsesickness virus genome. *J Gen Virol,* 71 (Pt 4)**,** 793-9.

BRONKHORST, A. W. & VAN RIJN, R. P. (2014) The long and short of antiviral defense: small RNA-based immunity in insects. *Curr Opin Virol*, 7c, 19-28.

BROOKES, S. M., HYATT, A. D. & EATON, B. T. (1993) Characterization of virus inclusion bodies in bluetongue virus-infected cells. *J Gen Virol,* 74 (Pt 3)**,** 525-30.

BURRAGE, T. G., TREVEJO, R., STONE-MARSCHAT, M. & LAEGREID, W. W. (1993) Neutralizing epitopes of African horsesickness virus serotype 4 are located on VP2. *Virology,* 196**,** 799-803.

BUSTIN, S.A., BENES, V., GARSON, J. A., HELLEMANS, J., HUGGETT, J., KUBISTA, MUELLER, R., NOLAN, T., PFAFFL, M. W. SHIPLEY, G. L., VANDESOMPELE, J. & WITTWER, C. T. (2009) The MIQE Guidelines: *M*inimum *I*nformation for publication of *Q*uantitative Real-Time PCR *E*xperiments. *Clin Chem*, 55, 611-622.

CALISHER, C. H. & MERTENS, P. P. (1998) Taxonomy of African horse sickness viruses. *Arch Virol Suppl,* 14**,** 3-11.

CLARKE, T. E. & CLEM, R. J. (2003) Insect defences against virus infection: the role of apoptosis. *Int Rev Immunol*, 22, 401-424.

COETZEE, P., VAN VUUREN, M., STOKSTAD, M., MYRMEL, M., GENNIP, R. G. P., VAN RIJN, P. A. & VENTER, E. H. (2014) Viral replication kinetics and *in vitro* cytopathogenicity of parental and reassortant strains of bluetongue virus serotype 1, 6 and 8. *Vet Microbiol*, 171, 53-65.

COETZEE, P., VAN VUUREN, M., STOKSTAD, M., MYRMEL, M. & VENTER, E. H. (2012) Bluetongue virus genetic and phenotypic diversity: towards identifying the molecular determinants that influence virulence and transmission potential. *Vet Microbiol* 161, 1-12.

COETZER, J. A. W. & GUTHRIE, A. J. (2004) African horse sickness. IN COETZER, J. A. W. & TUSTIN, R. C. (Eds.) *Infectious diseases of livestock.* Oxford University Press, Cape Town.

CONRADIE, A. M., STASSEN, L., HUISMANS, H. & POTGIETER, C. A. (2016) Establishment of different plasmid only-based reverse geetics systems for the recovery of African horse sickness virus. *Virol*, 499, 144-155.

COWLEY, J. A. & GORMAN, B. M. (1987) Genetic reassortants for identification of the genome segment coding for the bluetongue virus hemagglutinin. *J Virol,* 61**,** 2304-6.

COWLEY, J. A. & GORMAN, B. M. (1989) Cross-neutralization of genetic reassortants of bluetongue virus serotypes 20 and 21. *Vet Microbiol,* 19**,** 37-51.

DE LA POZA, F., CALVO-PINILLA, E., LÓPEZ-GIL, E., ALEJANDRO MARÍN-LÓPEZ, A., MATEOS, F., CASTILLO-OLIVARES, J., LORENZO, G. &, ORTEGO, J. (2013) Ns1 Is a Key Protein in the Vaccine Composition to Protect Ifnar(2/2) Mice against Infection with Multiple Serotypes of African Horse Sickness Virus. *PLoS ONE*, 8, e7097.

DE WAAL, P. J. & HUISMANS, H. (2005) Characterization of the nucleic acid binding activity of inner core protein VP6 of African horse sickness virus. *Arch Virol,* 150**,** 2037-50.

DEMAULA, C. D., JUTILA, M. A., WILSON, D. W. & MACLACHLAN, N. J. (2001) Infection kinetics, prostacyclin release and cytokine-mediated modulation of the mechanism of cell death during

bluetongue virus infection of cultured ovine and bovine pulmonary artery and lung microvascular endothelial cells. *J Gen Virol*, 82, 787-794.

DIPROSE, J. M., BURROUGHS, J. N., SUTTON, G. C., GOLDSMITH, A., GOUET, P., MALBY, R., OVERTON, I., ZIENTARA, S., MERTENS, P. P., STUART, D. I. & GRIMES, J. M. (2001) Translocation portals for the substrates and products of a viral transcription complex: the bluetongue virus core. *Embo J,* 20**,** 7229-39.

DORTMANS, J. C., KOCH, G., ROTTIER, P. J. & PEETERS, B. P. (2011) Virulence of Newcastle disease virus: what is known so far? *Vet Res*, 42, 122.

FEENSTRA, F., VAN GENNIP, R. G. P., SCHREUDER, M. & VAN RIJN, P. A. (2016) Balance of RNA sequence requirement and NS3/NS3a expression of segment 10 of orbiviruses. *J Gen Virol*, 97, 411-421.

FEENSTRA, F., VAN GENNIP, R. G. P., VAN DE WATER, S. G. P. & VAN RIJN, P. A. (2014) RNA elements in open reading frames of the bluetongue virus genome are essential for virus replication. *PLoS One*, 9, e92377.

FENG, Y., YANG, T., XU, Q., SUN, E., LI, J., LV, S., WANG, H., ZHANG, Q., ZHANG, J. & WU, D. (2015) Detectio, discrimination and quantitation of 22 bluetongue virus serotypes using real-time RT-PCR with TaqMan MGB probes. *Arch Virol*, 160, 2249-2258.

FERNANDEZ-PINERO, J., FERNANDEZ-PACHECO, P., RODRIGUEZ, B., SOTELO, E., ROBLES, A., ARIAS, M.& SANCHEZ-VIZCAINO, J. M. (2009) Rapid and sensitive detection of African horse sickness virus by real-time PCR. *Res Vet Sci*, 86, 353-358.

FIRTH, A. E. (2008) Bioinformatic analysis suggests that the Orbivirus VP6 cistron encodes an overlapping gene. *Virol J*, 5, 48.

FORZAN, M., WIRBLICH, C. & ROY, P. (2004) A capsid protein of nonenveloped Bluetongue virus exhibits membrane fusion activity. *Proc Natl Acad Sci U S A,* 101**,** 2100-5.

FREISTADT, M. S. & EBERLE, K. E. (1996) Correlation between poliovirus type 1 Mahoney replication in blood cells and neurovirulence. *J Virol*, 70, 686-6492.

FRENCH, T. J., INUMARU, S. & ROY, P. (1989) Expression of two related nonstructural proteins of bluetongue virus (BTV) type 10 in insect cells by a recombinant baculovirus: production of polyclonal ascitic fluid and characterization of the gene product in BTV-infected BHK cells. *J Virol,* 63**,** 3270-8.

FURUICHI, Y., MUTHUKRISHNAN, S. & SHATKIN, A. J. (1975) 5'-Terminal m-7G(5')ppp(5')G-m-p in vivo: identification in reovirus genome RNA. *Proc Natl Acad Sci U S A,* 72**,** 742-5.

FURUICHI, Y., MUTHUKRISHNAN, S., TOMASZ, J. & SHATKIN, A. J. (1976) Mechanism of formation of reovirus mRNA 5'-terminal blocked and methylated sequence, m7GpppGmpC. *J Biol Chem,* 251**,** 5043-53.

GOULD, A. R. & HYATT, A. D. (1994) The orbivirus genus. Diversity, structure, replication and phylogenetic relationships. *Comp Immunol Microbiol Infect Dis,* 17**,** 163-88.

GOULD, E. A. & HIGGS, S. (2008) Impact of climate change and other factors on emerging arbovirus diseases. *Trans R Soc Trop Med Hyg***,** 1-13.

GRAHAM, D. Y., DUFOUR, G. R. & ESTES, M. K. (1987) Minimal infective dose of rotavirus. *Arch Virol*, 92, 261-271.

GRIMES, J. M., BURROUGHS, J. N., GOUET, P., DIPROSE, J. M., MALBY, R., ZIENTARA, S., MERTENS, P. P. & STUART, D. I. (1998) The atomic structure of the bluetongue virus core. *Nature,* 395**,** 470-8.

GRUBMAN, M. J. & LEWIS, S. A. (1992) Identification and characterization of the structural and nonstructural proteins of African horsesickness virus and determination of the genome coding assignments. *Virology,* 186**,** 444-51.

HAMBLIN, C., SALT, J. S., MELLOR, P. S., GRAHAM, S. D., SMITH, P. R. & WOHLSEIN, P. (1998) Donkeys as reservoirs of African horse sickness virus. *Arch Virol Suppl,* 14**,** 37-47.

HAN, Z. & HARTY, R. N. (2004) The NS3 protein of bluetongue virus exhibits viroporin-like properties. *J Biol Chem,* 279**,** 43092-7.

HARRISON, R. E., BUCCI, C., VIEIRA, O. V., SCHROER, T. A. & GRINSTEIN, S. (2003) Phagosomes fuse with late endosomes and/or lysosomes by extension of membrane protrusions along microtubules : Role of Rab7 and RILP. *Mol. Cell. Biol.,* 23**,** 6494-6506.

HASSAN, S. H., WIRBLICH, C., FORZAN, M. & ROY, P. (2001) Expression and functional characterization of bluetongue virus VP5 protein: role in cellular permeabilization. *J Virol,* 75**,** 8356-67.

HASSAN, S. S. & ROY, P. (1999) Expression and functional characterization of bluetongue virus VP2 protein: role in cell entry. *J Virol,* 73**,** 9832-42.

HAY, B. A., WASSARMAN, D. A. & RUBIN, G. M. (1995)*Drosophila* homologs of baculovirus inhibitor of apoptosis proteins function to block cell death. *Cell*, 83, 1253-1262.

HEWAT, E. A., BOOTH, T. F., WADE, R. H. & ROY, P. (1992) 3-D reconstruction of bluetongue virus tubules using cryoelectron microscopy. *J Struct Biol,* 108**,** 35-48.

HOUSE, J. A. (1993) African horse sickness. *Vet Clin North Am Equine Pract,* 9**,** 355-64.

HUISMANS, H. (1979) Protein synthesis in bluetongue virus-infected cells. *Virol*, 92, 385-396.

HUISMANS, H. & ELS, H. J. (1979) Characterization of the tubules associated with the replication of three different orbiviruses. *Virology,* 92**,** 397-406.

HUISMANS, H. & ERASMUS, B. J. (1981) Identification of the serotype-specific and group-specific antigens of bluetongue virus. *Onderstepoort J Vet Res,* 48**,** 51-8.

HUISMANS, H., VAN DER WALT, N. T., CLOETE, M. & ERASMUS, B. J. (1987a) Isolation of a capsid protein of bluetongue virus that induces a protective immune response in sheep. *Virology,* 157**,** 172-9.

HUISMANS, H., VAN DER WALT, N. T. & ERASMUS, B. J. (1985) Immune response against the purifies serotype specific antigen of bluetongue virus and initial attempts to clone the gene that codes for the synthesis of this protein. In *Proceedings of the International Symposium on Bluetongue and Related Orbiviruses,* pp. 347-353. Edited by Barber, T. L. & Jochim, M. M. Alan R. Liss, New York.

HUISMANS, H. & VAN DIJK, A. A. (1990) Bluetongue virus structural components. *Curr Top Microbiol Immunol,* 162**,** 21-41.

HUISMANS, H., VAN DIJK, A. A. & BAUSKIN, A. R. (1987b) In vitro phosphorylation and purification of a nonstructural protein of bluetongue virus with affinity for single-stranded RNA. *J Virol,* 61**,** 3589-95.

HUISMANS, H., VAN DIJK, A. A. & ELS, H. J. (1987c) Uncoating of parental bluetongue virus to core and subcore particles in infected L cells. *Virology,* 157**,** 180-8.

HUISMANS, H., VAN STADEN, V., FICK, W. C., VAN NIEKERK, M. & MEIRING, T. L. (2004). A comparison of different orbivirus proteins that could affect virulence and pathogenesis. *Veterinaria italiana*, 40, 417-425.

HYATT, A. D., EATON, B. T. & BROOKES, S. M. (1989) The release of bluetongue virus from infected cells and their superinfection by progeny virus. *Virology,* 173**,** 21-34.

HYATT, A. D., ZHAO, Y. & ROY, P. (1993). Release of bluetongue virus-like particles from insect cells is mediated by BTV nonstructural protein NS3/NS3A. *Virology* 193, 592-603.

JANOWICZ, A., CAPORALE, M., SHAW, A., GULLETTA, S., DI GIALLEONARDO, L., RATINIER, M. & PALMARINI, M. (2015) Multiple genome segments determine virulence of bluetongue virus serotype 8. *J Virol*, 89: 5238-5249.

KANAI, Y., VAN RIJN, P. A., MARIS-VELDHUIS, M., KANAME, Y., ATHMARAM, T. N. & ROY, P. (2014) Immunogenicity of recombinant VP2 proteins of all nine serotypes of African horse sickness virus. *Vacc,* 32: 4932-4937.

KAR, A. K., BHATTACHARYA, B. & ROY, P. (2007) Bluetongue virus RNA binding protein NS2 is a modulator of viral replication and assembly. *BMC Mol Biol,* 8**,** 4.

KAR, A. K., GHOSH, M. & ROY, P. (2004) Mapping the assembly pathway of Bluetongue virus scaffolding protein VP3. *Virology,* 324**,** 387-99.

KAR, A. K., IWATANI, N. & ROY, P. (2005) Assembly and intracellular localization of the bluetongue virus core protein VP3. *J Virol,* 79**,** 11487-95.

KAR, A. K. & ROY, P. (2003) Defining the structure-function relationships of bluetongue virus helicase protein VP6. *J Virol,* 77**,** 11347-56.

KOBAYASHI, N., KOJIMA, K., TANIGUCHI, K., URASAWA, T. & URASAWA, S. (1995) Non-random selection of gene segment 3 and random selection of gene segment 5 observed in reassortants generated in vitro between rotavirus SA11 and RRV. *Res Virol*, 146, 53-59.

LAEGREID, W. W., BURRAGE, T. G., STONE-MARSCHAT, M. & SKOWRONEK, A. (1992). Electron microscopic evidence for endothelial infection by African horsesickness virus. *Vet Pathol*, 29, 554-556.

LE BLOIS, H., FAYARD, B., URAKAWA, T. & ROY, P. (1991) Synthesis and characterization of chimeric particles between epizootic hemorrhagic disease virus and bluetongue virus: functional domains are conserved on the VP3 protein. *J Virol,* 65**,** 4821-31.

LE BLOIS, H. & ROY, P. (1993) A single point mutation in the VP7 major core protein of bluetongue virus prevents the formation of core-like particles. *J Virol,* 67**,** 353-9.

LIMN, C. K. & ROY, P. (2003) Intermolecular interactions in a two-layered viral capsid that requires a complex symmetry mismatch. *J Virol,* 77**,** 11114-24.

LIMN, C. K., STAEUBER, N., MONASTYRSKAYA, K., GOUET, P. & ROY, P. (2000) Functional dissection of the major structural protein of bluetongue virus: identification of key residues within VP7 essential for capsid assembly. *J Virol,* 74**,** 8658-69.

LIU, H. M., BOOTH, T. F. & ROY, P. (1992) Interactions between bluetongue virus core and capsid proteins translated in vitro. *J Gen Virol,* 73 (Pt 10)**,** 2577-84.

LOUDON, P. T. & ROY, P. (1992) Interaction of nucleic acids with core-like and subcore-like particles of bluetongue virus. *Virology,* 191**,** 231-6.

LYMPEROPOULOS, K., NOAD, R., TOSI, S., NETHISINGHE, S., BRIERLEY, I. & ROY, P. (2006) Specific binding of Bluetongue virus NS2 to different viral plus-strand RNAs. *Virology,* 353**,** 17-26.

LYMPEROPOULOS, K., WIRBLICH, C., BRIERLEY, I. & ROY, P. (2003) Sequence specificity in the interaction of Bluetongue virus non-structural protein 2 (NS2) with viral RNA. *J Biol Chem,* 278**,** 31722-30.

MAAN, N. S., MAAN, S., BELAGANAHALI, M., PULLINGER, G., MONTES, A. J., GAPARINI, M. R., GUIMERA, M., NOMIKOU, K. & MERTENS, P.P. (2015) A quantitative real-time reverse transcription PCR (qRT-PCR) assay to detect genome segment 9 of all 26 bluetongue virus serotypes. *J Virol Methods*, 213, 118-126.

MAAN, S., MAAN, N. S., ROSS-SMITH, N., BATTEN, C. A., SHAW, A. E., ANTHONY, S. J., SAMUEL, A. R., DARPEL, K. E., VERONESI, E., OURA, C. A., SINGH, K. P., NOMIKOU, K., POTGIETER, A. C., ATTOUI, H., VAN ROOIJ, E., VAN RIJN, P., DE CLERCQ, K., VANDENBUSSCHE, F., ZIENTARA, S., BREARD, E., SAILLEAU, C., BEER, M., HOFFMAN, B., MELLOR, P. S. & MERTENS, P. P. (2008) Sequence analysis of bluetongue virus serotype 8 from the Netherlands 2006 and comparison to other European strains. *Virology,* 377**,** 308-18.

MACLACHLAN, N. J., CRAFFORD, J. E., VERNAU, W., GARDNER, I. A., GODDARD, A., GUTHRIE, A. J. & VENTER, E. H. (2008) Experimental reproduction of severe bluetongue in sheep. *Vet Pathol,* 45**,** 310-315.

MACLACHLAN, N. J. & GUTHRIE, A. J. (2010) Re-emergence of bluetongue, African horse sickness, and other orbivirus diseases. *Vet Res*, 41, 35.

MANOLE, V., LAURINMÄKI, P., VAN WYNGAARDT, W., POTGIETER, C. A., WRIGHT, I. M., VENTER, G. J., VAN DIJK, A. A., SEWELL, B. T. & BUTCHER, S. J. (2012) Structural insight into African horse sickness virus infection. *J Virol*, 86, 7858-7866.

MAREE, S., DURBACH, S. & HUISMANS, H. (1998). Intracellular production of African horsesickness virus core-like particles by expression of the two major core proteins, VP3 and VP7, in insect cells. *J Gen Virol* 79 (Pt 2), 333-337.

MAREE, F. F. & HUISMANS, H. (1997) Characterization of tubular structures composed of nonstructural protein NS1 of African horsesickness virus expressed in insect cells. *J Gen Virol,* 78 (Pt 5)**,** 1077-82.

MARONICHE, G.A., SAGADÍN, M., MONGELLI, V.C., TRUOL, G.A. & DEL VAS, M., (2011) Reference gene selection for gene expression studies using RT-qPCR in virus-infected planthoppers. *J Virol*, 8, 308.

MARTIN, L. A., MEYER, A. J., O'HARA, R. S., FU, H., MELLOR, P. S., KNOWLES, N. J. & MERTENS, P. P. (1998) Phylogenetic analysis of African horse sickness virus segment 10: sequence variation, virulence characteristics and cell exit. *Arch Virol Suppl,* 14**,** 281-93.

MARTINEZ-COSTAS, J., SUTTON, G., RAMADEVI, N. & ROY, P. (1998) Guanylyltransferase and RNA 5'-triphosphatase activities of the purified expressed VP4 protein of bluetongue virus. *J Mol Biol,* 280**,** 859-66.

MARTINEZ-TORRECUADRADA, J. L. & CASAL, J. I. (1995) Identification of a linear neutralization domain in the protein VP2 of African horse sickness virus. *Virology,* 210**,** 391-9.

MARTINEZ-TORRECUADRADA, J. L., DIAZ-LAVIADA, M., ROY, P., SANCHEZ, C., VELA, C., SANCHEZ-VIZCAINO, J. M. & CASAL, J. I. (1996) Full protection against African horsesickness (AHS) in horses induced by baculovirus-derived AHS virus serotype 4 VP2, VP5 and VP7. *J Gen Virol,* 77**,** 1211-21.

MARTINEZ-TORRECUADRADA, J. L., IWATA, H., VENTEO, A., CASAL, I. & ROY, P. (1994) Expression and characterization of the two outer capsid proteins of African horsesickness virus: the role of VP2 in virus neutralization. *Virology,* 202**,** 348-59.

MATSUO, E., CELMA, C. C. & ROY, P. (2010) A reverse genetics system of African horse sickness virus reveals existence of primary replication. *FEBS Lett*, 584, 3386-3391.

MAYRAN, N., PARTON, R. G. & GRUENBERG, J. (2003) Annexin II regulates multivesicular endosome biogenesis in the degradation pathway of animal cells. *EMBO Journal,* 22**,** 3242-3253.

MCINTOSH, B. M. (1958) Immunological types of horsesickness virus and their significance in immunization. *Onderstepoort J Vet Res,* 27**,** 465-538.

MEIRING, T. L., HUISMANS, H., & VAN STADEN, V. (2009) Genome segment reassortment identifies non-structural protein NS3 as a key protein in African horsesickness virus release and alteration of membrane permeability. *Arch Virol*, 154, 263-271.

MELLOR, P. S. & HAMBLIN, C. (2004) African horse sickness. *Vet Res,* 35**,** 445-66.

MELLOR, P. S., RAWLINGS, P., BAYLIS, M. & WELLBY, M. P. (1998) Effect of temperature on African horse sickness virus infection in *Culicoides*. *Arch Virol Suppl,* 14**,** 155-63.

MERTENS, P. P., BROWN, F. & SANGAR, D. V. (1984) Assignment of the genome segments of bluetongue virus type 1 to the proteins which they encode. *Virology,* 135**,** 207-17.

MERTENS, P. P. & DIPROSE, J. (2004) The bluetongue virus core: a nano-scale transcription machine. *Virus Res,* 101**,** 29-43.

MERTENS, P. P. & SANGAR, D. V. (1985) Analysis of the terminal sequences of the genome segments of four orbiviruses. *Virology,* 140**,** 55-67.

MERTENS, P. P. C., DIPROSE, J., MAAN, S., SINGH, K. P., ATTOUI, H. & SAMUEL, A. R. (2004) Bluetongue virus replication, molecular and structural biology. *Vet Ital,* 40**,** 426-437.

MILLS, M. K., NAYDUCH, D. & MICHEL, K. (2015) Inducing RNA interference in the arbovirus vector, *Cullicoides sonorensis*. *Insect Mol Biol*, 24, 105-114.

MIRCHAMSY, H., HAZRATI, A., BAHRAMI, S. & SHAFYI, A. (1970) Growth and persistent infection of African horse sickness virus in a mosquito cell line. *Am J Vet Res*, 31, 1755-1761.

MODROF, J., LYMPEROPOULOS, K. & ROY, P. (2005) Phosphorylation of bluetongue virus nonstructural protein 2 is essential for formation of viral inclusion bodies. *J Virol,* 79**,** 10023-31.

MONACO, F., POLCI, A., LELLI, R., PINONI, C., DI MATTIA, T., MBULU, R. S., SCACCHIA, M. & SAVINI, G. (2011) A new duplex real-time RT-PCR assay for sensitive and specific detection of African horse sickness virus. *Moll Cell Probes*, 25, 87-93.

MONASTYRSKAYA, K., BOOTH, T., NEL, L. & ROY, P. (1994) Mutation of either of two cysteine residues or deletion of the amino or carboxy terminus of nonstructural protein NS1 of bluetongue virus abrogates virus-specified tubule formation in insect cells. *J Virol,* 68**,** 2169-78.

MOODY, M. D. & JOKLIK, W. K. (1989) The function of reovirus proteins during the reovirus multiplication cycle: analysis using monoreassortants. *Virology,* 173**,** 437-46.

MOSS, S. R., AYRES, C. M. & NUTTALL, P. A. (1987) Assignment of the genome segment coding for the neutralizing epitope(s) of orbiviruses in the Great Island subgroup (Kemerovo serogroup). *Virology,* 157**,** 137-44.

NASON, E. L., ROTHAGEL, R., MUKHERJEE, S. K., KAR, A. K., FORZAN, M., PRASAD, B. V. & ROY, P. (2004) Interactions between the inner and outer capsids of bluetongue virus. *J Virol,* 78**,** 8059-67.

NAYDUCH, D., COHNSTAEDT, L. W., SASKI, C., LAWSON, D., KERSEY, P., FIFE, M. & CARPENTER, S. (2014) Studying *Cullicoides* vectors of BTV in the post-genomic era: resources, bottlenecks to progress and future directions. *Vir Res*, 182, 43-49.

NOMIKOU, K., HUGHES, J., WASH, R., KELLAM, P., BREARD, E., ZIENTARA, S., PALMARINI, M., BIEK, R. & MERTENS, P. (2015) Widespread Reassortment Shapes the Evolution and Epidemiology of Bluetongue Virus following European Invasion. *PLoS Path*, 1, e1005056.

O'HARA, R. S., MEYER, A. J., BURROUGHS, J. N., PULLEN, L., MARTIN, L. A. & MERTENS, P. P. (1998) Development of a mouse model system, coding assignments and identification of the genome segments controlling virulence of African horse sickness virus serotypes 3 and 8. *Arch Virol Suppl,* 14**,** 259-79.

OBERST, R. D., SQUIRE, K. R. E., STOTT, J. L., CHUANG, R. Y., & OSBURN, B. I. (1985) The coexistence of multiple bluetongue virus electropherotypes in individual cattle during natural infection. *J Gen Vir*, 66, 1901-1909.

OBERST, R. D., STOTT, J. L., BLANCHARD-CHANNELL, M. & OSBURN, B. I. (1987) Genetic reassortment of bluetongue virus serotype 11 strains in the bovine. *Vet Microbiol*, 15, 11-18.

OELLERMANN, R. A., ELS, H. J. & ERASMUS, B. J. (1970) Characterization of African horsesickness virus. *Arch Gesamte Virusforsch,* 29**,** 163-74.

OLDFIELD, S., ADACHI, A., URAKAWA, T., HIRASAWA, T. & ROY, P. (1990) Purification and characterization of the major group-specific core antigen VP7 of bluetongue virus synthesized by a recombinant baculovirus. *J Gen Virol,* 71**,** 2649-56.

OOMS, L. S., KOBAYASHI, T., DERMODY, T. S., & CHAPPELL, J. D. (2010) A post-entry step in the mammalian orthoreovirus replication cycle is a determinant of cell tropism. *J Biol Chem*, 285, 41604-41613.

OSAWA, Y. & HAZRATI, A. (1965) Growth of African horse sickness virus in monkey kidney cell cultures. *Am J Vet Res*, 25, 505-511.

OWENS, R. J., LIMN, C. & ROY, P. (2004) Role of an arbovirus nonstructural protein in cellular pathogenesis and virus release. *J Virol,* 78**,** 6649-56.

PAWESKA, J. T., PRINSLOO, S. & VENTER, G. J. (2003) Oral susceptibility of South African Culicoides species to live-attenuated serotype-specific vaccine strains of African horse sickness virus (AHSV). *Med Vet Entomol*, 17, 436-447.

POTGIETER, A. C., CLOETE, M., PRETORIUS, P. J. & VAN DIJK, A. A. (2003) A first full outer capsid protein sequence data-set in the Orbivirus genus (family Reoviridae): cloning, sequencing, expression and analysis of a complete set of full-length outer capsid VP2 genes of the nine African horsesickness virus serotypes. *J Gen Virol,* 84**,** 1317-26.

PRETORIUS, J. M., HUISMANS, H., & J. THERON, J. (2015) Establishment of an entirely plasmid-based reverse genetics system for Bluetongue virus. *Vir*, 486: 71-77.

PURDY, M., PETRE, J. & ROY, P. (1984) @P39 Cloning of the bluetongue virus L3 gene. *J Virol,* 51**,** 754-9.

QUAN, M., LOURENS, C. W., MACLACHLAN, N. J., GARDNER, I. A. & GUTHRIE, A. J. (2010) Development and optimisation of a duplex real-time reverse transcription quantitative PCR assay targeting the VP7 and NS2 genes of African horse sickness virus. *J Virol Methods*, 167, 45-52.

RAMADEVI, N., BURROUGHS, N. J., MERTENS, P. P., JONES, I. M. & ROY, P. (1998) Capping and methylation of mRNA by purified recombinant VP4 protein of bluetongue virus. *Proc Natl Acad Sci U S A,* 95**,** 13537-42.

RAMADEVI, N. & ROY, P. (1998) Bluetongue virus core protein VP4 has nucleoside triphosphate phosphohydrolase activity. *J Gen Virol,* 79 (Pt 10)**,** 2475-80.

RAMIG, R. F., GARRISON, C., CHEN, D. & BELL-ROBINSON, D. (1989) Analysis of reassortment and superinfection during mixed infection of Vero cells with bluetongue virus serotypes 10 and 17. *J Gen Virol,* 70 (Pt 10)**,** 2595-603.

RATHOGWA, N. M., QUAN, M., SMIT, J. Q., LOURENS, C., GUTHRIE, A. J. & VAN VUUREN, M. (2014) Development of a real time polymerase chain reaction assay for equine encephalosis virus. *J Virol Methods*, 195, 205-210.

RAY, B. K., BRENDLER, T. G., ADYA, S., DANIELS-MCQUEEN, S., MILLER, J. K., HERSHEY, J. W., GRIFO, J. A., MERRICK, W. C. & THACH, R. E. (1983) Role of mRNA competition in regulating translation: further characterization of mRNA discriminatory initiation factors. *Proc Natl Acad Sci U S A,* 80**,** 663-7.

RODRIGUEZ-SANCHEZ, B., FERNANDEZ-PINERO, J., SAILLEAU, C., ZIENTARA, S., BELAK, S., ARIAS, M.& SANCHEZ-VIZCAINO, J. M. (2008) Novel gel-based and real-time PCR assays for the improved detection of African horse sickness virus. *J Virol Methods*, 151, 87-94.

RONER, M. R. & MUTSOLI, C. (2007) The use of monoreassortants and reverse genetics to map reovirus lysis of a ras-transformed cell line. *J Virol Methods,* 139**,** 132-42.

ROY, P. (1996) Orbivirus structure and assembly. *Virology,* 216**,** 1-11.

ROY, P. (2001) Orbiviruses IN KNIPE, D. M. & HOWLEY, P. M. (Eds.) *Fields' virology.* 4th ed., Lippincott Williams & Wilkins, Philadelphia, USA

ROY, P. (2005) Bluetongue virus proteins and particles and their role in virus entry, assembly, and release. *Adv Virus Res,* 64**,** 69-123.

ROY, P. (2008a) Bluetongue virus: dissection of the polymerase complex. *J Gen Virol*, 89, 1789-1804.

ROY, P. (2008b) Functional mapping of bluetongue virus proteins and their interactions with host proteins during virus replication. *Cell Biochem Biophys,* 50**,** 143-57.

ROY, P., ADACHI, A., URAKAWA, T., BOOTH, T. F. & THOMAS, C. P. (1990) Identification of bluetongue virus VP6 protein as a nucleic acid-binding protein and the localization of VP6 in virus-infected vertebrate cells. *J Virol,* 64**,** 1-8.

ROY, P., BISHOP, D. H., HOWARD, S., AITCHISON, H. & ERASMUS, B. (1996) Recombinant baculovirus-synthesized African horsesickness virus (AHSV) outer-capsid protein VP2 provides protection against virulent AHSV challenge. *J Gen Virol,* 77**,** 2053-7.

ROY, P., BISHOP, D. H., LEBLOIS, H. & ERASMUS, B. J. (1994a) Long-lasting protection of sheep against bluetongue challenge after vaccination with virus-like particles: evidence for homologous and partial heterologous protection. *Vaccine*, 12, 805-811.

ROY, P., MERTENS, P. P. & CASAL, I. (1994b) African horse sickness virus structure. *Comp Immunol Microbiol Infect Dis,* 17**,** 243-73.

SAMAL, S. K., EL-HUSSEIN, A., HOLBROOK, F. R., BEATY, B. J. & RAMIG, R. F. (1987a) Mixed infection of Culicoides variipennis with bluetongue virus serotypes 10 and 17: evidence for high frequency reassortment in the vector. *J Gen Virol,* 68 (Pt 9)**,** 2319-29.

SAMAL, S. K., LIVINGSTON, C. W., JR., MCCONNELL, S. & RAMIG, R. F. (1987b) Analysis of mixed infection of sheep with bluetongue virus serotypes 10 and 17: evidence for genetic reassortment in the vertebrate host. *J Virol,* 61**,** 1086-91.

SAMBROOK, J., & Russel, D.W. (2001) Molecular cloning. A laboratory manual. Volume 1 (3rd ed.). Cold Spring Harbor Laboratory Press, Cold Spring Harbor, NY.

SAVINI, G., MACLACHLAN, N. J., SANCHEZ-VIZCAINO, J. M. & ZIENTARA, S. (2008) Vaccines against bluetongue in Europe. *Comp Immunol Microbiol Infect Dis,* 31**,** 101-20.

SCHWARTZ-CORNILL, I., MERTENS, P. P., CONTRERAS, V., HEMATI, B., PASCALE, F., BREARD, E., MELLOR, P. S., MACLACHLAN, N. J. & ZIENTARA, S. (2008) Bluetongue virus: virology, pathogenesis and immunity. *Vet Res,* 39**,** 46.

SHAW, A. E., MONAGHAN, P., ALPAR, H. O., ANTHONY, S., DARPEL, K. E., BATTEN, C. A., GUERCIO, A., ALIMENA, G., VITALE, M., BANKOWSKA, K., CARPENTER, S., JONES, H., OURA, C. A., KING, D. P., ELLIOTT, H., MELLOR, P. S. & MERTENS, P. P. (2007) Development and initial evaluation of a real-time RT-PCR assay to detect bluetongue virus genome segment 1. *J Virol Methods*, 145, 115-126.

SHAW, A. E., BRUNING-RICHARDSON, A., MORRISON, E. E., BOND, J., SIMPSON, J., ROSS-SMITH, N., ALPAR, O., MERTENS, P. P. C. & MONAGHAN, P. (2013) Bluetongue virus infection induces aberrant mitosis in mammalian cells. *Virol J*, 10, 319.

SHMULEVITZ, M., GUJAR, S. A., AHN, D.-G., MOHAMED, A. & LEE, P. W. K. (2012) Reovirus Variants with Mutations in Genome Segments S1 and L2 Exhibit Enhanced Virion Infectivity and Superior Oncolysis. *J Virol*, 86, 7403-7413.

SLOSARIS, M., LEVY, B., KATZ, E., LEVY, R. & ZAKAY-RONES, Z. (1989) Elevated virulence of Newcastle disease virus strains following serial passages in kidney cells in vitro. *Avian Dis*, 33, 248-253.

SMITH, J. A., SCHMECHEL, S. C., RAGHAVAN, A. ABELSON, M., REILLY, C., KATZE, M. G., KAUFMAN, R. J., BOHJANEN, P. R. & SCHIFF, L. A. (2006) Reovirus induces and benefits from an integrated cellular stress response. *J Virol*, 80, 2019-2033.

STASSEN, L., HUISMANS, H. & THERON, J. (2012) African horse sickness virus induces apoptosis in cultured mammalian cells. *Virus Res*, 163, 385-389.

STAUBER, N., MARTINEZ-COSTAS, J., SUTTON, G., MONASTYRSKAYA, K. & ROY, P. (1997) Bluetongue virus VP6 protein binds ATP and exhibits an RNA-dependent ATPase function and a helicase activity that catalyze the unwinding of double-stranded RNA substrates. *J Virol,* 71**,** 7220-6.

STOLTZ, M. A., VAN DER MERWE, C. F., COETZEE, J. & HUISMANS, H. (1996) Subcellular localization of the nonstructural protein NS3 of African horsesickness virus. *Onderstepoort J Vet Res,* 63**,** 57-61.

STOTT, J. L., OBERST, R. D., CHANNELL, M. B. & OSBURN, B. I. (1987) Genome segment reassortment between two serotypes of bluetongue virus in a natural host. *J Virol,* 61**,** 2670-4.

SUNG, P.-Y. & ROY, P. (2014) Sequential packaging of RNA genomic segments during the assembly of bluetongue virus. *Nucl Acid Res*, 42, 13824-13838.

SUTTON, G., GRIMES, J. M., STUART, D. I. & ROY, P. (2007) Bluetongue virus VP4 is an RNA-capping assembly line. *Nat Struct Mol Biol*.

SVOBODOVÁ, K., BÍLEK, K. & KNOLL, A. (2008) Verification of reference genes for relative quantification of gene expression by real-time reverse transcription PCR in the pig. *J Appl Genet*, 49, 263-265.

TAMHANE, A. C. (1979) A comparison of procedures for multiple comparisons of means with unequal variances. *J Am Stat Ass*, 74, 471-480.

TAUSCHER, G. I. & DESSELBERGER, U. (1997) Viral determinants of rotavirus pathogenicity in pigs: production of reassortants by asynchronous coinfection. *J Virol,* 71**,** 853-7.

TENEV, T., DITZEL, M., ZACHARIOU, A. & MEIER, P. (2007) The antiapoptotic activity of insect IAPs requires activation by an evolutionarily conserved mechanism. *Cell Death Differ*, 14, 1191-1201.

THEILER, A. (1921) African horsesickness (*Pestis equorum*). *S Afr Dep Agric Sci Bull*, 19.

THOMAS, C. P., BOOTH, T. F. & ROY, P. (1990) Synthesis of bluetongue virus-encoded phosphoprotein and formation of inclusion bodies by recombinant baculovirus in insect cells: it binds the single-stranded RNA species. *J Gen Virol,* 71 (Pt 9)**,** 2073-83.

THOMPSON, G. M., JESS, S., & MURCHIE, A. K. (2012) A review of African horse sickness and its implications for Ireland. *Ir Vet J*, 65, 9.

TOUSSAINT, J. F., SAILLEAU, C., BREARD, E., ZIENTARA, S. & DE CLERCQ, K. (2007) Bluetongue virus detection by two real-time RT-qPCRs targeting two different genomic segments. *J Virol Methods*, 140, 115-123.

TSCHERNE, D. M. & GARCIA-SASTRE, A. (2011) Virulence determinants of pandemic influenza viruses. *J Clin Invest*, 121, 6-13.

UITENWEERDE, J. M., THERON, J., STOLTZ, M. A. & HUISMANS, H. (1995) The multimeric nonstructural NS2 proteins of bluetongue virus, African horsesickness virus, and epizootic hemorrhagic disease virus differ in their single-stranded RNA-binding ability. *Virology,* 209**,** 624-32.

URAKAWA, T., RITTER, D. G. & ROY, P. (1989) Expression of largest RNA segment and synthesis of VP1 protein of bluetongue virus in insect cells by recombinant baculovirus: association of VP1 protein with RNA polymerase activity. *Nucleic Acids Res,* 17**,** 7395-401.

VAN DE WATER, S. G., VAN GENNIP, R. G., x POTGIETER, R. G., WRIGHT, I. M. & VAN RIJN, P. A. (2015) VP2 Exchange and NS3/NS3a Deletion in African Horse Sickness Virus (AHSV) in Development of Disabled Infectious Single Animal Vaccine Candidates for AHSV. *J Virol*, 89, 8764-8772.

VAN DIJK, A. A. & HUISMANS, H. (1988) In vitro transcription and translation of bluetongue virus mRNA. *J Gen Virol*, 69, 573-581.

VAN GENNIP, R. G. P., VAN DE WATER, S. G. P. & VAN RIJN, P. A. (2014) Bluetongue Virus Nonstructural Protein NS3/NS3a Is Not Essential for Virus Replication. *PLoS One*, 9, e85788.

VAN NIEKERK, M., SMIT, C. C., FICK, W. C., VAN STADEN, V. & HUISMANS, H. (2001a) Membrane association of African horsesickness virus nonstructural protein NS3 determines its cytotoxicity. *Virology,* 279**,** 499-508.

VAN NIEKERK, M., VAN STADEN, V., VAN DIJK, A. A., & HUISMANS, H. (2001b) Variation of African horsesickness virus nonstructural protein NS3 in southern Africa. *J Gen Virol*, 82, 149-158.

VAN RIJN, P. A., VAN DER WATER, S. G. P., FEENSTRA, F. & VAN GENNIP, R. G. P. (2016) Requirements and comparative analysis of reverse genetics for bluetongue virus (BTV) and African horse sickness virus (AHSV). *Virol*, 13, 119.

VAN STADEN, V. & HUISMANS, H. (1991) A comparison of the genes which encode non-structural protein NS3 of different orbiviruses. *J Gen Virol,* 72 (Pt 5)**,** 1073-9.

VAN STADEN, V., SMIT, C. C., STOLTZ, M. A., MAREE, F. F. & HUISMANS, H. (1998) Characterization of two African horse sickness virus nonstructural proteins, NS1 and NS3. *Arch Virol Suppl,* 14**,** 251-8.

VAN STADEN, V., STOLTZ, M. A. & HUISMANS, H. (1995) Expression of nonstructural protein NS3 of African horsesickness virus (AHSV): evidence for a cytotoxic effect of NS3 in insect cells, and characterization of the gene products in AHSV infected Vero cells. *Arch Virol,* 140**,** 289-306.

VANDESOMPELE, J., DE PRETER, K., PATTYN, F., POPPE, B., VAN ROY, N., DE PAEPE, A. & SPELEMAN, F. (2002) Accurate normalization of real-time quantitative RT-PCR data by geometric averaging of multiple internal control genes. *Genome Biol*, 3, 1-12.

VENDE, P., PIRON, M., CASTAGNE, N. & PONCET, D. (2000) Efficient translation of rotavirus mRNA requires simultaneous interaction of NSP3 with the eukaryotic translation initiation factor eIF4G and the mRNA 3' end. *J Virol,* 74**,** 7064-71.

VENTER, E. (2014) Factors contributing to AHSV pathogenesis in infected mammalian and insect cells. PhD thesis, University of Pretoria, Pretoria, RSA.

VENTER, E., VAN DER MERWE, C. F., BUYS, A. V., HUISMANS, H. & VAN STADEN, V. (2014) Comparative ultrastructural characterisation of African horse sickness virus-infected mammalian and insect cells reveals novel potential virus release mechanism from insect cells. *J Gen Virol*, 95, vir.0.060400-060400.

VENTER, G. J., GRAHAM, S. D. & HAMBLIN, C. (2000) African horse sickness epidemiology: vector competence of South African *Culicoides* species for virus serotypes 3, 5 and 8. *Med Vet Entomol,* 14**,** 245-50.

VERMAAK, E., CONRADIE, A. M., MAREE, F. F. & THERON, J. (2016) African horse sickness virus infects BSR cells through micropinocytosis. *Virol*, 497, 217-232.

VERMAAK, E., PATERSON, D. J., CONRADIE, A. & THERON, J. (2015) Directed genetic modification of African horse sickness virus by reverse genetics. *SA J Sci*, 111, 1-8.

VERWOERD, D. W., ELS, H. J., DE VILLIERS, E. M. & HUISMANS, H. (1972) Structure of the bluetongue virus capsid. *J Virol,* 10**,** 783-94.

VERWOERD, D. W. & ERASMUS, B. J. (2004) Bluetongue. IN COETZER, J. A. W. & TUSTIN, R. C. (Eds.) *Infectious diseases of livestock.* Oxford University Press, Cape Town.

VERWOERD, D. W. & HUISMANS, H. (1969) On the relationship between bluetongue, African horsesickness and reoviruses: hybridization studies. *Onderstepoort J Vet Res,* 36**,** 175-9.

VERWOERD, D. W., HUISMANS, H. & ERASMUS, B. J. (1979) Orbiviruses. *Comprehensive Virology.* Plenum Publishing Corporation.

VREEDE, F. T. & HUISMANS, H. (1994) Cloning, characterization and expression of the gene that encodes the major neutralization-specific antigen of African horsesickness virus serotype 3. *J Gen Virol,* 75 (Pt 12)**,** 3629-33.

VREEDE, F. T., & HUISMANS, H., 1998 Sequence analysis of the RNA polymerase gene of African horse sickness virus. *Arch Virol*, 143, 413-419.

VON TEICHMAN, B. F. & SMIT, T. K. (2008) Evaluation of the pathogenicity of African Horsesickness (AHS) isolates in vaccinated animals. *Vacc*, 26, 5014-5021.

WALKER III, W. B. & ALLEN, M. L. (2011) RNA interference-mediated knockdown of IAP in *Lygus lineolaris* induces mortality in adult and pre-adult life stages. *Entomol Exp Appl*, 138, 83-92.

WALKER, P. J., TAYLOR, J. & GORMAN, B. M. (1989) Detection of reassortant orbiviruses (Wallal serogroup) in a prototype strain isolated from a pool of biting midges (*Culicoides dycei*). *J Gen Virol,* 70 (Pt 4)**,** 1011-6.

WANG, H., GORT, T., BOYLE, D. L. & CLEM, R. J. (2012) Effects of manipulating apoptosis on Sinbis virus infection of *Aedes aegypti* mosquitoes. *J Virol*, 86, 6546-6554.

WEHRFRITZ, J. M., BOYCE, M., MIRZA, S. & ROY, P. (2007) Reconstitution of bluetongue virus polymerase activity from isolated domains based on a three-dimensional structural model. *Biopolymers,* 86**,** 83-94.

WEYER, C. T., JOONEA, C., LOURENSA, C. W., MONYAIA, M. S., KOEKEMOER, O., GREWARD, J. D., VAN SCHALKWYK, A., MAJIWA, P. O. A., MACLACHLAN, N. J. & GUTHRIEA, A. J. (2015) Development of three triplex real-time reverse transcription PCR assays for the qualitative molecular typing of the nine serotypes of African horse sickness virus. *J Virol Methods*, 223, 69-74.

WILLIAMS, C. F., INOUE, T., LUCUS, A. M., ZANOTTO, P. M. & ROY, P. (1998) The complete sequence of four major structural proteins of African horse sickness virus serotype 6: evolutionary relationships within and between the orbiviruses. *Virus Res*, 53, 53-73.

WILSON, A., DARPEL, K. & MELLOR, P. S. (2008) Where Does Bluetongue Virus Sleep in the Winter? *PLOS Biology,* 6**,** 1612-1617.

WINSTON W. M., MOLODOWITCH, C. & HUNTER, C. P. (2002) Systemic RNAi in *C. elegans* requires the putative transmembrane protein SID-1. *Sci*, 295, 2456-2459.

WIRBLICH, C., BHATTACHARYA, B. & ROY, P. (2006) Nonstructural protein 3 of bluetongue virus assists virus release by recruiting ESCRT-I protein Tsg101. *J Virol,* 80**,** 460-73.

WU, X., CHEN, S. Y., IWATA, H., COMPANS, R. W. & ROY, P. (1992) Multiple glycoproteins synthesized by the smallest RNA segment (S10) of bluetongue virus. *J Virol,* 66**,** 7104-12.

ZIENTARA, S. & SÁNCHEZ-VIZCAÍNO, J. M. (2013) Control of bluetongue in Europe. *Vet Microbiol*, 165, 33-37.

ZWART, L., POTGIETER, C. A., CLIFT, S. J. & VAN STADEN, V. (2015) Characterising non-structural protein NS4 of African horse sickness virus. *PLoS One*, 10, e0124281.